A Numerical Study on the Accuracy of Nonlinear Wave Generation and Wave-Current Coupling in OpenFOAM

孫, 浩東
九州大学大学院総合理工学府総合理工学専攻機械・システム理工学メジャー

Master Thesis

A Numerical Study on the Accuracy of Nonlinear Wave Generation and Wave-Current Coupling in OpenFOAM

Marine Environment and Energy Engineering Laboratory,
Mechanical and Systems Engineering Major,
Interdisciplinary Graduate School of Engineering Sciences,
Kyushu University

SUN HAODONG

Supervisor(s) 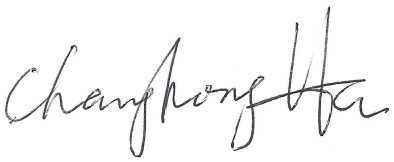

Date: 04, February, 2026

Contents

Contents of Table

Contents of Figure

Abstract

Tension Leg Platform (TLP), is a type of floating platform gaining its popularity in marine engineering in recent years, featured in its high vertical stability (Roll, Pitch, Heave), been moored through a tension mooring system that anchors it to the seabed. However, this structure has a relevantly lower stability in the horizontal direction, typically under the influence of waves and currents, the motion amplitudes of Surge, Sway, Roll, and Pitch might increase significantly. As a result, precisely generate the waves and reproduce wave-current coupling phenomena are significant for the design of TLP.

This study focuses on the verification of nonlinear wave generation in OpenFOAM and the development of two solvers - stokesSecondwCurrent and overWaveDyMFoam within the framework of waves2Foam, aiming to extend the function of waves2Foam by adding these two solvers to the program and providing guidelines on wave generation as well as wave-current coupling reproduction for the engineering design of TLP. This research consist of three parts - wave generation, development of wave-current coupling solver and development of overset-mesh-based 6DOF motion solver.

In the first part of the research, the feasibility and numerical accuracy of nonlinear wave generation using OpenFOAM and waves2Foam are systematically investigated. To validate the feasibility of these programs, simulations are conducted to generate identical waves using various wave models in both OpenFOAM and waves2Foam across multiple mesh resolutions. The accuracy performance of these wave models are evaluated and the model exhibiting the highest accuracy is selected for further study of its generality by generating wave with different parameters, including some extreme wave conditions. With the use of this model, a case which contains a 2D fixed floating body is simulated to confirm whether this model is capable of precisely forecasting hydrodynamic loads on marine structures. Subsequently, a study on improving numerical accuracy of nonlinear wave generation on relevantly coarser meshes is implemented, aiming to provide a guideline for achieving cost-effective numerical prediction for engineering application.

In the second part of the study, a user-defined wave-current coupling solver stokesSecondwCurrent is develop and its feasibility, accuracy performance and generality are evaluated. The solver is developed on the basis of Stokes nonlinear wave theory and be verified by

comparing the numerical predication with theoretical values. The accuracy performance of the solver is subsequently investigated under multiple mesh resolutions and wave conditions, obtaining a guidelines for achieving high accuracy in terms of mesh requirements and the applicability of the solver. After that, the capability of the solver to accurately predict hydrodynamic loads on a floating body is validated by comparing the numerical results with benchmark experimental data. Finally, in order to seize cost-effective numerical results about wave-current interaction using the solver in practical engineering applications, this study also explores approaches to improve computational accuracy on relevantly coarser meshes.

In the last part of the study, an overset-mesh-based 6DOF motion solver overWaveDyMFoam is developed and verified. The solver is created by combing the relaxation zone related code of waves2Foam with the source code of overInterDyMFoam, an application in OpenFOAM to conduct simulation based on overset mesh. By using this solver, the dynamic response of a 2D cubic-shaped free floating structure under wave loads is analyzed and be compared with the experimental data of a benchmark, validating the correctness and feasibility of the solver overWaveDyMFoam.

In conclusion, this research verifies the feasibility of generate large or even extreme nonlinear wave by waves2Foam and develops two solvers to address the lacks of the program - no built-in solver for wave-current interaction and does not support overset-mesh-based simulations. Practical recommendations for nonlinear wave generation using waves2Foam are provided, detailing the requirements for mesh resolution, computational domain configuration, and discretization schemes for physical variables. Moreover, through the symmetrical investigation on the stokesSecondwCurrent and overWaveDyMFoam solvers, the feasibility of them are verified and guidelines detailing their generality, suggested mesh resolutions and recommended numerical settings are also provided.

This study developed a wave-current coupling solver and an overset-meshed-based 6DOF motion solver, which largely extend the function of waves2Foam, providing crucial numerical toolbox and reference for researchers and engineering applications. Also, this research provide technical support and practical guideline for load analysis process of the design of TLP.

1 Introduction

1.1 Background

In 2010, fossil fuels accounted for a dominant share of total primary energy consumption in key East Asian economies: approximately 82% in South Korea, over 80% in Japan, and around 84% in China. Renewable energy sources such as wind, solar, and biomass collectively made up a much smaller portion of total energy consumption, roughly 3%, 8%, and 7% in these countries, respectively. More recent data indicates that the share of renewable energy has risen significantly in the electricity sector, with Japan achieving around 22% renewable generation by 2023 and South Korea around 9%, reflecting ongoing transitions toward cleaner energy sources.[1-4] With the ongoing of this transition, there are increasing demands on the exploitation of green energy, which promotes the development of relevant technology as well as related researches. Studies about this topic has gaining its' popularity in the past decade, growing to one of the most popular direction in multiple academic fields, including Naval Architecture and Ocean Engineering.

In Naval Architecture and Ocean Engineering field, researchers are focusing on the development of offshore wind turbine and its foundation in order to promote the exploitation of offshore wind energy, which exhibits a higher resource density compared to the land-based wind energy. This resource is even richer in the far offshore areas than in the costal areas, however, with the increase of the distance to the coastline and water depth, the difficulty of utilization also steeply rises. There are thus growing tendency that global scientists are dedicated to the research on exploitation of far offshore wind energy, addressing challenges such as the foundation structure of offshore wind turbine in deep or extreme deep water. In order to overcome this problem, floating foundation structures such as spar platform, semi-submersible platform and tension leg platform were hired to support the wind turbine in far offshore areas. Among them, tension leg platform, showing great potential for application in deep-sea , has been widely occupied as the foundation of floating wind turbine.

1.2 Tension leg platform (TLP)

Tension leg platform is a type of floating platform mainly be adopted as the foundation of offshore oil drilling platform and offshore oil production platform and gradually be employed to support the

offshore wind turbine in recent years. The concept of the structure appeared in 1950s, scientists back to the time proposed a floating platform which vertically anchored to the seabed, while the practical application of it was in 1970s. In 1974, American ConocoPhillips Company initially launched a verification research about the TLP aiming to design a platform for offshore oil exploitation in deep water and verify its' feasibility. After a decade of study, the company finally accomplished the design of TLP and through the cooperation with British government the fist structure of this kind was establish in Hutton Field in North Sea where the water depth is 148m.[5] This early stage structure consists of four columns and a rectangular base frame, being secured to the seabed by 16 tension tendons. In 1989, the second TLP in the world was installed for offshore oil exploitation by ConocoPhillips Company in Green Canyon block of the Gulf of Mexico where the water depth is 535m.[6] The the installation of which demonstrated the capability of TLP being applied in greater water depth. The operating water depth of the structure was further extended to 872m in 1994 with the application of Auger TLP in the Gulf of Mexico designed by Shell plc.[7] The company subsequently established Mars TLP (operating water depth 896m), Ram-Powell TLP (operating water depth 980m) and Ursa TLP (operating water depth 1185m) in the gulf from 1996 to 2001, enabling the Gulf of Mexico to be region with the highest concentration of TLP applications in the world.[8] In the same place, TLP with the deepest operation depth of 1584m Big Foot TLP for offshore oil resource was installed in 2013 and was donated to operation in 2018 designed Chevron Corporation.[9] These practical engineering examples verified the feasibility of the application this platform in deep or extreme deep water.

The application of TLP in floating wind turbine, however, appears much later than that on the offshore oil drilling platform. The concept of Tension Leg Platform - Floating Offshore Wind Turbine (TLP-FOWT) was devised in 1990s and researched by Massachusetts Institute of Technology (MIT) America, National Renewable Energy Laboratory (NREL) America as well as Kyushu University (KU) Japan.[10] Globally, the engineer examples of TLP-FOWT are mainly experimental demonstration projects. The first experimental TLP-FOWT in the world Blue H, equipped with a 80 kW two-blade wind turbine, was sent to service in Offshore Puglia, Adriatic Sea, Italy in 2007, however was subsequently demolished in 2008.[11] In the 2010s, MIT and NREL developed a concept design of a TLP-FOWT with a rated power output of 5 MW for water depths ranging from 200 m to 500 m. In 2013, KU and New Energy and Industrial Technology Development Organization (NEDO) installed a

small-scale prototype of the structure, the power output of which was 100kW, in Nagasaki and sent to service.[12] Pivot Buoy X30 a structure of the kind equipped with a modified 225kW Vestas V29 wind turbine, was established in 2022 in the PLOCAN offshore test site in the Canary Islands Spain where the water depth is 50m.[13] France also established its' first TLP-FLOWT called Provence Grand Large which referred to the design of TLP offshore oil drilling platform in 2023 and be sent to generate electricity in July 2025.[14] Institutes in Europe such as IFP Energies Nouvelles (IFPEN) France, The Foundation for Industrial and Technical Research (SINTEF) Norway are also developing the similar concept, however no prototype has been established yet and they have mainly focused on Spar-FOWT. In recent years, the relevant academic institutes are continuously conducting researches about TLP-FOWT to promote its' popularization.

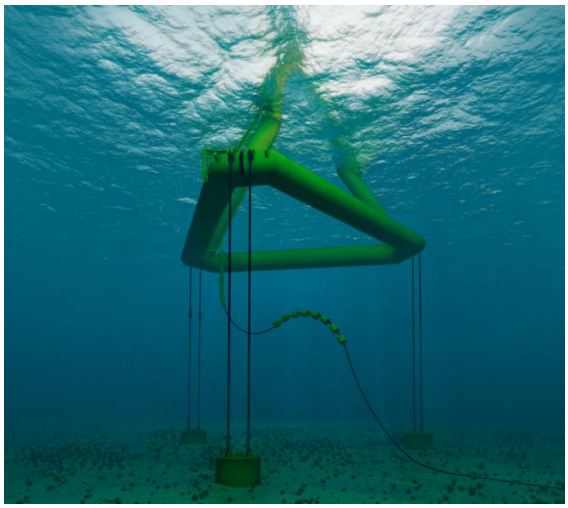

[Figure 1.1] The figure of a typical TLP

As a semi-compliant structure, tension leg platform shows distinctive stability and survivability in its practical operational life owing to its form of constraint, being anchored to the seabed through a mooring system and tension tendons. The hull of this type of platform, commonly consist of buoyant pontoon, columns and deck, has a larger displacement compared to its weight, therefore, the buoyancy of a TLP is greater than the gravity. The difference between these two forces, known as excess buoyancy, is compensated by the tension in the tendons, which constrains the motion of the platform. Owing to this mechanism, the structure exhibits remarkable stability in the vertical direction, with small amplitudes of heave, pitch, and roll. However, its stability in the horizontal directions is

relatively weak compared with other floating platform structures, thus under extreme conditions, the horizontal motions may become excessive, which could result in tendon failure or even platform overturning. These failure commonly appear when the motion of TLP is too large leading to the tension on the tendons decrease to zero. As a result, the analysis of the dynamic response of this platform should be given particular attention during the design process.

1.3 OpenFOAM and waves2Foam

Open Source Field Operation and Manipulation (OpenFOAM) is one of the most widely adopted open-source computational fluid dynamic (CFD) tools in both academia and industry. This toolbox was initially proposed by Henry Weller with his colleagues in late 1980s and continuously developed since its release in 2004.[15] OpenFOAM also provides a flexible object-oriented framework for the numerical solution of partial differential equations (PDEs), making it particularly suitable for simulating complex fluid flow and multiple problems. This software has been widely adopted to solve multiple engineering problems involved with both hydrodynamic, aerodynamic and thermodynamic. The feasibility and generality of OpenFOAM were systematically discussed by Jasak.H in 2009, and the extensibility of the code was also investigated in the research.[16] An official user's manual about the the numerical methods, solver structure, and extension mechanisms for secondary development of OpenFOAM was proposed by Greenshields.C.J in 2021.[17]

Volume of fluid (VOF) theory is also introduced to OpenFOAM, enabling the software to be highly capable of handling multiple-phase flow simulations. The VOF theory, initially developed by Hirt.C.W and Nichols.B.D in 1981, tracks free-surface motion by solving a transport equation for the fluid volume fraction, allowing complex interface deformation to be captured on fixed grids.[18] The cell is considered to be liquid phase if volume fraction equals to 1 and is consider to be air phase if volume fraction equals to 0. Whereas, the grid is consider to be the interface between two phases when volume fraction varies from 1 to 0 and thus the position of free-surface is identified. Ubbink.O and Issa.R.I improved the mathematical method of free-surface capture, increased the numerical accuracy of free-surface capture.[19] In 2002, Rusche.H finially established a core numerical implementation framework for multi-phase flow and interface transport equations and introduced VOF theory to OpenFOAM.[20]

One of the key advantages of OpenFOAM is that the software provides researchers to

conveniently modify the source code or develop their own users-defined libraries, boundary conditions or solvers. Some of these user-developed libraries will be absorbed by the developers of OpenFOAM and added to the following versions. Furthermore, this software also supports a wide range of plug-in code such as waves2Foam, olaFlow or HiSA which allows users to further customize the code to fulfill their demand of research.

The plug-in code waves2Foam is a widely used plug-in code of OpenFOAM to simulate the propagation of wave and fluid-structure interactions (FSI). Specifically waves2Foam was developed by Jacobsen.N.G et.al in 2012 which achieved the objective of generating both regular and irregular waves.[21] This code introduced the relaxation zone to the OpenFOAM, minimizing undesired wave reflections at domain boundaries, to simulate the surface wave with satisfying accuracy within the framework of OpenFOAM. In OpenFOAM, wave generation is commonly achieved using the internal wave-maker concept originally proposed by Lin.P and Liu.P.L.F in 1999, in which target waves are generated by introducing source terms into the Navier-Stokes equations.[22] However, in the waves2Foam framework, waves are generated using the relaxation-zone method, whose underlying concept was first proposed by Larsen.B.E and Dancy.H in 1983, featuring simple implementation and the capability of simultaneous wave generation and absorption, thereby providing stable numerical solutions.[23]

The feasibility of generating waves by waves2Foam has been verified by researchers, and this code has been adopted to solve multiple engineering problems. Higuera.P not only reproduced and absorbed high-fidelity wave using waves2Foam but also comprehensively validated the feasibility of waves2Foam on engineering applications.[24] He also concluded the capability and application scope in coastal and offshore engineering in 2013.[25] Additionally, he enhanced the ability of the code on generating 3D waves, enabling the solver to be capable of handling complex wave fields with strong non-linearity.[26] Similarly, Shuaiwen Huo from Shanghai Jiao Tong University conducted simulation with the application of waves2Foam to analyze the wave-current coupling problems based on a floating production storage and offloading unit (FPSO), verifying the outstanding performance of the toolbox in wave generation and absorption under complex sea states.[27]

Apart from waves2Foam, there are various plug-in codes available for the wave generation in the framework of OpenFOAM. For example, olaFlow developed by Pablo Higuera.P and his team also generates wave by relaxation zone wave generation method which is consistent to waves2Foam,

demonstrating high performance on the generation of shallow water waves.[28] IHFOAM, another wave generation toolbox developed on the basis of waves2Foam by Environmental Hydraulics Institute (IH Cantabria) of a Spanish school - University of Cantabria. This solver further enhance the capability of OpenFOAM in shallow-water wave modelling and WSI simulations.[29]

On comparison to the above mentioned models, waves2Foam shows a higher accuracy in capturing nonlinear waves, reproducing non-linearity induced wave breaking and analyzing the viscous effect. Moreover, waves2Foam also leaves an user-friendly interface in its source code, allowing researchers to conveniently developer their own user-defined solvers or wave theories to fulfill their research need such as overset-mesh-based dynamic simulations. Both linear and nonlinear wave theories, regular and irregular wave theories are allowed to be introduced into the framework of waves2Foam for the implementation of a wide range of simulations.[30] Because of this advantage, waves2Foam has become a widely-accepted tool in marine and offshore engineering research, particularly in the study of wave loading on offshore structures, floating platforms, and renewable energy devices such as floating offshore wind turbines and wave energy converters.

1.4 Nonlinear wave generation

In wave theories, regular wave might be describe by neither linear theory or nonlinear theory. Linear wave theory or Airy model is a commonly used simplified model, providing researchers a convenient approach to study the propagation of wave and its physical characteristics. In linear wave theory, waves are idealized as small-amplitude sinusoidal waves, and the motion of a fluid particle is assumed to follow a closed elliptical orbit. These assumptions allow the Airy model to reproduce wave kinematics with reasonable reliability in calm sea states. However, in real physical cases, the fluid particles has a lateral drift motion, known as Stokes drift, which might be ignore in calm sea states but non-negligible in higher sea states. Thus in high sea states, the non-linearity of the wave is significant and waves can no longer be assumed to be linear, and Airy model may fail to provide results with satisfying accuracy. The limitations of linear wave theory further manifest in its failure on reproducing wave deformation and wave breaking.

The limitations of the linear wave is even more evident when studying Fluid-Structure Interaction (FSI) problems. This theory neglects the nonlinear free-surface elevation and higher-order velocity potential terms, thus its direct application to the dynamic analysis of floating bodies such as

TLP-FOWT often leads to an underestimation of dynamic response, typically in extreme conditions.

To address these above-mentioned deficiencies, nonlinear theories have been devised to precisely analyze the kinematics of waves as well as investigate the FSI problems. This models might provide a better description of a floating body's added mass, radiation damping and second-order wave loads, which are essential for the evaluation of a marine structure's survivability in extreme cases.

However, the introduction of nonlinear wave may poses significant challenge for numerical simulation. The reproduction of Stokes waves requires high mesh density and tiny time steps to precisely capture the free-surface deformation as well as higher-order harmonic components of the wave, which remarkably increases the consumption of calculation resources. For instance, OpenFOAM together with its plug-in code waves2Foam are capable of generating waves with significant non-linearity, accurately simulating the wave deformation or wave breaking by numerically solving the Navier-Stokes equation in a numerical water tank (NWT). However, the requirements of this kind of high-accuracy simulations in terms of mesh density and computational resources, far exceed the acceptable range for engineering applications. Enormous consumption of computational resources will be inevitable if industrial designers aim to obtain precise second-order motion responses of the floating body and the associated second-order wave loads, which lack cost-effectiveness and practical feasibility. To issue this problem, in academia user-defined applications might be proposed by researchers to fulfill their requirement of obtaining precise results with limited use of calculation resources, whereas in industrial applications, designers mainly rely on original source codes of OpenFOAM or waves2Foam for numerical analysis.

Therefore, it is essential to investigate how to achieve a precise and cost-effective reproduction of nonlinear wave while ensuring the use of computational resources within an acceptable range, through appropriate parameter settings and mesh optimization.

2 Research overview

2.1 Research gap

OpenFOAM and its plug-in code waves2Foam, featured by their the open-source flexibility and powerful solving capability, has been widely adopted for the simulation of various the nonlinear free-surface flow in the ocean environment and FSI problems including the dynamic response of marine platforms. The feasibility of these two toolboxes have been widely studied by researchers.

Although waves2Foam is capable of reproducing waves with a wide range of theories including both linear wave theory, nonlinear wave theory such as Stokes fifth-order theory, shallow-water solitary wave theory together with irregular waves. Due to the absence of built-in code for wave-current coupling, waves2Foam can not easily reproduce the wave-current coupling phenomena. Additionally, waves2Foam can not handle simulations involved with overset meshes which is necessary when analyzing the dynamic response of marine structures under wave loads.

Due to the above mentioned drawbacks of waves2Foam, this study proposes two solvers - stokesSecondwCurrent and overWaveDyMFoam - to fill this gap. The feasibility of these solvers is validated and the performance of them under multiple conditions are also assessed.

2.2 Research target

This study is committed to comprehensively investigating the accuracy of OpenFOAM and its plug-in code waves2Foam in terms of nonlinear wave generation, providing systematic guideline for improving the accuracy of wave reproduction with moderate mesh density and time steps. On this basis, this research also devises an application for the wave-current coupling reproduction as well as an overset-mesh-based 6 degree of freedom (6DOF) motion solver in the framework of OpenFOAM and waves2Foam. Their feasibility and performance evaluated through the 6DOF dynamic response analysis of a small-scale TLP under the combined loads of wave, current and wind. The applicability of utilizing OpenFOAM and waves2Foam to investigate the motion response of a floating body is also tested. The practical targets of this thesis are as follows:

This paper examines the feasibility of nonlinear wave generation by OpenFOAM and its plug-in code waves2Foam. The accuracy performance between these software and between various wave

models are compared, the theory with the best resolution is subsequently selected. Further study is conducted to assess the function and precision performance of this model in different wave conditions.

The effect of mesh density on accuracy of nonlinear wave generation is estimated. From the perspectives of mesh distribution optimization and algorithmic improvement, this study explores methods to increase the accuracy of nonlinear wave generation while maintaining a moderate level of mesh density and restricting computational resource consumption within an acceptable range. A guideline within the framework of OpenFOAM and waves2Foam for cost-effective nonlinear wave reproduction and high-order wave load analysis is devised, oriented towards the practical engineering applications.

A wave-current coupling solver is created within the framework of waves2Foam. Its feasibility is systematically, and its performance is assessed under various wave and current conditions. This module address the limitation of the existing plug-in, thereby facilitating future research and industrial application.

Within the environment of waves2Foam, an overset-mesh-based 6DOF motion solver is developed to evaluate the 6DOF dynamic response of a floating body under multiple loads, including the high-order wave loads reproduced by waves2Foam. The feasibility of the application is then examined though reproducing the 6DOF dynamic response analysis of a regular-shaped floating body in the benchmark.

2.3 Research plan

Based on the open-source computational fluid dynamics toolbox OpenFOAM and its plug-in waves2Foam, this study is centered on the generation of nonlinear waves and the analysis of their accuracy. The first stage of the research verifies the feasibility of generating nonlinear waves using OpenFOAM and waves2Foam. Specifically, the second-order Stokes model and the fifth-order Stokes model of both the OpenFOAM and the waves2Foam, are respectively applied to numerically reproduce an identical wave but with different mesh densities. The numerical results of wave height and period are compared against theoretical values given by a Matlab code, while the wave loads on a fixed floating body are compared with benchmark from other researchers, in order to analyze the feasibility of nonlinear wave generation using these two numerical toolboxes. In this process, this paper gives special attention to the analysis of the effect of mesh density towards the precision of the

numerical result. The wave model that achieves the most accurate reproduction of the given parameters are subsequently identified, the performance and versatility of which is further studied in different wave conditions. Based on this model, this research then investigate, under medium or even coarse mesh densities, how to improve computational accuracy of wave generation through optimizing mesh distribution and algorithmic, while ensuring computational costs remain within an acceptable range, for the engineering applications.

The second stage of this study focuses on the development of wave-coupling solver, stokesSecondwCurrent, within the framework of waves2Foam. The feasibility of this model is, similarly, verified by comparing the numerical result of wave height and period with theoretical values and by comparing the simulation result of wave loads on a fixed floating body with benchmark from other scholars. By varying the parameters of wave as well as current velocities in the wave-current coupling system, the performance and versatility of the module is further assessed. Likewise, this part of the study will also explore how to maximize the accuracy of wave-current coupling reproduction by optimizing the mesh distribution and algorithms while the mesh density is medium or even low. A systematic guideline is commentated for engineering applications or further researches.

In addition, a 6DOF motion solver based on over-set mesh, overWaveDyMFoam, is devised. The feasibility of the solver is subsequently validated, and the performance of which is examined under multiple conditions.

A detailed flowchart of the research framework is presented in Figure 2.1.

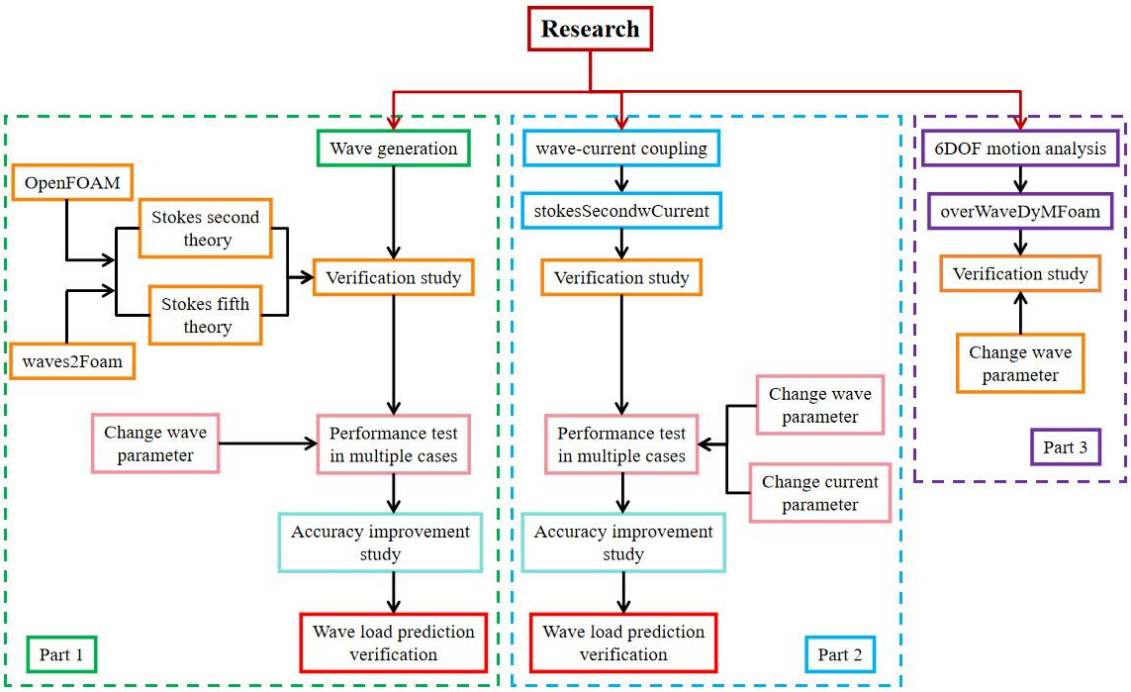

[Figure 2.1] Flowchart of the research

3 Methodology

In this chapter, the developments of linear as well nonlinear wave theory are explained in detail, and mathematical basis of user-developed solver stokesSecondwCurrent and overWaveDyMFoam is also proposed. Noting that, in order to improve the robustness of the solver and reduce computational cost, second-order Stokes wave theory is adopted as the foundation of the wave-current coupling solver. Moreover, the second-order Stokes model is capable of capturing a substantial portion of nonlinear wave effects, and, following discussions with the academic supervisor, it was therefore selected as the theoretical basis for further solver development.

3.1 Nonlinear wave theory

In this research, Stokes wave theory, a classic nonlinear wave model for periodic gravity waves, is adopted for wave generation. Based on potential flow theory, this theory is developed, with the assumption of in-viscid and in-compressible ideal fluid of constant depth for describing steady state periodic wave motion. The Stokes model is often employed to reproduce the regular nonlinear waves under deep water conditions, providing prediction of free-surface deformation and fluid dynamic load on the structure in the marine engineering applications.

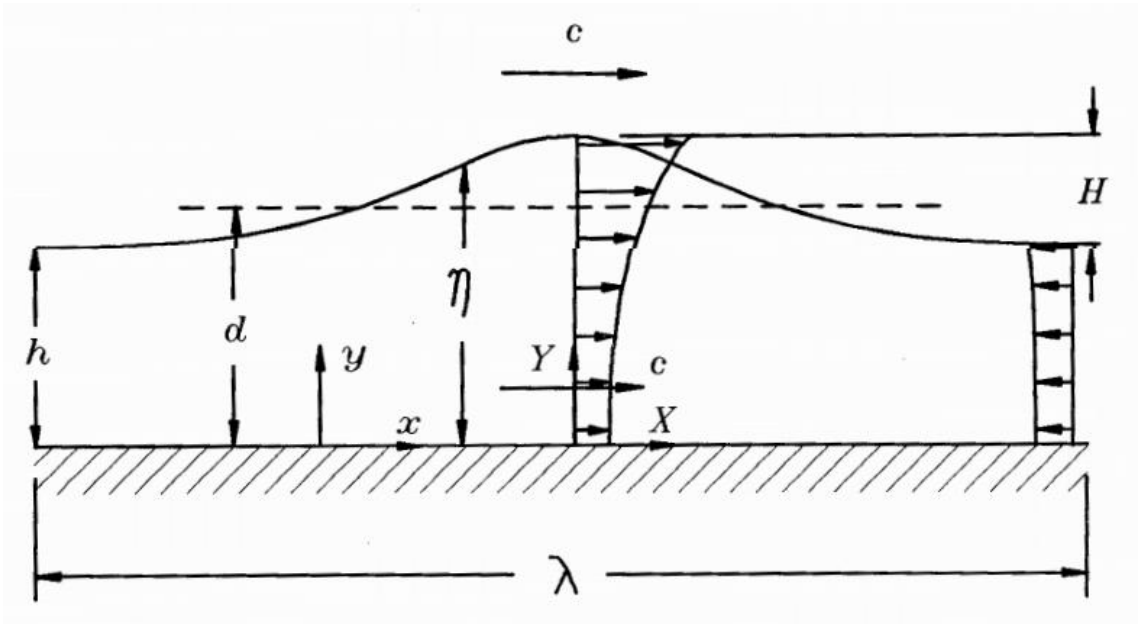

[Figure 3.1] 2D fluid field for the theory development in Chapter 3

The theory development in this study follows the paper proposed by the researcher John D. Fenton.[31] The fundamental ideal of Stokes wave theory is introducing the non-linearity of the wave by perturbation expansion, in which process the free-surface elevation η and velocity potential ϕ are described as a series expansion in a small parameter, typically the wave steepness ε, which is the product of the wave number k and the wave amplitude a or the ratio of wave height H and wave length λ. On the basis of that, approximate solution can be established to progressively approach the real characteristics of finite-amplitude waves, and be expanded to second-order, fifth-order or even higher order. The second-order Stokes wave theory is often adopted to generate waves with moderate height and non-linearity, whereas under conditions, where wave elevation is higher and the non-linearity becomes significant, fifth-order or even higher order models are required for accurate prediction of the wave profile.

Stokes wave model is developed under the framework of potential flow theory, and assumes no vortex and turbulence existing in the calculation domain. Thus, the velocity potential follows the Laplace equation and can be expressed in 2D cases as:

$$\nabla^2\phi = 0 \tag{3-1}$$

Within the above mentioned framework, in a 2D fluid field illustrated in Figure 3.1, the Stokes model under all orders must satisfy the following three fundamental boundary conditions.

1. Dynamic Boundary Condition (Pressure Continuity)

The dynamic boundary condition ensures that the pressure at the free-surface equals the atmospheric pressure. On the interface of fluid and air, by employing Bernoulli's equation, this condition can be expressed in 2D cases as:

$$\frac{\partial\phi}{\partial t} + \frac{1}{2}|\nabla\phi|^2 + g\eta = 0, \quad z = \eta(x,t) \tag{3-2}$$

This equation indicates the balance between hydrodynamic pressure, kinetic energy, and gravitational potential energy on the free-surface.

2. Kinematic Boundary Condition (Surface Particle Consistency)

The Kinematic Boundary Condition grantees that fluid particles on the free-surface remain on it and the vertical velocity of the surface equals that of the fluid. Under 2D conditions, this condition can be mathematically described as:

$$\frac{\partial\eta}{\partial t} + \frac{\partial\phi}{\partial x}\frac{\partial\eta}{\partial x} = \frac{\partial\phi}{\partial z}, \quad z = \eta(x,t) \tag{3-3}$$

This formula ensures the shape of the free-surface, preventing the unwanted velocity vectors which might lead to the free-surface breaking exist on the interface between fluid and air phase.

3. Bottom Boundary Condition (Impermeability)

The Bottom Boundary Condition defines the bottom of a NWT, where no fluid particle can penetrate the boundary. This condition, in 2D cases, can be expressed as:

$$\frac{\partial \phi}{\partial z} = 0, \quad z = 0 \tag{3-4}$$

With these boundary conditions, Stokes wave theory under different orders can be mathematically described.

1. Stokes first-order theory (linear wave)

The first-order model is equivalent to the linear wave theory, also known as Airy wave theory, which is often adopted under the conditions where the wave height is small and the nonlinear effect in the fluid field is negligible. In this kind of cases, where the non-linearity in the calculation domain is ignored, assumption is made that the wave amplitude is small (small-amplitude assumption) and the motion orbit of fluid particle is considered as a closed ellipse under the free-surface. Under these assumptions, the theoretical formulation of free-surface elevation η and velocity potential ϕ are as follows:

$$\eta(x,t) = d + \frac{\varepsilon}{k}\cos\left[k(x-ct)\right] \tag{3-5}$$

$$\phi(x,z,t) = (c-\overline{U})x + \frac{\varepsilon}{\sinh(kd)}\left[\tanh(kd)\right]^{\frac{1}{2}}\left(\frac{g}{k^3}\right)^{\frac{1}{2}}\cosh(kz)\sin\left[k(x-ct)\right] \tag{3-6}$$

From the mathematical expression of these two physical elements, conclusion is obtained that the wave generated by first-order Stokes model is a simple sinusoidal wave. In the Eq. (3-5) and Eq. (3-6), d represents the water depth. k denotes the wave number, being calculated by:

$$k = \frac{2\pi}{\lambda} \tag{3-7}$$

ε is the wave steepness , being given by:

$$\varepsilon = \frac{ka}{\pi} = \frac{H}{\lambda} \tag{3-8}$$

c is the phase velocity, which denotes the speed of wave shape propagation in the field, being calculated by two formulas:

$$c = \overline{u_E} + \overline{U} \tag{3-9}$$

$$c = \overline{u_S} + \frac{Q}{d} \tag{3-10}$$

Here u_E denotes the Euler speed, which represents the instantaneous horizontal velocity of fluid particle at a fixed point in the inertial coordinate system, and $\overline{u_E}$ is its time average over one wave period. u_S is the Stokes drift velocity, representing the forward horizontal velocity of a fluid particle resulting from nonlinear wave motion, and $\overline{u_S}$ is its time average over one wave period. $\overline{U}$ is the mean drift velocity, referring to the time-average horizontal velocity of fluid particles over one wave period measured in the stationary frame, which corresponds to the Stokes drift component in nonlinear wave theory. Q is the volume flow rate per unite span underneath the wave in the inertial coordinate system. In the first-order Stokes theory, $\overline{U}$ and Q can be obtained by:

$$\overline{U} = \left[\frac{\tanh(kd)}{\left(\frac{k}{g}\right)}\right]^{\frac{1}{2}} \tag{3-11}$$

$$Q = \frac{[\tanh(kd)]^{\frac{1}{2}} kd}{\left(\frac{k^3}{g}\right)} \tag{3-12}$$

2. Stokes second-order theory (weakly nonlinear wave)

The non-linearity is introduced to the fluid fields through the Stokes second-order model. Within the framework of this theory, the second-order perturbation term involving the square of wave steepness ε is incorporated into the expression of free-surface elevation and velocity potential. The introduction of this term enables the Stokes second-order model to reproduce weakly nonlinear waves. In such cases, the motion trajectory of fluid particles are no longer close eclipses, and a horizontal movement of fluid elements appears in the computational domain. The horizontal velocity of these elements is known as Stokes drift u_S, which equals 0 under linear wave conditions. Meanwhile, the wave profile loses its symmetry, exhibiting sharper crests and flatter troughs, which better agree with the realistic wave shape in natural, due to the involvement of second-order perturbation term. The free-surface elevation η and velocity potential ϕ of the theory can be mathematically expressed as:

$$\eta(x,t) = d + \frac{\varepsilon}{k}\cos[k(x-ct)] + \frac{\varepsilon^2}{k}\coth(kd)\frac{1+2S}{2(1-S)}\cos[2k(x-ct)] \tag{3-13}$$

$$\phi(x,z,t) = (c-\overline{U})x + \frac{\varepsilon}{\sinh(kd)}[\tanh(kd)]^{\frac{1}{2}}\left(\frac{g}{k^3}\right)^{\frac{1}{2}}\cosh(kz)\sin[k(x-ct)] + \frac{\varepsilon^2(3S^2)}{2(1-S)^2}\cosh(2kz)\sin[2k(x-ct)] \tag{3-14}$$

Here, S is a coefficient calculated by:

$$S = \operatorname{sech}(2kd) \tag{3-15}$$

From the mathematical expression of the second-order theory, the existence of second-order terms leads to the mean water level rise, which is a typical feature of Stokes nonlinear wave theory. The appearance of this phenomenon is caused by the non-linearity in the filed, specifically, it attributes to the constant term in the second-order boundary conditions, being introduced to ensure the mass conservation of the fluid field. Physically, this mean free-surface elevation arises from the asymmetry of the wave profile, sharper crests and flatter troughs, and Stokes drift, the non-closed trajectories of fluid particles.

3. Stokes fifth-order theory (highly nonlinear wave)

With the further increase of wave height as well as wave steepness, the non-linearity in the fluid fields becomes more significant, higher-order of nonlinear terms are thus introduced to the Stokes theory to maintain the numerical accuracy. Third-order, forth-order and fifth-order perturbation terms are introduced to the formula of free-surface elevation and velocity potential, enabling the theory to precisely reproduce wave under high non-linearity conditions. In these cases, the waves generated by Stokes fifth-order model demonstrate a more accurate relationships between wave crest steepness and the wave dispersion, with sharper crests and flatter troughs comparing with second-order nonlinear waves. It should be noted that the high non-linearity of these waves leads to remarkable mass transport effect, the horizontal motion of fluid elements, Stokes drift, must be introduced to the theory to satisfy the mass conservation condition in the computational domain. The expression of free-surface elevation and velocity potential are given by:

$$\eta(x,t) = d + \frac{1}{k}\sum_{i=1}^{5}\varepsilon^i\sum_{j=1}^{j}B_{ij}\cos[jk(x-ct)] \tag{3-16}$$

$$\phi(x,z,t) = (c-\overline{U})x + [\tanh(kd)]^{\frac{1}{2}}\left(\frac{g}{k^3}\right)^{\frac{1}{2}}\sum_{i=1}^{5}\varepsilon^i\sum_{j=1}^{j}A_{ij}\cosh(jkz)\sin[jk(x-ct)] \tag{3-17}$$

Here, A_{ij} and B_{ij} are coefficients which can be calculated by the formulas given by Appendix 1.

Due to the introduction of higher-order terms, waves generated with Stokes-fifth model exhibit a more obvious mean water level rise.

In OpenFOAM and waves2Foam, Stokes theory is a commonly employed model for wave generation in numerical simulations, and widely adopted to report the wave loads on various marine structure. However, fifth-order model is the model with the highest order in the engineering application attributing to the introduction of higher order terms remarkably increase the resource consumption of the calculations with limited improvement in accuracy.

Based on the Stokes wave theory, a Matlab code is developed to provide theoretical predictions of wave profiles, serving as a theoretical reference for this study. The expression of wave-induced free-surface elevation η, velocity potential ϕ as well as the other parameters in the expression of these two physical elements all follow the theory discussed above.

3.2 Wave-current coupling

To clarify the theoretical foundation of describing wave-current coupling based on Stokes wave theory, the definition and physical meanings of c, u_E, u_S and $\overline{U}$ needs to be further discussed. Although these parameters are closely related, they represent distinct physical meanings.

The phase velocity c can be considered as the speed of the wave shape, answering the question of how fast the wave profile travels through the space. This physical quantity provides an intuitive visualization of the wave propagation speed. In linear wave theory, $c = 0$ indicates that the wave shape does not advance over time; for an observer in a stationary frame, the waves fluctuate but the crests and trough remain fixed in position.

The Euler velocity u_E describes the instantaneous horizontal velocity of different fluids particles, passing trough a fixed spatial point, at a designated location. This parameter is observed in a stationary coordinate system, focusing on a specific point within the field. The value of u_E fluctuates over time in both linear and nonlinear cases, which attributed to the motion of fluid particles exist in both cases. In linear waves, the motion forms a closed ellipse, so the time-average of Euler velocity u_E is 0, $\overline{u_E} = 0$, suggesting that particles only move periodically under the free-surface without propagation over time. Under nonlinear conditions, the particle trajectories are no longer closed ellipses, however, the time average of Euler speed $\overline{u_E}$ still remains zero, $\overline{u_E} = 0$.

The parameter u_S is also observed in a stationary coordinate. Unlike the definition of Euler

velocity u_E, this parameter focusing on the velocity of one designated fluid particle yet not the velocity on a fixed point. The value of u_S also oscillates over time as the motion of fluid particle and remains nonzero in both linear and nonlinear cases. However, under linear conditions, the time average of u_S, $\overline{u_S}$, remains 0 over one wave period, whereas in nonlinear conditions $\overline{u_S} \neq 0$. This also well agrees with the physical observation that due to the influence of non-linearity, stokes drift exist in the field leading to the propagation of fluid particles.

The mean velocity $\overline{U}$ represents the mean horizontal flow observed in a wave-following reference frame. It is obtained by performing a spatial average over one wavelength at a fixed elevation, rather than by tracking the motion of an individual fluid particle. Therefore, $\overline{U}$ should be interpreted as a coordinate-induced mean flow associated with the steady wave description, rather than a Lagrangian drift velocity.

In the absence of background current, $\overline{U}$ arises from the transformation between the stationary and wave-following reference frames and does not correspond to the Stokes drift. When a background current with velocity U_C exist, the Eulerian mean velocity in the stationary frame becomes non-zero, while $\overline{U}$ continues to represent the mean flow in the wave-following frame. The Stokes drift u_S, which characterizes the Lagrangian mean transport of fluid particles induced by nonlinear wave motion, is treated as a separate quantity and is not directly induced in the definition of $\overline{U}$.

Under linear conditions, the following relationships exist.

$$u_E \neq 0, \ \overline{u_E} = 0 \tag{3-18}$$
$$u_S \neq 0, \ \overline{u_S} = 0 \tag{3-19}$$
$$\overline{U} = 0 \tag{3-20}$$
$$c = \overline{u_E} + \overline{U} = 0 \tag{3-21}$$

As shown above, in linear condition $c = 0$, which consistent with the result that waves only fluctuate but do not propagate over time, and the motion of fluid particles follows a close ellipse-shape orbit.

However, under nonlinear condition, the relationships given in Eq. (3-18), Eq. (3-19), Eq. (3-20) and Eq. (3-21) change into:

$$u_E \neq 0, \ \overline{u_E} = 0 \tag{3-22}$$
$$u_S \neq 0, \ \overline{u_S} \neq 0 \tag{3-23}$$
$$\overline{U} \neq 0 \tag{3-24}$$
$$c = \overline{u_E} + \overline{U} \tag{3-25}$$

The physical meaning of equations listed above also consistent with realistic physical observations:

in nonlinear conditions, the presence of non-linearity induces horizontal propagation not only of the wave profile but also of the fluid particles within the flow field. Noting that, Eq. (3-25) represents a kinematic relation between the stationary and wave-following reference frames rather than a decomposition of fluid particle velocities.

When as background current with a speed of U_C is introduced to the fluid field, the relationship between c, u_E, u_S, $\overline{U}$ and U_C can be described as:

$$u_E \neq 0, \ \overline{u_E} = U_C \tag{3-26}$$

$$u_S \neq 0, \ \overline{u_S}' = \overline{u_S} + U_C \tag{3-27}$$

$$\overline{U} \neq 0 \tag{3-28}$$

$$c' = \overline{u_E} + \overline{U} = U_C + \overline{U} = c + U_C \tag{3-29}$$

Here, $\overline{u_E}$ and $\overline{u_S}$ respectively denote the time-average of Euler velocity and Stokes drift of the nonlinear wave in the absence of current. c represents the phase velocity of the nonlinear wave, whereas $\overline{u_S}'$ and c' represents the variables under wave-current conditions.

The wave-current coupling phenomenon can be reproduced by substituting Eq. (3-29) into the expressions of the wave-induced free-surface elevation and velocity potential in Stokes theory, as given in Eq. (3-16) and Eq. (3-17). Notice that the Doppler effect has already been considered in the process of modifying the expression of phase velocity.

Similarly, by implementing the same process on the Matlab code introduced in Chapter 3.1, the code can also be used to predict theoretical values of waves under wave-current coupling conditions.

3.3 Relaxation zone

In CFD toolboxes, there are few methods for wave generation, the commonly used ones are: boundary-condition wave generation; wave paddle (moving-boundary) generation; source-term wave generation and relaxation-zone wave generation. The waves2Foam adopted relaxation-zone wave generation method to reproduce both linear and nonlinear wave in the NWT.

The relaxation-zone wave generation method is a special form of source-term wave generation. The fundamental concept of this method is to smoothly blend the analytical wave solution with the numerical solution of the Navier-Stokes equations within a specified spatial region, known as relaxation zone, using a weighting function. In waves2Foam, relaxation zones are defined both near the wave-making boundary and wave-absorbing boundary, where the flow filed gradually transitions from the theoretical solution to the numerical one. Due to these efforts, the wave reflection and

numerical instability can be effectively suppressed, stabilizing the wave generation as well as wave propagation in the viscous-NWT.

Within the relaxation zone, physical elements are expressed as the weighted average of analytical and numerical solutions, the equation of which is as follows:

$$\Phi = \chi(x)\Phi_{theory} + [1 - \chi(x)]\Phi_{numrical} \tag{3-30}$$

In Eq. (3-30), Φ denotes a physical parameter of any kind such as velocity, pressure or free-surface elevation in the fluid filed, while Φ_{theory} and $\Phi_{numrical}$ is its corresponding theoretical value and numerical solution. $\chi(x)$ is a spatially varying weighting function, usually defined as a smooth function ranging from 0 to 1, such as cosine or exponential forms. Within the wave-making relaxation zone, the value of the function gradually rises from 0 to 1, enabling the numerical solutions approach the theoretical values. Whereas this process is reverse in the wave-absorption relaxation zone that the value of weighting function gradually decreases to 0, preventing the reflection wave from entering the calculation domain. A typical cosine-type weighting function being commonly used in waves2Foam is defined as:

$$\chi(x) = \frac{1}{2}\left[1 - \cos\left(\pi\frac{x - x_0}{L_{relax}}\right)\right] \tag{3-31}$$

Here, L_{relax} represents the length of the relaxation zone and x_0 represent the x-coordinate of the beginning boundary of the relaxation zone. Moreover, at both boundaries of the relaxation zone, this function ensures that the first-order derivative of $\chi(x)$ equals 0, thereby eliminating discontinuities in the velocity and pressure gradients and leading to a smooth transmission of wave energy on the interface between relaxation zone and calculation domain.

In terms of applying relaxation-zone wave generation to generate Stokes nonlinear waves, Φ represents physical elements of waves such as wave-induced free-surface elevation or velocity. In the inlet relaxation zone, the value of weighting function $\chi(x)$ gradually rise from 0 to 1, indicating that the fluid filed is progressively guided to the theoretical wave field condition. Where as in the outlet boundary, the weighting function $\chi(x)$ gradually drops to 0, enabling the physical parameters of the wave, for example wave-induce free-surface elevation, approaches to numerical solution. In this process, the waves in the region are absorbed to prevent the wave reflection and maintain the numerical stability in the calculation domain. Moreover, in order to avoid flow fluctuation caused by the sudden imposition of the wave field soon after the launching of simulation, waves2Foam also

introduced $f(t)$, a function to progressively generate in the field. The definition of which is commonly given by:

$$f(t) = \sin\left(\frac{\pi t}{2T_{soft}}\right), \quad t \le T_{soft} \tag{3-32}$$

Here, T_{soft} is the soft-start time defined by users, often being defined as 2 times of wave period. The involvement of this concept further improves the numerical stability of the simulation. Therefore, in waves2Foam, the formula of Stokes wave theory with the introduction of $f(t)$ can written as:

$$\eta(x,t) = d + f(t)\left\{\frac{1}{k}\sum_{i=1}^{5}\varepsilon^i\sum_{j=1}^{j}B_{ij}\cos[jk(x-ct)]\right\} \tag{3-33}$$

$$\phi(x,z,t) = f(t)\{(c-\overline{U})x + [\tanh(kd)]^{\frac{1}{2}}\left(\frac{g}{k^3}\right)^{\frac{1}{2}}\sum_{i=1}^{5}\varepsilon^i\sum_{j=1}^{j}A_{ij}\cosh(jkz)\sin[jk(x-ct)]\Bigg\} \tag{3-34}$$

3.4 Development of stokesSecondwCurrent model

The Stokes nonlinear wave theory is adopted for wave generation in OpenFOAM and waves2Foam. In the source codes of these toolboxes, however, the original theoretical expressions of free-surface elevation and velocity potential in the theory are complicated and thus simplified to reduce the computational resource consumption, improving the convergence and stability of the numerical simulation. The modified formulas of η and ϕ in the Stokes theory are as follows:

$$\eta(x,t) = d + f(t)\left[\frac{1}{k}\sum_{i=1}^{5}\varepsilon^i\sum_{j=1}^{j}B_{ij}\cos(j\theta)\right] \tag{3-35}$$

$$u_x = f(t)\left[c-\overline{U}+k[\tanh(kd)]^{\frac{1}{2}}\left(\frac{g}{k^3}\right)^{\frac{1}{2}}\sum_{i=1}^{5}\varepsilon^i\sum_{j=1}^{j}A_{ij}\cosh(jkz)\cos(j\theta)\right] \tag{3-36}$$

$$u_z = f(t)\left\{k[\tanh(kd)]^{\frac{1}{2}}\left(\frac{g}{k^3}\right)^{\frac{1}{2}}\sum_{i=1}^{5}\varepsilon^i\sum_{j=1}^{j}A_{ij}\sinh(jkz)\sin(j\theta)\right\} \tag{3-37}$$

In these equations, the expression of phase speed c is simplified, and θ is a parameter. The expression of them are:

$$c = \frac{\omega}{k} \tag{3-38}$$

$$\theta = kx - \omega t + \varphi \tag{3-39}$$

In this equation, ω is the angular frequency of wave, which can be obtain through $\omega = 2\pi f$

where f denotes the wave frequency; while φ is the initial phase of the target wave.

As demonstrated in Eq. (3-36) and Eq. (3-37), in waves2Foam, in stead of calculating the velocity potential, the velocity in each directions are directly calculated. Also, this toolbox neglected the complicate calculation of phase velocity c, which significantly improves the robustness and efficiency of the simulation. Moreover, the parameter θ is introduced to simply the phase term inside the cosine function in the equation of wave-induced free-surface elevation, the phase term inside the cosine function of u_x and the phase term inside the sine function of u_z.

Under the condition where background current exist, the expression of parameter θ needs to be further modified to include the Doppler effect. Thus, the modified θ is defined as:

$$\theta = kx + (U_C k - \omega t) + \varphi \tag{3-40}$$

By plugging the modified expression to Eq. (3-35), Eq. (3-36) and Eq. (3-37), the equations of Stokes theory for wave-current coupling within the framework are obtained. On the basis of that, the stokesSecondwCurrent model is programmed by C++.

3.5 Development of overWaveDyMFoam solver

From the above mentioned discussion, conclusion can be made that the fundamental of waves2Foam is the introduction of relaxation zone into the OpenFOAM. While in the framework of OpenFOAM, there are viscous solvers with overset mesh capability for simulating the motion of floating bodies. Among which, a solver called overInterDyMFoam, being developed on the basis of a classic viscous solver known as interFoam for multi-phase flow simulation by Bruinsma.N .et.al in 2017, is a commonly used application for the analysis of 6DOF dynamic response of a floating body in overset meshes.[32] Therefore, by modifying the mathematical expressions of physical quantities such as pressure and velocity vector in the relaxation zone, a weighting function is incorporated in these formulas within the region, through which the concept of relaxation zone is introduced into the source code of overInterDyMFoam. After the compilation, a solver called overWaveDyMFoam is then developed in the framework of waves2Foam for analyzing the 6DOF motion of floating bodies under the overset meshes.

4 Numerical water tank and wave conditions

4.1 2D viscous numerical water tank

In this study,a 2D viscous numerical water tank (viscous NWT) is established in the framework of OpenFOAM, parameters of which is shown in Figure 4.1. In this graph, λ represents wave length and the scale of the viscous NWT is defined by the wave parameters. The velocity and volume fractions of wave incidence are prescribe in the inlet relaxation zone, the length of which is two wavelengths. At the inlet boundary, the pressure and velocity are specified with zeroGradient condition which means no variation of the variable in the normal direction at the boundary. The boundary conditions of outlet boundary are set to be consistent with those at the inlet boundary, and an outlet relaxation zone with a length of two wavelengths is also applied. At the bottom boundary, the pressure condition is set to the zeroGradient type, the velocity condition, however, is specified as fixedValue with a value of zero. In this case, the bottom is treated as a no-slip wall. At the top boundary, totalPressure boundary condition specifies a fixed total pressure, allowing the static pressure at the boundary to vary with the local flow velocity according to Bernoulli's principle, while the velocity condition is defined as zeroGradient. Front and back boundary are specified to be empty since this viscous NWT is two dimensional.

Quadrilateral structured meshes are adopted throughout the entire computational domain in all 2D simulations, a typical mesh configuration is given by Figure 4.2 and Figure 4.3. In order to effectively allocate the computational resources and reduce the overall simulation cost, the vertical size of cell is progressively reduced from the bottom of water tank and top of the air layer toward the free-surface. For the same purpose, the grid in x-direction is uniformly distributed within both the inlet relaxation zone and computational domain. Whereas starting from the let boundary of the outlet relaxation zone, corresponding to a location approximately 100 m downstream of the inlet boundary, the density of mesh in x-direction smoothly drops and the size of cell in that direction gradually expands. This mesh layout also applies a numerical damping to the waves within the outlet relaxation zone, further preventing the wave reflection reflection at the outlet boundary. Moreover the mesh is gradually refined towards the free-surface, reaching the finest resolution within a region extending two wave heights above and below the free-surface, aiming to precisely capture wave deformation and free-surface motion. Since the mesh is 2D, only one mesh is specified in y-direction.

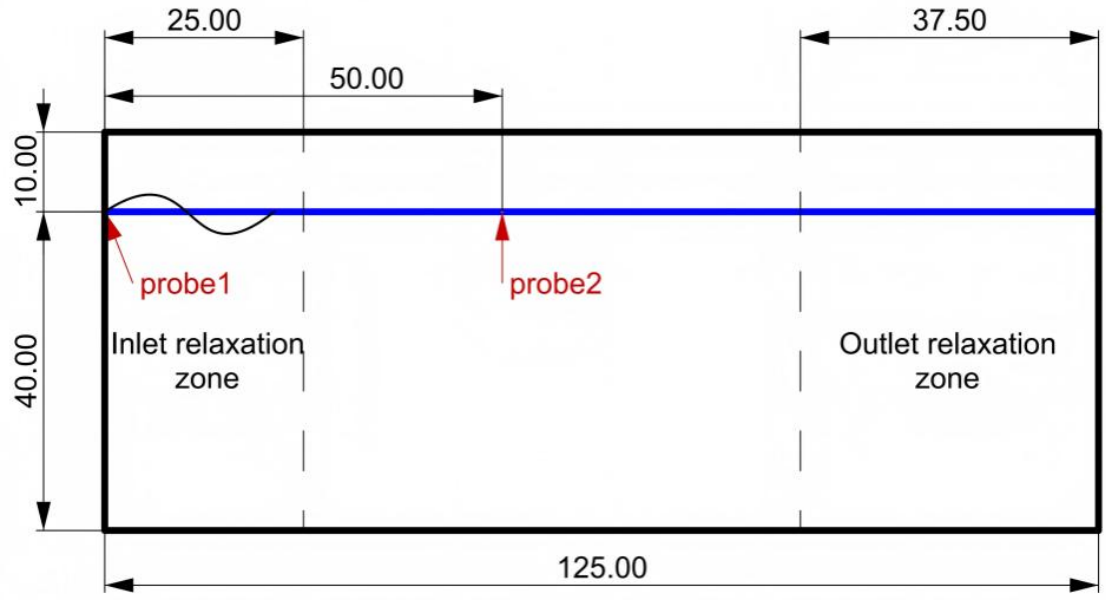

[Figure 4.1] The definition of 2D viscous-NWT

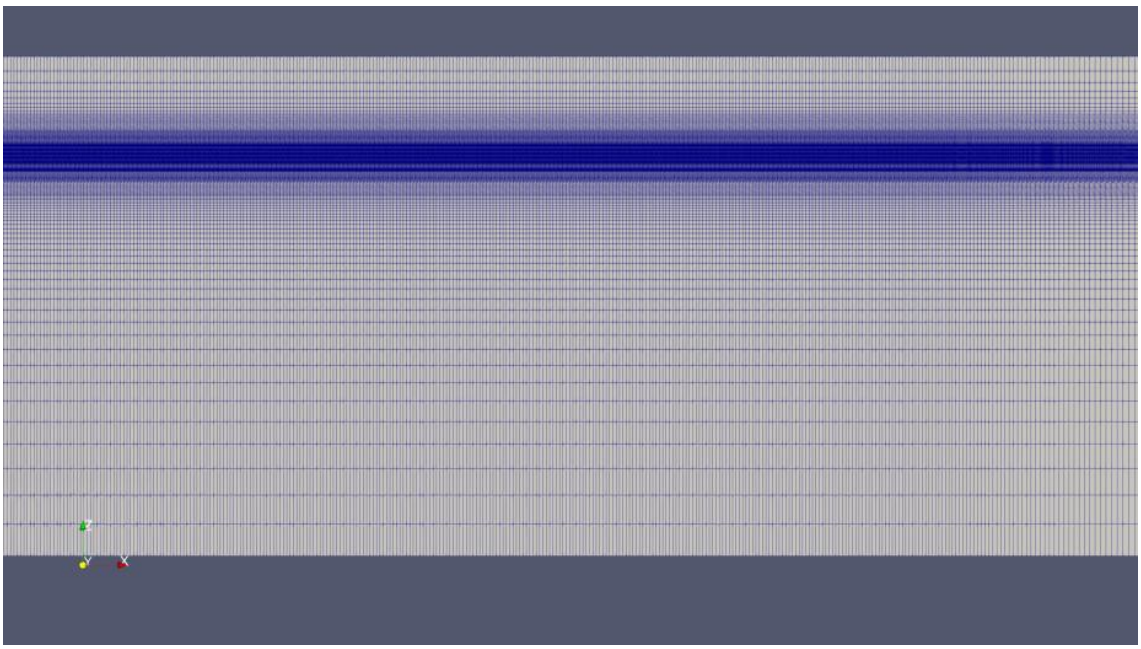

[Figure 4.2] A representative mesh configuration for 2D cases

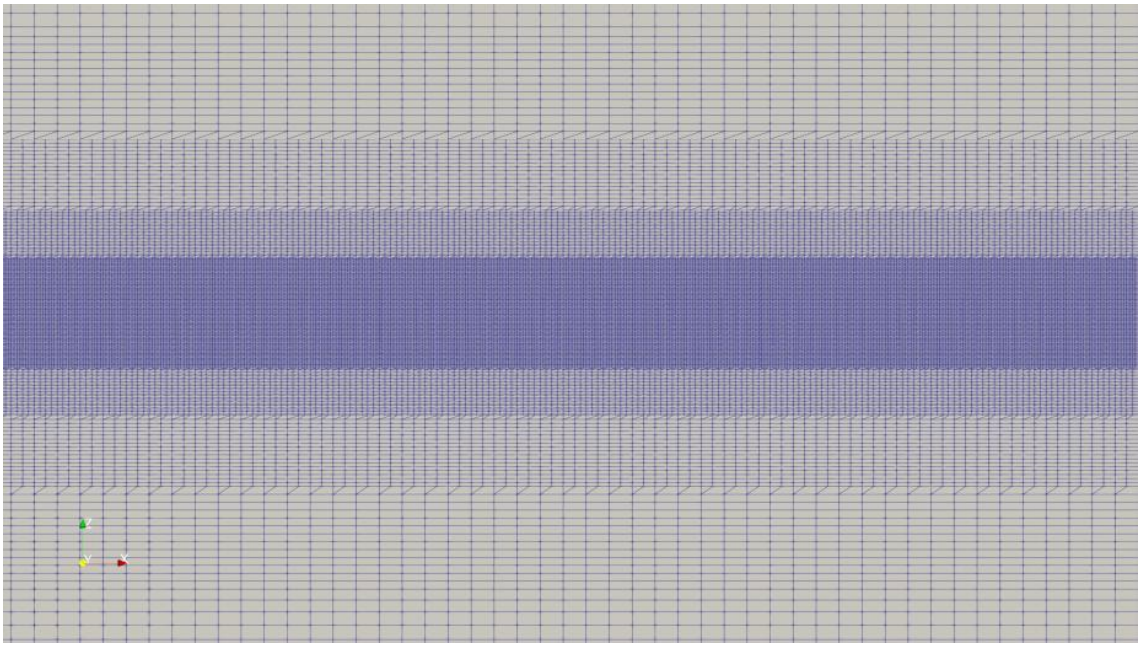

[Figure 4.3] A representative mesh configuration for 2D cases (partially enlarged view)

Professor Milovan Perić suggests that in order to precisely generate nonlinear wave within a NWT, 10 to 20 cells are necessary within one wave height in his paper.[33] Professor Mostafa Amini-Afshar proposes that aiming to accurately reproduce the velocity potential and pressure of an nonlinear wave in OpenFOAM, 200 cells should be specified in one wave length and the mesh density in this direction should be improved with the increase of the wave steepness. Otherwise, the accumulation of error eventually leads to the premature wave breaking, severe numerical wave damping or even non-physical free-surface breaking.[34] With reference to these previous studies, in this research the size of the cell is relatively determined according to the wave length and wave height of the target wave. The size of grid in each might be calculated as follows:

$$\frac{\lambda}{N_x} = \Delta_x \tag{4-1}$$

$$\frac{H}{N_z} = \Delta_z \tag{4-2}$$

Here, N_x and N_z respectively represent the number of cells in one wave length and one wave height, while Δ_x and Δ_z denote the absolute grid size in the corresponding directions. According to the number of cells in each direction, the meshes are categorized into four different levels, which are detailed in table 4.1. It should be noted that the absolute cell size and cell number in the table refer to the grids located near the free-surface, in other word, in the region with the highest mesh density, while the size of background meshes are calculated based on the absolute mesh size listed out in the

table. This mesh definition is applied to all the 2D simulations on both wave generation and wave-current reproduction in this paper.

[Table 4.1] The definition of 2D mesh levels

2D Mesh level	N_x	N_z
Coarse 2D	200	20
Medium 2D	250	25
Fine 2D	300	30
VeryFine 2D	350	35
ExtremeFine 2D	450	45

4.2 3D numerical water tank

On the basis of the 2D viscous NWT, the 3D viscous NWT is established in OpenFOAM. Length of water tank, water depth, air layer thickness as well as distribution of relaxation zone and calculation are all consistent with the 2D case. The length of the viscous numerical wave tank (NWT) in this direction is set to half the wavelength of the target wave. Moreover, the definitions of boundary conditions are also in agreement with the 2D tank, except for the front and back boundary - being set as symmetry.

In this research, 3D meshes are generated on the basis of 2D meshes. 2D simulations are initially conducted to study the feasibility of multiple models for wave generation or wave-current coupling reproduction. 3D calculations is subsequently implemented to further study the performance and generality of these solvers. In terms of 3D cases, a 2D mesh is selected and then expanded in the third direction, y-direction, to produce 3D grids with different levels. A typical layout of the 3D mesh is as shown in Figure 4.4 and Figure 4.5. Similar to the 2D meshes, the cell size in the y-direction is also determined according to the wave parameters and the absolute size of grid in the third direction can be evaluated by:

$$\frac{\lambda}{N_y} = \Delta_y \tag{4-3}$$

Here, N_y represents the number of cells in one wavelength and one wave height, and Δ_y denote the absolute grid size in the y-direction. In this direction, meshes are evenly distributed, while the refinement of the mesh in the x-direction and z-direction is consistent with that of the 2D case. The

definition of the 3D meshes is detailed in Table 4.2. Note that the table only defines the mesh configuration in the third direction, and the definition of the meshes in the other two directions depend on the 2D mesh used as the basis for the 3D extension in this study. The settings in the table are also applied to all the 3D simulations of this paper.

[Table 4.2] The definition of 3D mesh levels

3D Mesh level	N_y
Coarse 3D	80
Medium 3D	120
Fine 3D	160

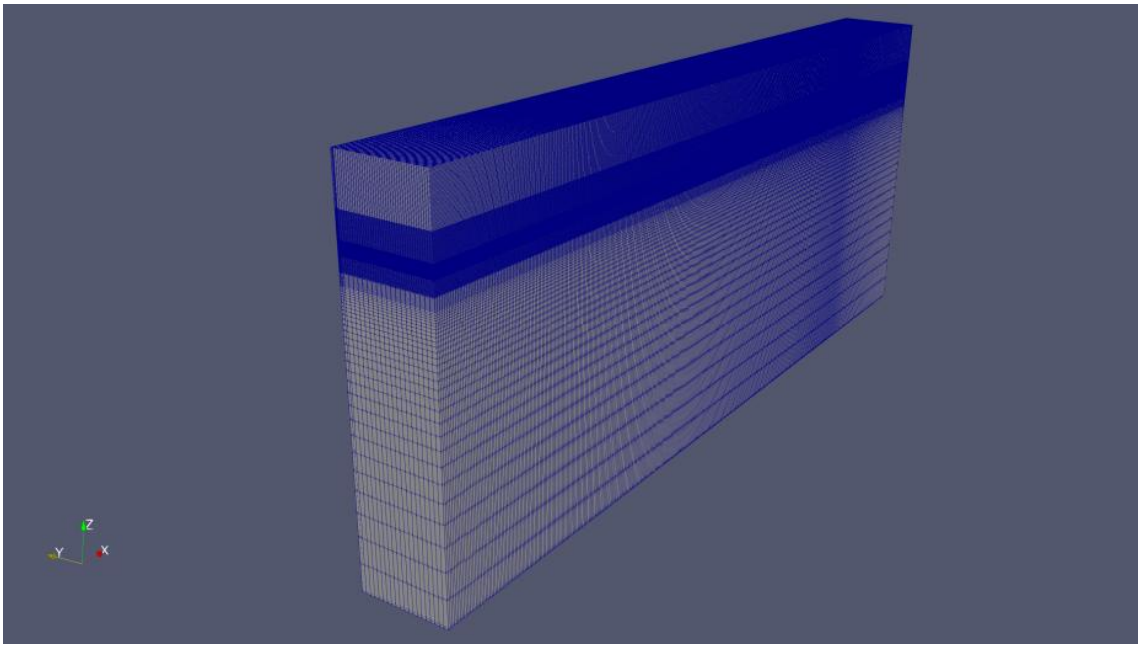

[Figure 4.4] A representative mesh configuration for 3D cases

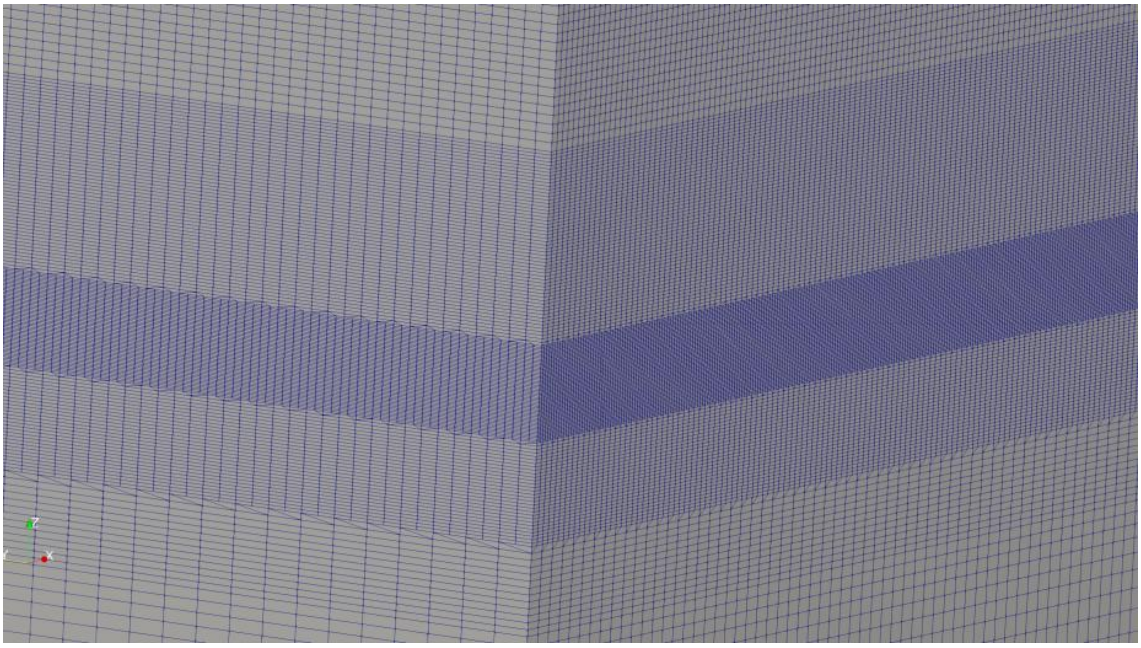

[Figure 4.5] A representative mesh configuration for 3D cases (partially enlarged view)

4.3 Wave conditions

This research studies several wave models including stokesSecond of OpenFOAM, stokesFifth of OpenFOAM as well as the their corresponding implementations in the framework of waves2Foam. These models are utilized to reproduce the same wave with meshes of different density to investigate the accuracy and performance of each solver. A reference wave is determined with a steepness ε of 0.04, wavelength λ of 12.5 m, wave height H 0.5 m and wave period T of 2.8295 s. On the basis of that, several additional wave cases are determined by modifying the wave height. The detailed wave parameters and their respective serial numbers are summarized in Table 4.3. Note that in all cases, the water depth d is fixed to be 40 m, and these waves can be considered as deep water waves. Moreover, in the wave-current coupling cases, the parameters listed in the table are original value without considering the Doppler effect.

This study also develops a wave-current coupling solver, stokesSecondwCurrent, to assess the accuracy of wave-current coupling reproduction of OpenFOAM and waves2Foam. Accordingly, multiple wave-current conditions are also proposed on the basis of the reference wave. By combining the reference wave listed in Table 4.3 with a current with a velocity of 0.6 m/s, a reference wave-current case is defined. Subsequently, more conditions are devised to further investigate the performance and generality of stokesSecondwCurrent model. The parameters of these conditions are

also detailed in Table 4.3.

[Table 4.3] The definition of wave conditions

Wave condition number	Water depth d (m)	Wave period T (s)	Wave height H (m)	Wave amplitude a (m)	Wave length λ (m)	Wave steepness ε	Current velocity U_C (m/s)
W0			0.5000	0.2500		1/25	0.0000
W16			0.7813	0.3906		1/16	0.0000
W10			1.2500	0.6250		1/10	0.0000
WC0			0.5000	0.2500		1/25	+0.6000
WC16	40	2.8295	0.7813	0.3906	12.5	1/16	+0.6000
WC10			1.2500	0.6250		1/10	+0.6000
WC+1.1			0.5000	0.2500		1/25	+1.1000
WC+2.2			0.5000	0.2500		1/25	+2.2000
WC-0.6			0.5000	0.2500		1/25	-0.6000

4.4 Computational environment and setting

All simulations in this study were conducted on the Genkai supercomputer, operated by the Research Institute for Information Technology (RIIT) of Kyushu University. Genkai represents the latest generation of high-performance computing (HPC) systems at the university, designed to provide computational support for large-scale numerical simulations, data-intensive computing, and artificial-intelligence-related research across various academic disciplines. The system consists of 3 node groups, interconnected via an InfiniBand NDR (400 Gbps) high-speed network. It is equipped with 32 racks and 1024 compute nodes, achieving a peak double-precision performance of approximately 7.76 PFLOPS (CPU) and 5.63 PFLOPS (GPU), with a total mixed-precision (FP16/BF16) capability exceeding 166 PFLOPS. The entire system adopts liquid cooling and is supported by dual shared storage systems, one high-capacity and one high-speed parallel file system, to ensure efficient I/O operations for massive datasets.

In this study, in order to evaluate the efficiency of different wave models under various meshes configurations, all simulations, unless otherwise stated, are implemented using identical computational settings of 5 nodes with 48 threads per node.

5 Wave generation

5.1 Feasibility study of wave generation by different toolboxes

In this section the feasibility of wave generation of both OpenFOAM and waves2Foam is investigated, and the accuracy of several wave models of these toolboxes are studied. By utilizing these wave theories, on the basis of meshes with different density, an identified wave is reproduced in the viscous NWT. The numerical results of these simulations are compared with the theoretical values given by a Matlab code which follows the wave theory, above mentioned in chapter 3.1, proposed by John D. Fenton in his paper. The accuracy of various wave models is subsequently discussed to identify the most precise and robust theory for wave generation applied for the the following sections of this research.

5.1.1 Wave generation by OpenFOAM

In this part wave models stokesII and stokesV of OpenFOAM are used to generate the wave case labeled with W0 in the Coarse 2D, Medium 2D, Fine 2D and VeryFine 2D meshes. Specifically, this wave is respectively generated by two models in four meshes and the physical time of these cases is 120 s. Moreover, two wave gauges are positioned at the inlet boundary and 50 m down stream from inlet boundary to capture the wave height and wave period. The results obtained from these probes are summarized and compared with theoretical predictions as part of the verification study of this section, and are discussed in detail in order to assess the performance of different wave models.

Simulations are conducted in the framework of OpenFOAM, and the results of these cases are detailed in Table 5.1, the wave profile of these cases as well as theoretical prediction are illustrated in Figure 5.1 and Figure 5.1, the visualized NWT of “VeryFine 2D stokesV W0” case is shown by Figure 5.3, and the results about accuracy of these cases are detailed in Table 5.1. In the table, the error of wave height at the location of two probes, calculation time, mesh level and the corresponding wave models are provided.

[Table 5.1] The calculation results given by

[Table 5.2] The calculation results given by

stokesII in OpenFOAM under 2D W0 condition

Mesh level	Time consumption	Error on wave height (x=50)
Coarse 2D	3h 39mins	-41.5397%
Medium 2D	4h 48mins	-35.8964%
Fine 2D	5h 55mins	-29.2875%
VeryFine 2D	7h 13mins	-23.2546%

stokesV in OpenFOAM under 2D W0 condition

Mesh level	Time consumption	Error on wave height (x=50)
Coarse 2D	3h 29mins	-42.8628%
Medium 2D	4h 35mins	-36.9726%
Fine 2D	5h 43mins	-30.4001%
VeryFine 2D	6h 51mins	-24.4289%

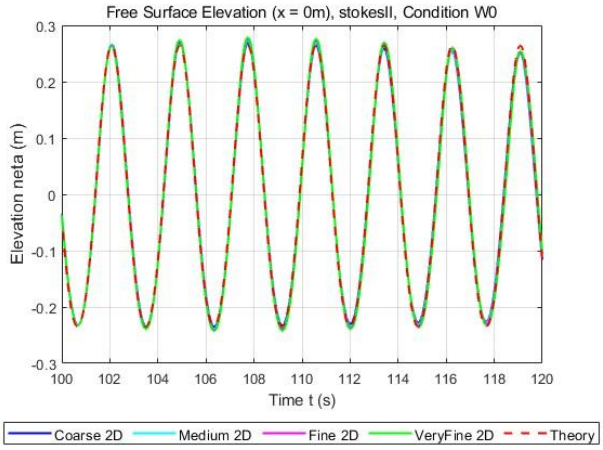

(a) The wave height at the inlet boundary

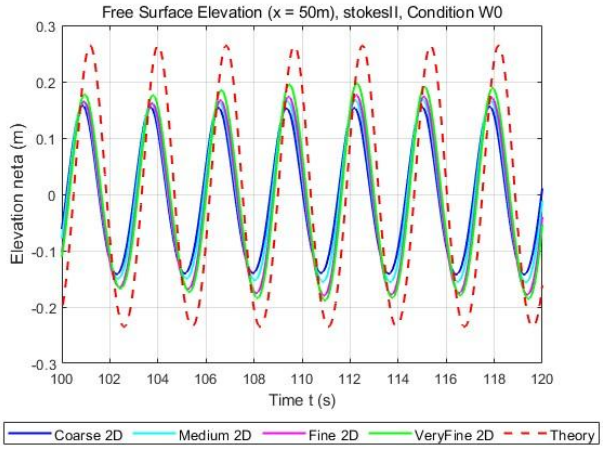

(b) The wave height at the location 50 m downstream from the inlet boundary

[Figure 5.1] The comparison on wave height between numerical results given by stokesII in OpenFOAM and theoretical values under W0 condition

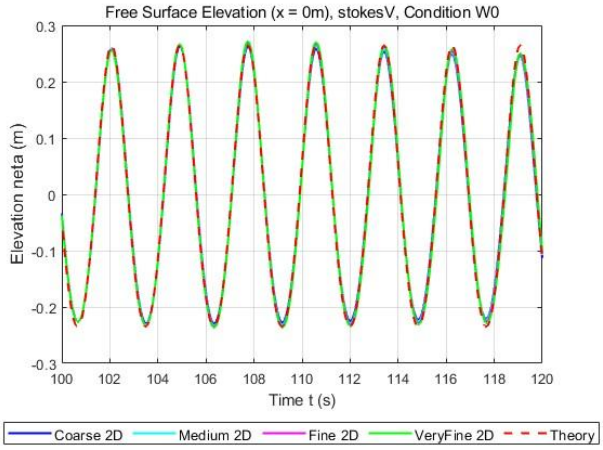

(a) The wave height at the inlet boundary

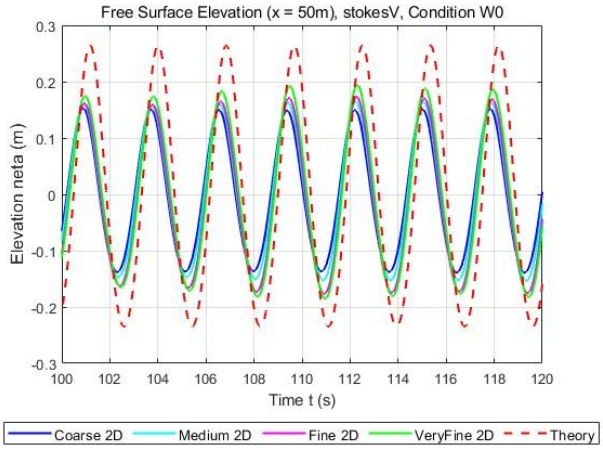

(b) The wave height at the location 50 m downstream from the inlet boundary

[Figure 5.2] The comparison on wave height between numerical results given by stokesV in OpenFOAM and theoretical values under W0 condition

(a) The wave-induced free-surface deformation in the viscous-NWT

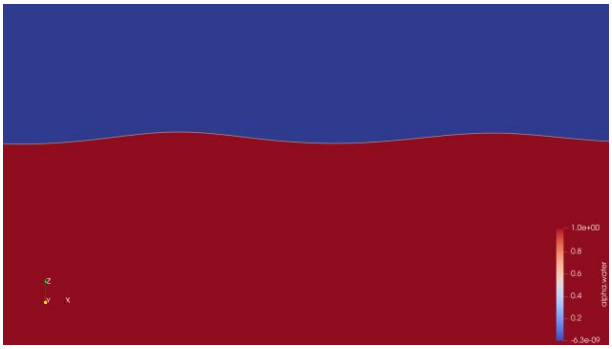

(b) The wave-induced free-surface deformation in the viscous-NWT (partially enlarged view)

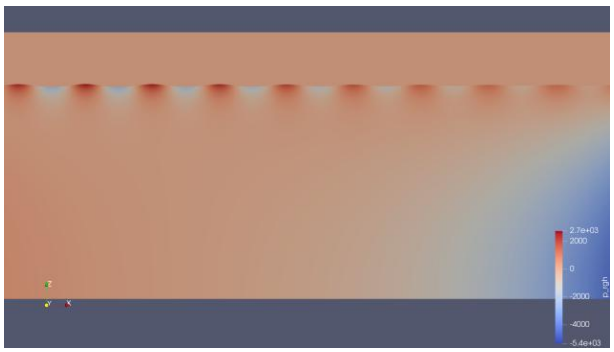

(c) The pressure distribution in the viscous-NWT

(d) The velocity contour of the case

[Figure 5.3] The visualized viscous-NWT of the “VeryFine 2D stokesV W0” case

According to Figure 5.1 and Figure 5.2, the numerical predictions about wave induced free-surface elevation given by both stokesII and stokesV model in OpenFOAM agree well with theoretical values at the inlet boundary, demonstrating the validity of these wave models. However, as shown in Figure 5.1 (b) and Figure 5.2 (b), waves generated by these models significantly damp at the location 50 m downstream from the inlet boundary. At that location, no abnormal fluctuation on wave period is observed, however, the wave height is remarkably underestimated, and the numerical error on wave height in these cases varies from −23.2546% to −42.8628%, indicating that nonlinear wave can not be precisely generated merely by using wave models in OpenFOAM. On comparison to stokesV model, stokesII model shows a higher performance on numerical accuracy, but the computational efficiency of these two models are almost identical, as the simulation time required under the same mesh density is nearly the same. Moreover, as the mesh quality increases, the accuracy performance of both the Stokes II and Stokes V model improves, which is consistent with expectations.

In conclusion, the validity of stokesII and stokesV model is verify, whereas generating large nonlinear wave by these models is infeasible,due to the sever numerical wave damping appeared in the

viscous-NWT. Therefore, it is necessary to introduce the plug-in code of OpenFOAM - waves2Foam, into the simulation in ordering to accurately reproduce large nonlinear waves.

5.1.2 Wave generation by waves2Foam

In this part wave models stokesSecond and stokesFifth of waves2Foam, a plug-in code of OpenFOAM, are utilized to generate the wave W0 in four meshes with different density. The process of this section is consistent with that of the Section 5.1.1.

[Table 5.3] The calculation results given by stokesSecond in waves2Foam under 2D W0 condition

Mesh level	Time consumption	Error on wave height (x=50)
Coarse 2D	3h 08mins	-12.5699%
Medium 2D	3h 36mins	-8.8886%
Fine 2D	5h 00mins	-5.8290%
VeryFine 2D	5h 59mins	-4.9813%

[Table 5.4] The calculation results given by stokesFifth in waves2Foam under 2D W0 condition

Mesh level	Time consumption	Error on wave height (x=50)
Coarse 2D	2h 48mins	-7.7978%
Medium 2D	3h 15mins	-3.7948%
Fine 2D	5h 47mins	-1.5234%
VeryFine 2D	6h 58mins	-0.4971%

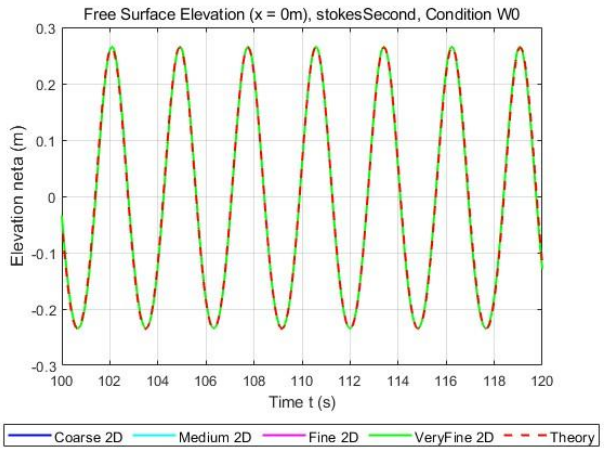

(a) The wave height at the inlet boundary

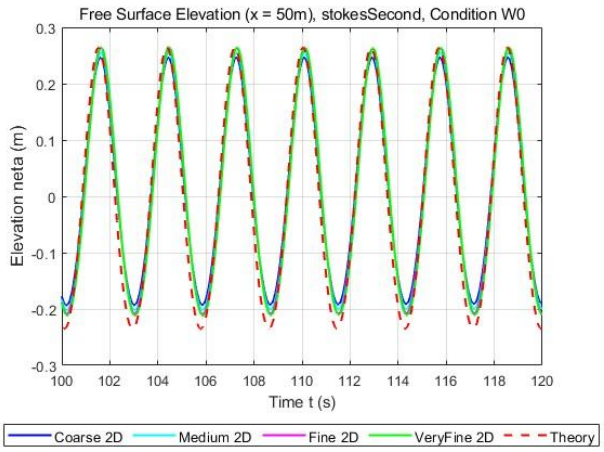

(b) The wave height at the location 50 m downstream from the inlet boundary

[Figure 5.4] The comparison on wave height between numerical results given by stokesSecond in waves2Foam and theoretical values under W0 condition

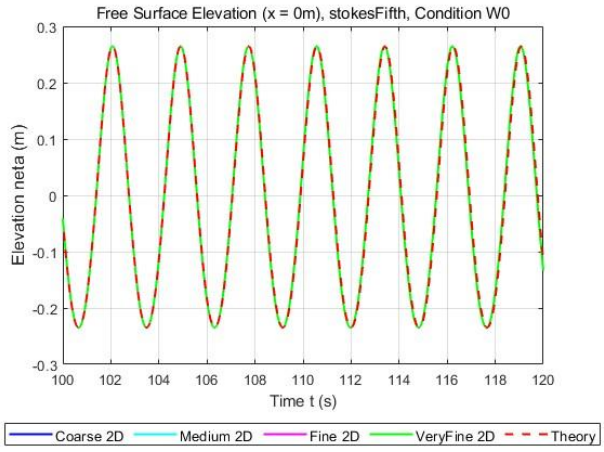

(a) The wave height at the inlet boundary

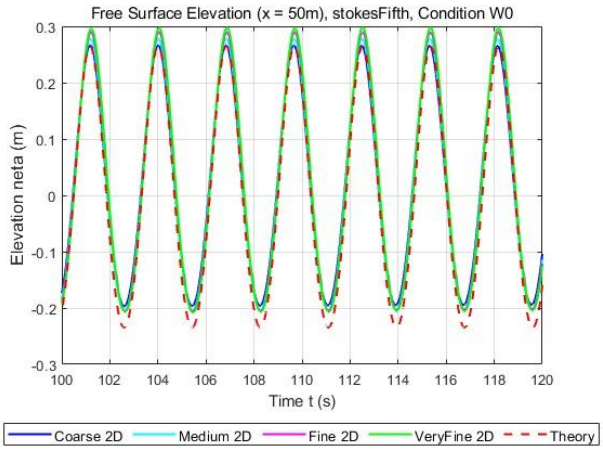

(b) The wave height at the location 50 m downstream from the inlet boundary

[Figure 5.5] The comparison on wave height between numerical results given by stokesFifth in waves2Foam and theoretical values under W0 condition

Simulations are conducted in the framework of waves2Foam for a physical time of 120 s, and the wave profile of these cases as well as theoretical prediction are illustrated in Figure 5.4 and Figure 5.5, the visualized NWT of "VeryFine 2D stokesFifth W0" case is shown by Figure 5.6, and the results about accuracy of these cases are detailed in Table 5.3 and Table 5.4. In the table, the error of wave height at the location of two wave gauges, calculation time, mesh level and the corresponding wave models are provided.

According to Figure 5.4 and Figure 5.5, both the stokesSecond and stokesFifth models in waves2Foam demonstrate the capability of precisely generating nonlinear wave and the visualized NWT in all simulations agree well with expected physical phenomena. The validity of these two models is confirmed by Figure 5.4 (a) and Figure 5.5 (a), where the computed free-surface elevations at the inlet boundary almost perfectly coincide with the theoretical predictions obtained from the MATLAB code mentioned above. However, at the location 50 m downstream from the inlet boundary, as shown in Figure 5.4 (b) and Figure 5.5 (b), wave damping is observed in all cases. The errors in wave elevation remain with in an controllable range and show a clear trend of decreasing with the increase of mesh quality. Moreover, in all the simulations, a mean water level rise is observed, which is consistent with the expectations of stokes nonlinear wave theory. These findings well confirm the feasibility of waves2Foam and its wave models, stokesSecond and stokesFifth, for nonlinear wave generation.

(a) The wave-induced free-surface deformation in the viscous-NWT

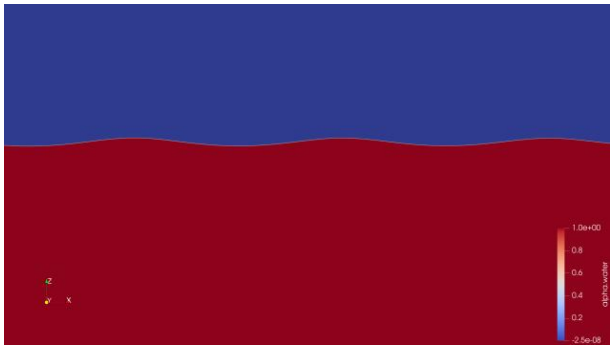

(b) The wave-induced free-surface deformation in the viscous-NWT (partially enlarged view)

(c) The pressure distribution in the viscous-NWT

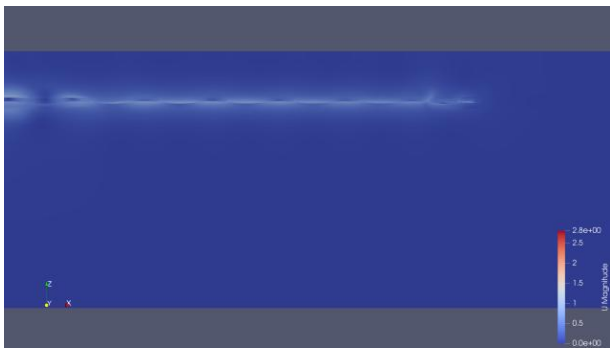

(d) The velocity contour of the case

[Figure 5.6] The visualized viscous-NWT of the "VeryFine 2D stokesFifth W0" case

Regarding the accuracy comparison between stokesSecond and stokesFifth model, the fifth-order model shows a higher potential for generating nonlinear wave precisely. In all simulations conducted with the stokesFifth model, the errors in wave height measured 50 m downstream from the inlet boundary are consistently smaller than those obtained from the stokesSecond model. The second-order wave model fails to accurately reproduce nonlinear wave in Coarse 2D, Medium 2D and Fine 2D meshes, as the errors of wave height are excessively large. The error is only reduced to under $\pm 5\%$ in VeryFine 2D mesh, yet the overall accuracy remains relatively low. In contrast, stokesFifth model shows higher precision even in the Coarse 2D as well as Medium 2D meshes, where the corresponding wave-elevation errors are -7.7978% and -3.7948% respectively. This model further provides more accurate results in the Fine 2D and VeryFine 2D meshes, with errors of -1.5234% and -0.4971%. Thus, conclusion can be obtained that the StokesFifth model in waves2Foam outperforms the stokesSecond model in terms of accuracy. This may be attributed to the absence of higher-order terms beyond the second order in the free-surface boundary equations, which leads to the lower accuracy of the second-order wave model compared with the fifth-order model.

It can be concluded that in ordering to accurately generate nonlinear wave, appropriate mesh density and stokesFifth model in waves2Foam is necessary are required. Specifically, to obtain highly accurate numerical predictions (wave-height error below ±2%) on nonlinear waves using fifth-order Stokes model, more than 300 cells and 30 cells are respectively required within one wave length and one wave height. Furthermore, the introduction of waves2Foam is recommended and thus in the rest part of this research, this plug-in code is adopted to generate nonlinear waves.

5.2 Performance test of the StokesFifth model in waves2Foam

In this section, the performance of the stokesFifth model in waves2Foam is evaluated, and potential methods for improving its accuracy are discussed. In the first place, this wave theory is applied to reproduce the reference waves in multiple 3D meshes to assess the applicability of this wave model in 3D simulations. The waves of varying steepness are subsequently generated based on a representative mesh as determined by the discussion about simulation results presented in chapter 5.1. Following a similar approach to the previous chapter, in this parts the computational results are compared with theoretical predictions to obtain the errors and assess the performance of stokesFifth model in waves2Foam under different wave circumstances. The theoretical values are also obtain using the Matlab code introduced in chapter 3.1.

5.2.1 Wave generation in 3D meshes

In this subsection, stokesFifth model in waves2Foam is utilized for 3D wave generation in ordering to verify the feasibility of the model in 3D cases. 3D meshes, as mentioned above, are created by expanding a specified 2D mesh, determined in the chapter 4.1, in y-direction with various mesh numbers.

Following this process, Coarse 3D, Medium 3D and Fine 3D meshes are proposed on the basis of criterion detailed in Table 5.5 for the analysis in this part. Similar to the study in the previous section, two wave gauges are placed at the inlet boundary and 50 m down stream from inlet boundary, positioned at the mid-span of the domain in the y-direction, to capture the wave height and wave period. The results of these probes are also compared against the theoretical prediction obtained from the Matlab code.

[Table 5.5] The calculation results given by stokesFifth in waves2Foam under 3D W0 condition

Mesh level	Time consumption	Error on wave height (x=50)
Coarse 3D	17h 54mins	+0.8941%
Medium 3D	19h 22mins	+0.7542%
Fine 3D	20h 37mins	+0.6057%

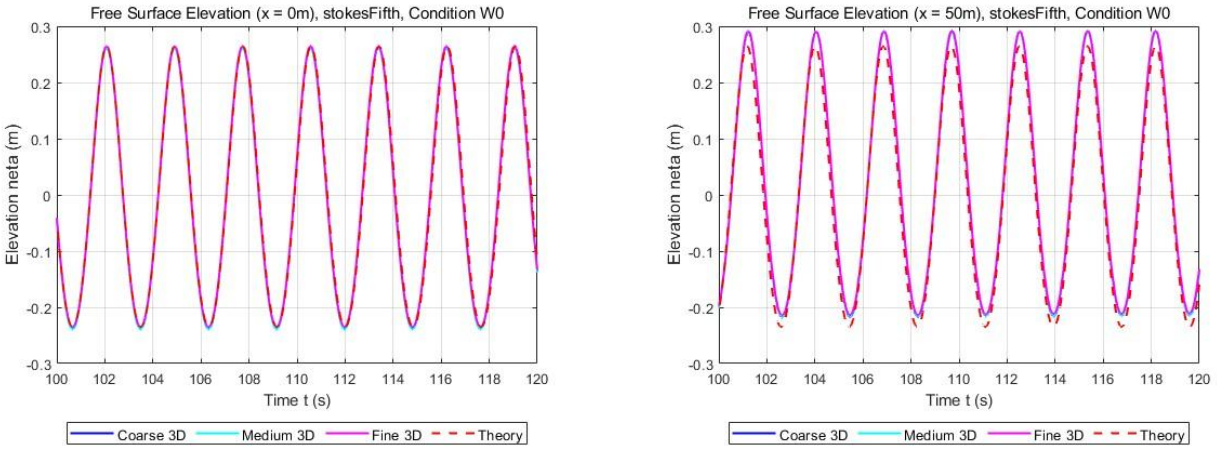

(a) The wave height at the inlet boundary

(b) The wave height at the location 50 m downstream from the inlet boundary

[Figure 5.7] The comparison on wave height between numerical results given by stokesFifth in waves2Foam and theoretical values under W0 condition (3D)

By using waves2Foam, 3D numerical analysis are implemented for a physical time of 120 s, and the wave profile of these cases are illustrated in Figure 5.7, the visualized NWT of "Fine 3D stokesFifth W0" case is shown by Figure 5.8, and the results of accuracy analysis are detailed in Table 5.3. In the table, the error of wave elevation at the location of two probes, calculation time, mesh level and the corresponding wave models are provided.

The results listed above demonstrate the feasibility and outstanding accuracy performance of stokesFifth model in waves2Foam for generating nonlinear wave under 3D conditions. As shown in Table 5.5 and Figure 5.7, the wave-elevation curves obtained from the numerical simulations almost perfectly overlap with the theoretical prediction at the inlet boundary, but deviates slightly from the theoretical curve at the location 50 m downstream, with maximum errors of +0.8941%, +0.7542% and +0.6057% for different mesh configurations. Apart from the well agreement in wave height, no fluctuation in period over time is captured in the simulations, confirming the stability of the stokesFifth

model. Furthermore, as illustrated in Figure 5.8, no unexpected free-surface breaking is observed in the viscous-NWT, and the distribution of pressure and velocity fields are well consistent with the expected physical behavior. These findings indicate that the numerical predictions obtained from the stokesFifth model are in excellent agreement with the theoretical values, precisely reproducing nonlinear waves behavior in 3D conditions.

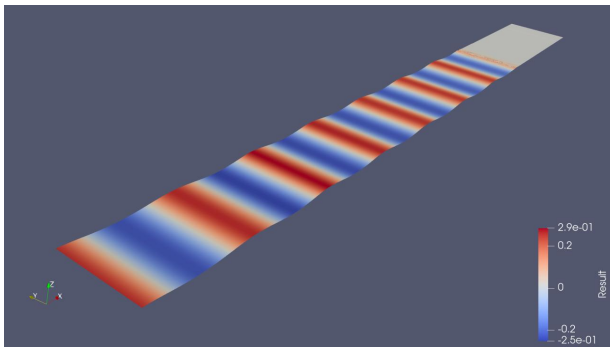

(a) The wave-induced free-surface deformation in the viscous-NWT

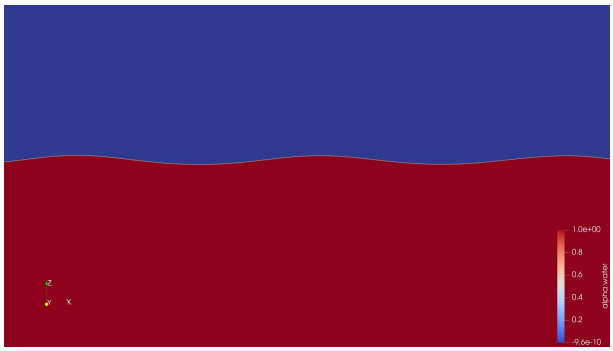

(b) The wave-induced free-surface deformation in the viscous-NWT (partially enlarged view)

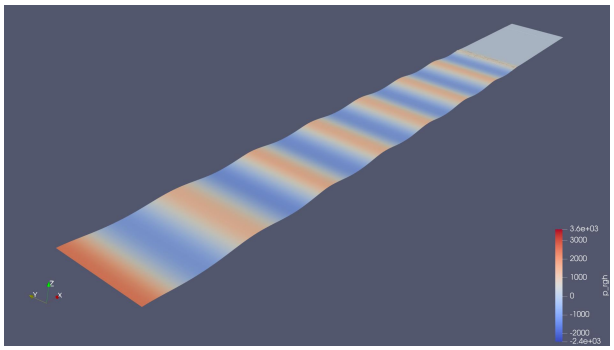

(c) The pressure distribution on the free-surface

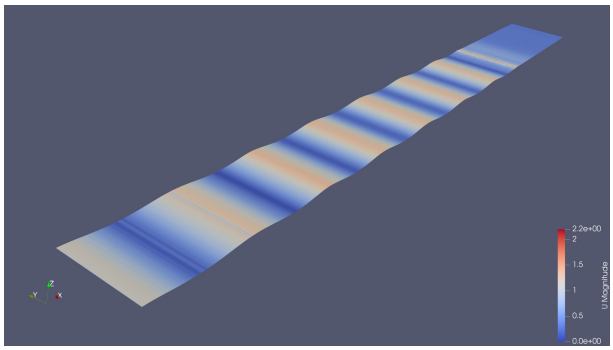

(d) The velocity contour on the free-surface

[Figure 5.8] The visualized viscous-NWT of the “Fine 3D stokesFifth W0” case

5.2.2 Wave generation with various wave parameters

In this part, the performance and generality of stokesFifth model in waves2Fom is assessed. Multiple waves with different steepness are generated based on VeryFine 2D mesh, identified in Section 5.1 which provides the most accurate numerical results. On the basis of this mesh, waves labeled with W16 and W10 are reproduced, and the accuracy of wave height are studied. To capture these data, two wave gauges are defined, and the setting of them are consistent with the setting in Section 5.1. Also, the result obtained by these probes are compared with the theoretical prediction obtained from the Matlab code.

By using waves2Foam, two simulations are conducted for a physical time of 120 s, and the wave profile of these cases are illustrated in Figure 5.9 and Figure 5.10, the visualized NWT of "VeryFine 2D stokesFifth W10" case is shown by Figure 5.11, and the results of accuracy analysis are detailed in Table 5.6 and Table 5.7. In the table, the error of wave height at the location of two wave gauges, calculation time and the corresponding wave condition are provided.

[Table 5.6] The calculation results given by stokesSecond in waves2Foam under 2D W16 conditions

Mesh level	Time consumption	Error on wave height (x=50)
VeryFine 2D	7h 05mins	-1.9203%
ExtremeFine 2D	9h 40mins	-0.4717%
VeryFine-Expanded RelaxationZone 2D	6h 41mins	-1.7718%

[Table 5.7] The calculation results given by stokesFifth in waves2Foam under 2D W10 condition

Mesh level	Time consumption	Error on wave height (x=50)
VeryFine 2D	9h 24mins	-9.6706%
ExtremeFine 2D	17h 47mins	-5.8550%
VeryFine-Expanded RelaxationZone 2D	8h 16mins	-9.2685%

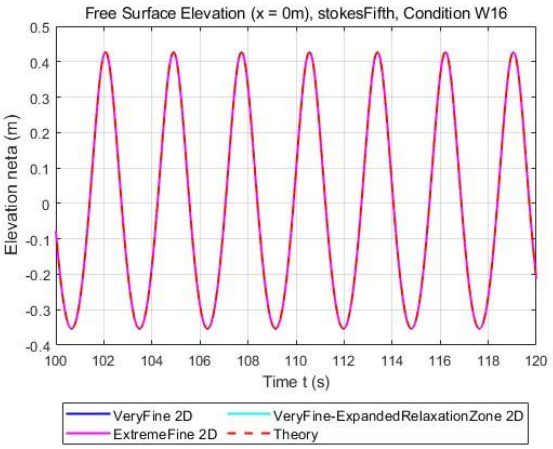

(a) The wave height at the inlet boundary

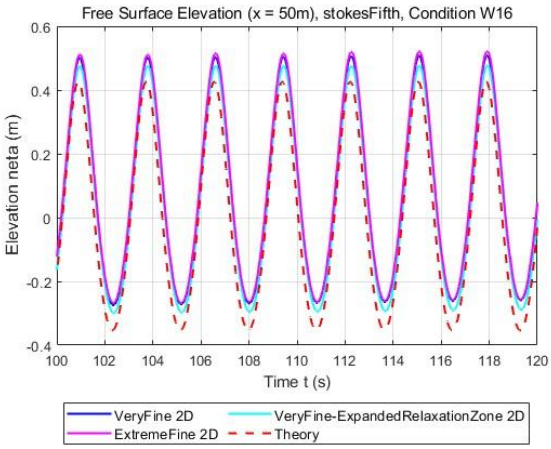

(b) The wave height at the location 50 m downstream from the inlet boundary

[Figure 5.9]The comparison on wave height between numerical results given by stokesFifth in waves2Foam and theoretical values under W16 condition

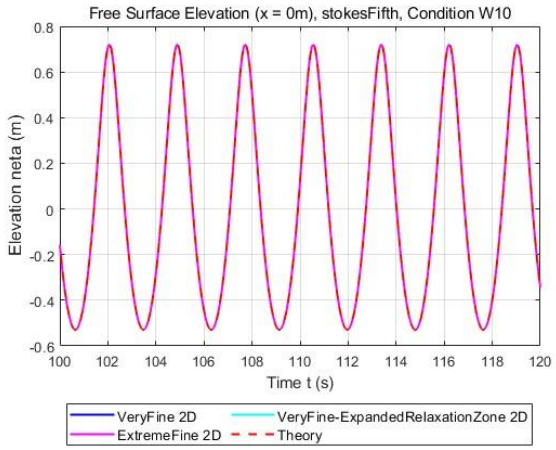

(a) The wave height at the inlet boundary

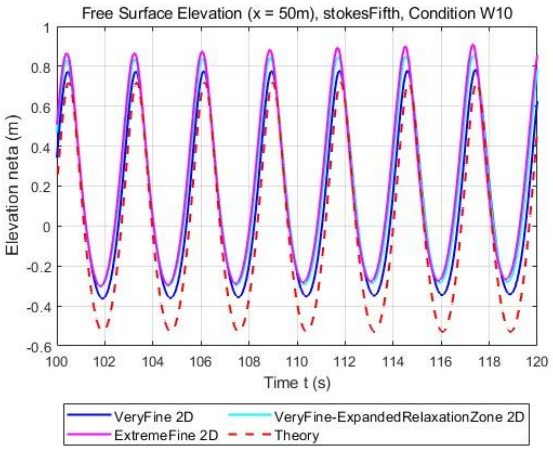

(b) The wave height at the location 50 m downstream from the inlet boundary

[Figure 5.10] The comparison on wave height between numerical results given by stokesFifth in waves2Foam and theoretical values under W10 condition

The results listed above reveal the performance of the stokesFifth model under different conditions. According to Figure 5.9 and Figure 5.10, the overall trend and shape of the curves agree well with the theoretical predictions, and the wave period shows no abnormal fluctuation over time. The curves of numerical results on wave height at the inlet boundary, shown in Figure 5.9 (a) and Figure 5.10 (a), almost perfectly overlap with the theoretical predictions, indicating the correctness of the stokesFifth model. However, at the position 50 m downstream from the in let boundary, the wave height exhibits varying degrees of attenuation. In the case with a wave steepness of $\frac{1}{25}$, the error of wave elevation at this point reaches -1.8203% which is significant larger than that in the case labeled with W0. The decrease in accuracy may be attributed to the increasing non-linearity, the influence of which becomes more significant as the wave steepness increases in the viscous-NWT.

To handle the strong non-linearity in the calculation domain, several attempts, including expanding the length of the outlet relaxation zone to 4 times of the wave length and further refining the mesh, were made to improve the simulation accuracy. By increasing the length of outlet relaxation zone from 3λ to 4λ, the error in free-surface elevation slightly decreases from $-1.9203\%$to -1.7718%, suggesting that expanding the relaxation zone is not an effective solution to enhance numerical precision under strong non-linearity conditions. In contrast, applying the ExtremeFine 2D mesh defined by Table 4.1 leads to highly accurate predictions, reducing the error of free-surface elevation at the place 50 m downstream from the inlet boundary to -0.4717%. It can be concluded that finer

meshes are required to precisely reproduce nonlinear waves under conditions with stronger non-linear effects, whereas increasing the length of relaxation zone does not remarkably influences the accuracy. This conclusion is further demonstrated by the computational results of simulations for waves with a steepness of $\frac{1}{10}$. Under this wave condition, the error in wave height at the location 50 m downstream from the inlet boundary reaches -9.6706%. Increasing the outlet relaxation zone length from 3λ to 4λ only slightly improves the accuracy, reducing the error in free-surface elevation to -9.2685%. However, further refining the mesh to ExtremeFine 2D level significantly decreases the error at the place to -5.8550%. It should be noted that under the WC10 wave condition, where numerical damping of wave is inevitable in the viscous-NWT, the errors in all simulations are higher than those under the WC16 wave condition, as the influence of non-linearity becomes more pronounced in waves with higher steepness.

From the visualized results in Figure 5.11, despite the extremely high wave steepness of $\frac{1}{10}$, no unexpected free-surface breaking is observed. The distribution of pressure and velocity fields are also consistent with physical expectations. The wave profile in the figure clearly exhibits the feature of sharp crests and broad troughs, which is a noticeable characteristic of fifth-order Stokes nonlinear wave.

However, as shown in Figure 5.9 and Figure 5.10, free-surface elevation of different magnitudes are observed in all simulations cases. This phenomenon might be attribute to the wave reflection at the boundary of the viscous-NWT, suggesting that the waves are not properly absorbed in the outlet relaxation zone. The wave reflection becomes more significant with the raise of wave steepness, leading to more obvious free-surface elevation induced by this phenomenon. However, as shown in Figure 5.9 and Figure 5.10, with the increase of outlet relaxation length the magnitudes of mean water-level elevation in the corresponding simulations are limited, suggesting that the length of the relaxation at the outlet boundary should further expanded to more than 4 times of the wave length when generating nonlinear wave with steepness higher than $\frac{1}{16}$.

In conclusion, the stokesFifth model in waves2Foam demonstrates excellent performance and generality under various wave conditions, showing strong potential for reproducing large or even extremely large nonlinear wave and providing numerical prediction with high accuracy.

(a) The wave-induced free-surface deformation in the viscous-NWT

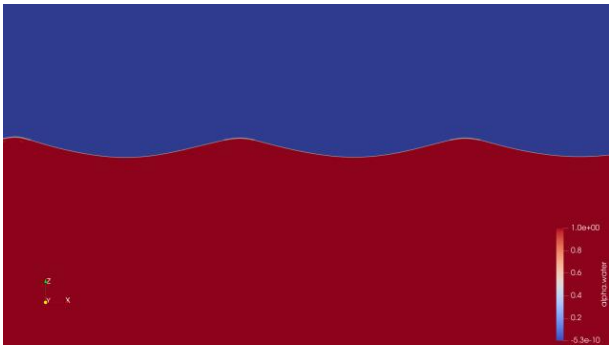

(b) The wave-induced free-surface deformation in the viscous-NWT (partially enlarged view)

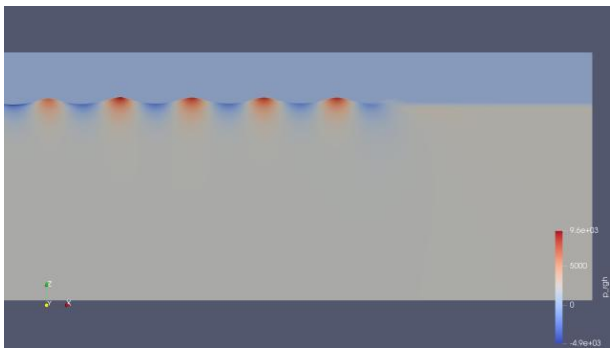

(c) The pressure distribution in the viscous-NWT

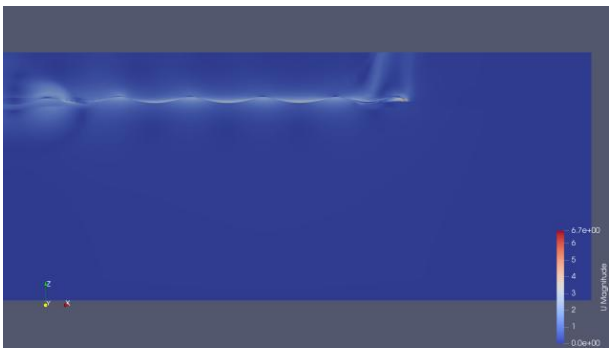

(d) The velocity contour of the case

[Figure 5.11] The visualized viscous-NWT of the “VeryFine 2D stokesFifth W10” case

5.3 Fluid dynamic force on a fixed floating-body under wave loads

This subsection verifies whether stokesFifth model reproduces wave loads on a marine structure precisely. In order to reach this goal, a benchmark (Bing Ren.et.al) is adopted as reference.[35] Following this paper, a viscous NWT, as illustrated in Figure 5.12, is established and a fixed 2D cubic floating body is created in the calculation domain. In this simulation, only wave load on the structure is considered, and the parameters of wave are given by Table 5.8. The mesh, illustrated in Figure 5.13, is generated with reference to the wave parameters, and the grid is refined around the floating body to capture the FSI phenomenon. In order to obtain the wave-induced forces in both directions and hydrodynamic moment acting on the body in the 2D plane, a force sensor and a moment sensor are respectively applied on the floating body. The results grabbed by these sensors are compared with the corresponding graphs in the benchmark. Noting that no turbulence model exists in the simulation of this section.

[Table 5.8] The parameters of waves in the simulation in Section 5.3

Wave parameters	Values
Water depth d (m)	1.2000
Wave period T (s)	1.2000
Wave height H (m)	0.0600
Wave amplitude a (m)	0.0300
Wave length λ (m)	2.0000
Wave steepness ε	1/33

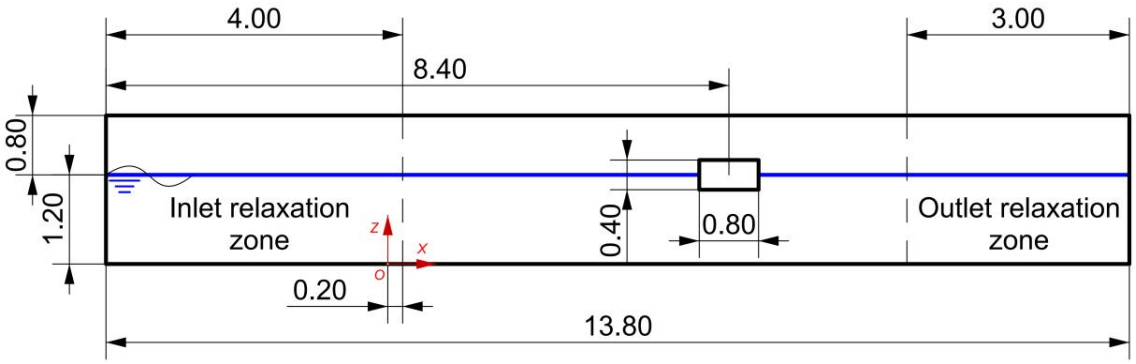

[Figure 5.12] The definition of 2D viscous-NWT for verification of wave loads predicted by stokesFifth

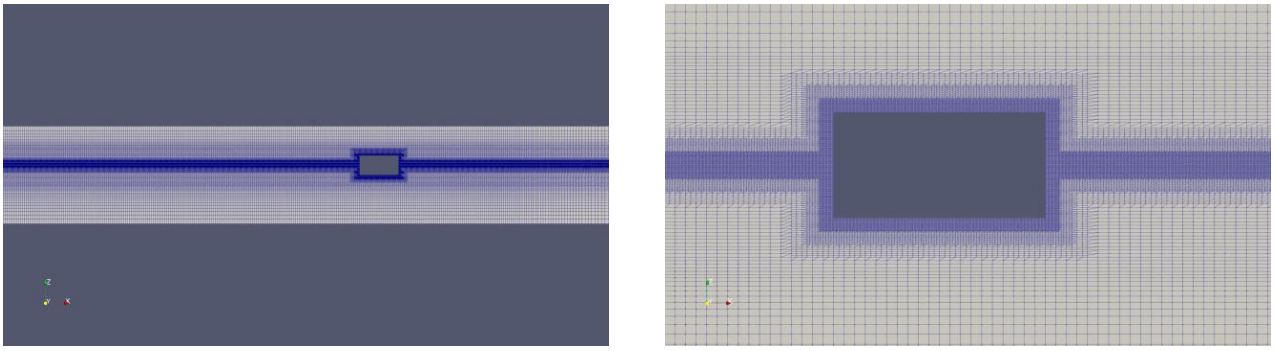

(a) The mesh configuration (overall view)

(b) The mesh configuration around target floating body

[Figure 5.13] The mesh configuration of 2D viscous-NWT for the verification of wave loads predicted by stokesFifth

Simulations are conducted in Genkai, the super computer of Kyushu University with the physical time of 20 s. Figure 5.14 shows the comparison between numerical results this study obtained and the experimental together with computational values proposed by benchmark. The visualized free-surface deformation, pressure distribution, velocity contour and velocity vector field around the cube are

shown in Figure 5.15.

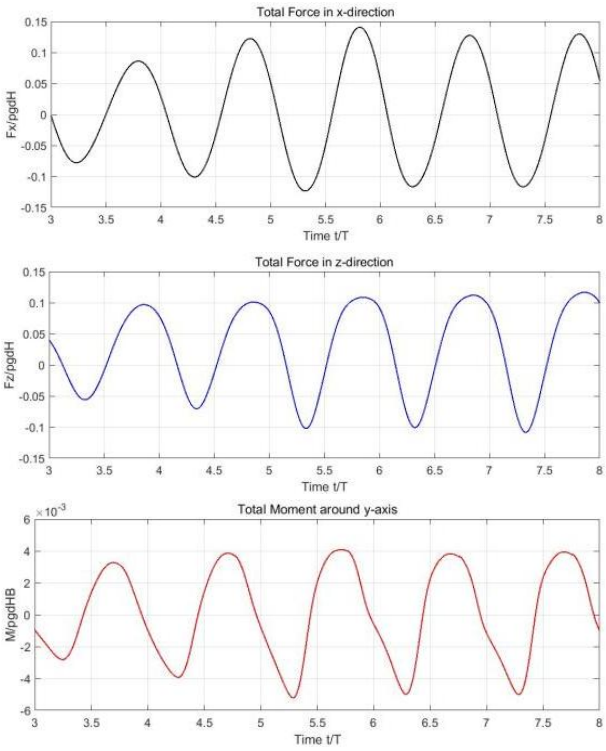

(a) The numerical results this research obtained

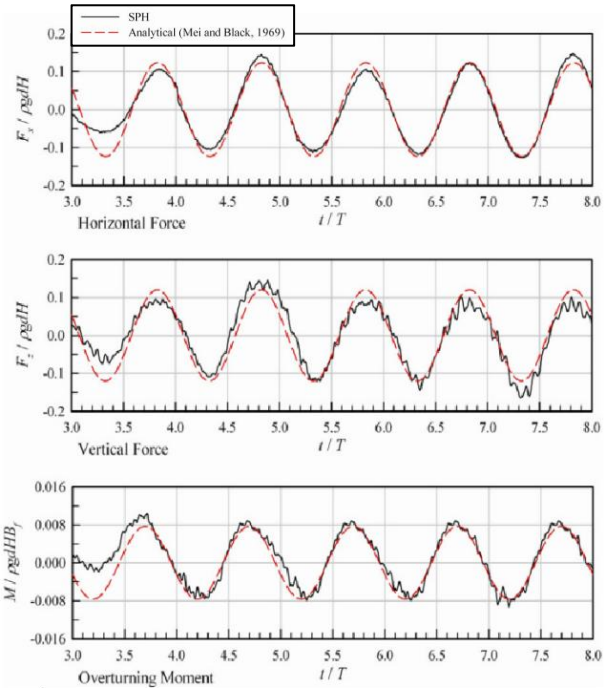

(b) The experimental and numerical results given by benchmark

[Figure 5.14] The comparison on wave loads between numerical results given by stokesFifth in waves2Foam and values given by benchmark

According to Figure 5.14, the numerical results given by stokesFifth model in waves2Foam agree well with the experimental as well as computational results proposed in the benchmark. The overall trend and shape of the curves, this study obtained, of both force and moment agree well with those of the reference results in the benchmark, the peak and trough values show good correspondence. The period of these curves agrees well with that of the curves reported in the reference paper, and shows no abnormal fluctuation over time which indicates the numerical stability of the simulation. Apart from the good agreement between results of this study and reference values, from graphs about the visualized NWT no abnormal free-surface deformation is observed around the floating body. Moreover, around the structure, the distribution of pressure and velocity fields are also consistent with the expected physical behavior, so does the velocity vector field. Therefore, result may be concluded from the analysis that stokesFifth model in waves2Foam is capable of forecasting the wave loads on a marine structure.

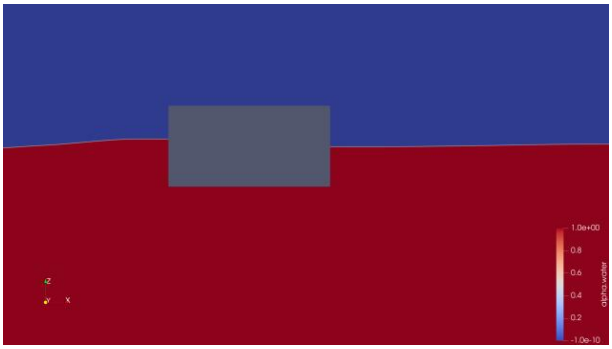

(a) The free-surface deformation around the floating body under investigation

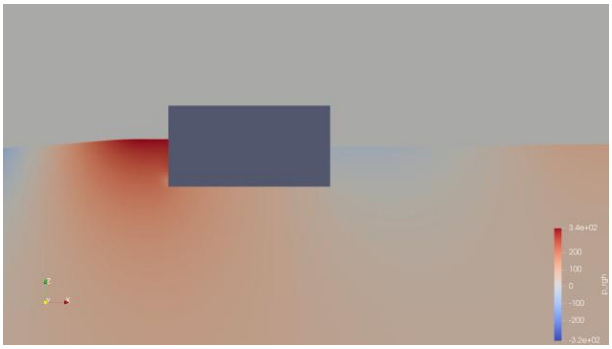

(b) The pressure distribution around the floating body under investigation

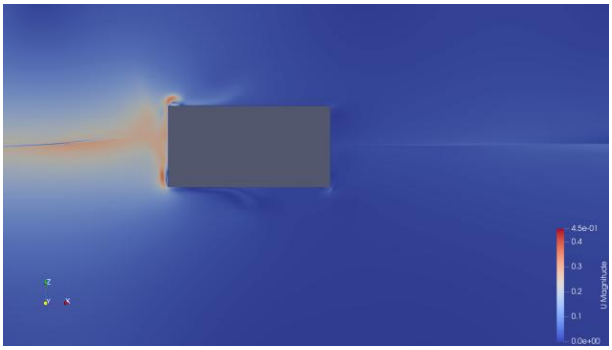

(c) The velocity contour around the floating body under investigation

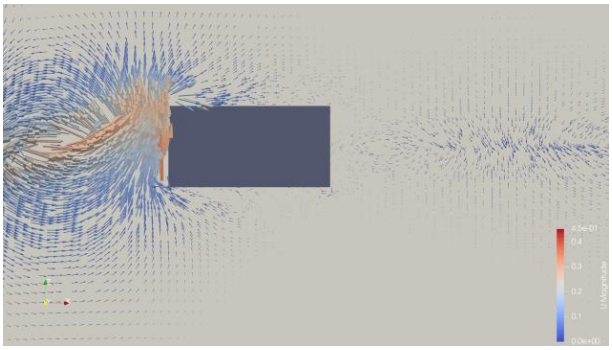

(d) The velocity vector distribution around the floating body under investigation

[Figure 5.15] The visualized viscous-NWT of the simulation for the verification of hydrodynamic loads predicted by stokesFifth

5.4 Investigation into accuracy improvement

This part explores the possibility of improving the accuracy of nonlinear wave generation on the basis of medium or even lower quality meshes in ordering to meet the requirement of engineering application. To achieve this objective, two methods, modifying the discretization scheme of each physical quantities and optimizing the relaxation zone layout, are examined. The effect of these two optimizing methods are initially tested based on the Medium 2D mesh, further investigation about the effort of two methods are implemented in the Coarse 2D mesh. Based on these two mesh levels, several modified simulation cases were constructed, and their corresponding labels as well as definitions are provided in Table 5.9. Noticing that all the modifications detailed in the table are based on the original “Medium 2D stokesFifth W0” case. Whereas, the unmodified content of the “fvSchemes” file in that original reference cases is given in the Appendix 2. All the simulations in this part focus on generating the reference wave labeled with W0 described in detail in Table 4.1. Similarly

to the chapters before, in order to investigate the accuracy of wave reproduction, two probes are positioned in the viscous-NWT which are located at the inlet boundary and 50 m down stream from inlet boundary. The data of these wave gauges are compared with theoretical prediction given by the Matlab code mentioned above in Section 3.1.

[Table 5.9] The modified cases as well as their definition

Case label	Definition
- TimeSecondOrder	Input of “ddtSchemes” in file “fvScheme” changed to “CrankNicolson 0.9”
- GradLimited	Input of “gradSchemes” in file “fvScheme” changed to “cellLimited Gauss linear”
- DivUSecondOrder	Input of “divSchemes/div(rhoPhi,U)” in file “fvScheme” changed to “Gauss linearUpwind grad(U)”
- DivAlphaCompressed	Input of “divSchemes/div(phirb,alpha)” in file “fvScheme” changed to “Gauss interfaceCompression”
- 35outlet	Length of outlet relaxation zone is expanded to 3.5λ
- 4outlet	Length of outlet relaxation zone is expanded to 4λ

Above mentioned modifications are implemented from the “Medium 2D stokesFifth W0” case, and coherent simulation cases are created. These simulations are also conducted for a physical time of 120 s, the wave profile of these cases are given by Figure 5.16 and the errors on wave height of each case, captured at the position that 50 m downstream from the inlet boundary, are listed in Table 5.10.

[Table 5.10] The numerical errors of the cases modified from the “Medium 2D stokesFifth W0” case

Case label	Time consumption	Error on wave height (x=50)
Medium 2D stokesFifth W0	3h 15mins	-3.7948%
Medium 2D stokesFifth W0 - TimeSecondOrder	Error	Error
Medium 2D stokesFifth W0 - GradLimited	4h 02mins	-4.1792%
Medium 2D stokesFifth W0 - DivUSecondOrder	9h 49mins	-3.8168%
Medium 2D stokesFifth W0 - DivAlphaCompressed	4h 32mins	-2.4056%
Medium 2D stokesFifth W0 - 35outlet	3h 47mins	-4.2739%
Medium 2D stokesFifth W0 - 4outlet	3h 26mins	-4.7472%

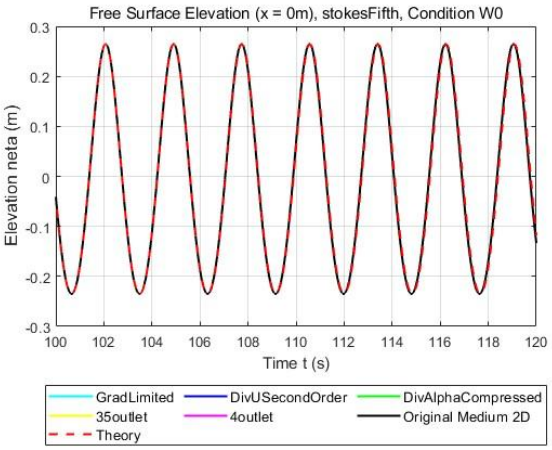

(a) The wave height at the inlet boundary

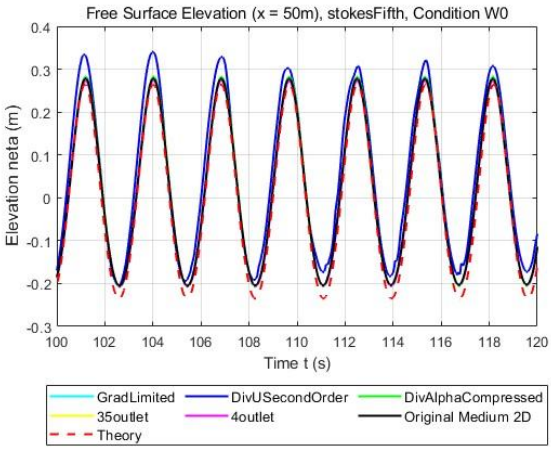

(b) The wave height at the location 50 m downstream from the inlet boundary

[Figure 5.16] The wave profile of the cases modified from the "Medium 2D stokesFifth W0" case

As shown in Figure 5.16 and Table 5.10, modifying the differencing schemes of the relevant physical terms has a significant influence on the numerical results. Changing the differencing method of time in file "fvScheme" from "Euler" to "CrankNicolson", a second-order time discretization scheme, leads to a numerical error called "floating point exception"which killed the simulation. As shown in Figure 5.17, the non-physical free-surface breaking is observed at the interface between relaxation zone and calculation domain and abnormal distribution of velocity vector is also identified in the NWT, suggesting that this error might be attribute to the accumulation of velocity errors.[34] The occurrence of these phenomena indicates the divergence of the case, suggesting that the convergence performance of "CrankNicolson" differencing method is relevantly poor and being unsuitable to handle the nonlinear wave generation simulation. Shifting the discretization method of the spatial gradient operator ∇ for physical variables except for fluid's volume fraction from "Gauss linear" to "cellLimited Gauss linear" in "fvScheme" file brings negative effect towards calculation efficiency as well as numerical accuracy, indicating that this redefinition does not contribute to improving nonlinear wave generation accuracy in medium mesh. Modifying the discretization scheme for the momentum convection term in Navier-Stokes equation from "Gauss upwind" to "Gauss linearUpwind grad(U)" in the file "fvScheme" results in a remarkable increase of computational time, almost tripled the time consumption under the same mesh density and end time, while showing no obvious effect on accuracy improvement. Moreover, as shown in Figure 5.16, the deep blue curve in the graph which represents the numerical result of the case "Medium 2D - DivUSecondOrder stokesFifth W0" shows measurable

fluctuation over the time, suggesting that this change has a negative impact on the numerical stability of the simulation. By modifying the discretization scheme of the artificial interface-compression flux in the VOF formulation from “Gauss linear” to “Gauss interfaceCompression”, the resource consumption increased, as the calculation time increased by approximately 39% - from 3 hours 15 minutes to 4 hours 32 minutes - compared with the original “Medium 2D stokesFifth W0” case, whereas the numerical accuracy of wave generation improved significantly. The error on wave height at 50 m downstream of the inlet boundary decreases from -3.7948% to -2.4056%, demonstrating the strong potential of this modification for improving numerical accuracy. This redefinition enables simulations in Medium 2D mesh achieves a wave generation accuracy slightly inferior to that in the Fine 2D mesh, while requiring substantially fewer computational resources. This discovery demonstrates that this modification is capable to meet the intended objective: improving the numerical accuracy of nonlinear wave generation on a relatively coarse grid with a controllable resource consumption, obtaining reliable but economical-friendly numerical results.

As shown in Figure 5.16 and Table 5.10, the relaxation optimization does not show potential on accuracy improvement, but demonstrates negative influence on the resource consumption. The calculation time of the modified cases increases from 3 hours 15 minutes - the runtime of the unmodified case - to 3 hours 47 minutes and 3 hours 26 minutes for the “Medium 2D - 35outlet stokesFifth W0” and “Medium 2D - 4outlet stokesFifth W0” cases, respectively, whereas the numerical accuracy of both cases decreases substantially. However, as shown in Figure 5.16, the average water level in these two cases decrease, indicating that expanding the outlet relaxation zone reduces the unwanted wave reflections when fluid exit the NWT, thereby limiting the abnormal free-surface rise induced by reflected waves.

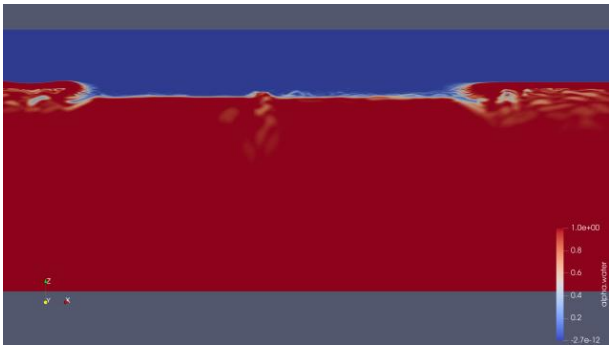

(a) The breaking free-surface in the viscous-NWT

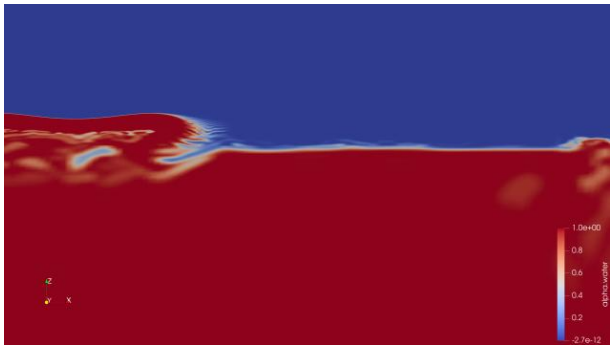

(b) The breaking free-surface in the viscous-NWT (partially enlarged view)

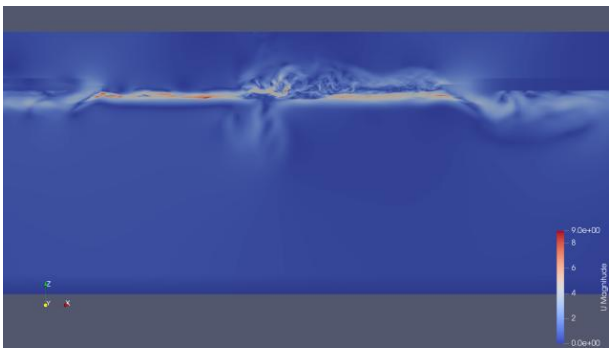

(c) The velocity contour of the case

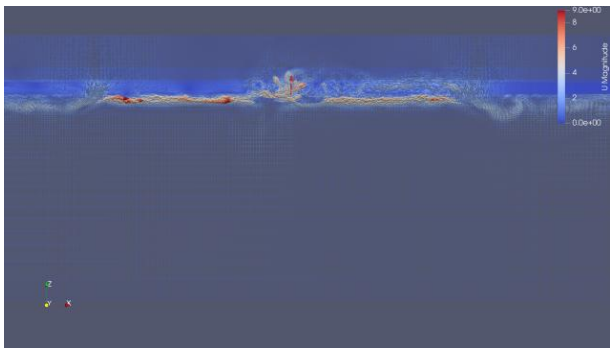

(d) The velocity vector distribution in the NWT

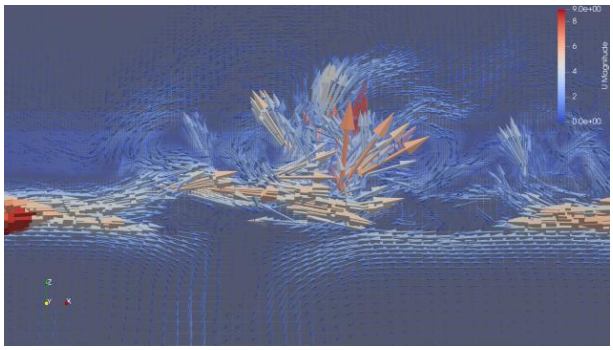

(e) The velocity vector distribution in the viscous-NWT (partially enlarged view)

[Figure 5.17] The visualized viscous-NWT of the“Medium 2D stokesFifth W0 - TimeSecondOrder” case at the moment when error occurs

Subsequently, the same process of accuracy improvement study is implemented on the Coarse 2D mesh. The same modifications detailed in the Table 5.9 are conducted on the basis of the “Coarse 2D stokesFifth W0” case, and the corresponding cases are created. These simulations are conducted for 120 s, and their numerical results as well as corresponding accuracy performance are respectively given by Figure 5.18 and Table 5.11. From Figure 5.18 and Table 5.11, a conclusion consistent with that obtained in the accuracy-improvement study based on the Medium 2D mesh can be drawn

regarding the effect of the aforementioned modification. Meanwhile, the correctness of the conclusion this section obtained is verified.

[Table 5.11] The numerical errors of the cases modified from the “Coarse 2D stokesFifth W0” case

Case label	Time consumption	Error on wave height (x=50)
Coarse 2D stokesFifth W0	2h 48mins	−7.7978%
Coarse 2D stokesFifth W0 - TimeSecondOrder	Error	Error
Coarse 2D stokesFifth W0 - GradLimited	2h 57mins	−8.6538%
Coarse 2D stokesFifth W0 - DivUSecondOrder	5h 41mins	−7.3586%
Coarse 2D stokesFifth W0 - DivAlphaCompressed	4h 02mins	−6.5726%
Coarse 2D stokesFifth W0 - 35outlet	3h 13mim	−8.8651%
Coarse 2D stokesFifth W0 - 4outlet	3h 09mins	−9.2686%

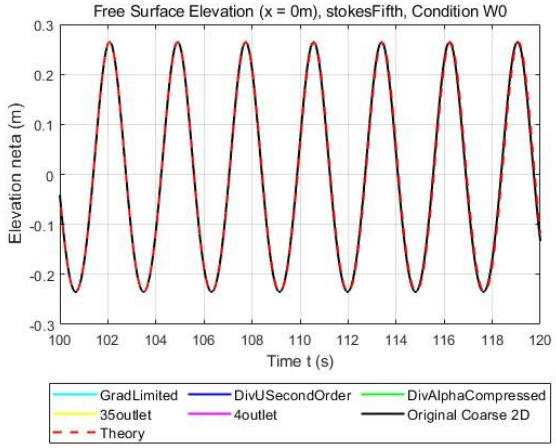

(a) The wave height at the inlet boundary

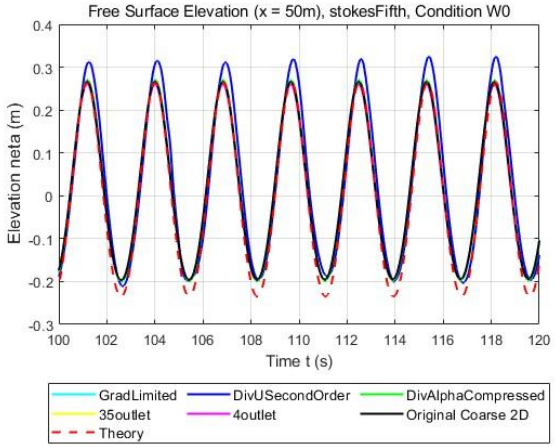

(b) The wave height at the location 50 m downstream from the inlet boundary

[Figure 5.18]The wave profile of the cases modified from the “Coarse 2D stokesFifth W0” case

5.5 Conclusion and discussion

In Chapter 5, the nonlinear wave generation in OpenFOAM are systematically investigated, waves are respectively generated by wave models in both OpenFOAM and its plug-in code waves2Foam and convergence study based on different mesh levels are substantially implemented. After that, the suitable wave model providing highly accurate numerical results is identified, the performance of which under 3D meshes and various wave conditions is also discussed. Then, this chapter tests the accuracy of numerical prediction about wave loads on a fixed floating structure given by the selected wave model, and finally investigation is conducted to identify the methods to increase numerical

accuracy of simulations in relevantly coarse meshes.

Section 5.1 verifies the feasibility of generating large nonlinear wave by OpenFOAM and its plug in code waves2Foam and the accuracy performance of them is also discussed. The feasibility of nonlinear wave generation by OpenFOAM is validated, while the accuracy of both stokesII and stokesV models - the models in the software for nonlinear wave - are poor being attribute to the numerical damping in the fluid field and the wave height errors of these two models in cases of VeryFine 2D mesh are -23.2546% and -24.4289% respectively. Therefore, this study introduces waves2Foam to accurately generate nonlinear waves. The feasibility of this plug-in code is verified and the precision of its wave models - stokesSecond and stokesFifth - is studied and the result of the investigation suggests the accuracy performance of the stokesFifth model is superior to that of the stokesSecond model. In the VeryFine 2D mesh, the free-surface elevation error of wave W0 generated by the fifth-order model is -0.4971%, which is remarkably lower than the wave-height error obtained with the stokesSecond model under the same conditions. Moreover, it can be concluded that for generating nonlinear waves with steepness no more than $\frac{1}{25}$ in OpenFOAM with high accuracy - typically requiring the wave height error to be kept below $\pm 2\%$ - the use of waves2Foam is essential, together with a spatial resolution of approximately 300 cells per wavelength and 30 cells per wave height.

In Section 5.2, the performance of the stokesFifth model is evaluated under multiple conditions, including 3D NWT and waves of varying steepness. In 3D meshes with different density, fifth order Stokes model properly performs in all cases, providing highly accurate numerical predictions as errors under all mesh conditions below $\pm 1\%$. Furthermore, simulations are conducting under the W16 and W10 wave conditions, the results demonstrating that the wave model also exhibits favorable performance when simulating extreme large nonlinear waves. However, as the wave steepness increases, the numerical damping in the viscous-NWT is unavoidable resulting in the numerical accuracy deteriorates and the unwanted mean water-level elevation appears in the fluid field. Through the investigation, conclusion can be made that when generating nonlinear waves with steepness ranging from $\frac{1}{25}$ to $\frac{1}{16}$ in OpenFOAM, achieving a wave-height error below $\pm 2\%$ requires the use of waves2Foam and a mesh density requirement - no fewer than 350 cells per wavelength and 35 cells per wave height specifically. Whereas, when the wave steepness exceeds $\frac{1}{16}$, the numerical damping in

the fluid field become significant and mesh density with 450 cells per wavelength and 45 cells per wave height is necessary to obtain results with satisfactory precision. However, if the wave height increases further and the wave steepness is greater than $\frac{1}{10}$, the numerical accuracy of the wave generation simulations noticeably drops due to the numerical damping induced by strong non-linearity. Under such conditions, even the ExtremeFine 2D mesh defined in Section 3.1 may no longer provide results with adequate precision. Moreover, as the wave steepness increases, the magnitude of the undesired mean water-level elevation also rises. This effect can be mitigated by extending the outlet relaxation zone to four wavelengths (4λ) or longer.

Section 5.3 examines whether stokesFifth model in waves2Foam can reproduce wave loads on a structure correctly. Simulation is conducted to obtain the numerical prediction of forces and moments on a 2D cubic shaped fixed floating body and the results of which are compared against a benchmark.

The last section of the chapter - Section 5.4 - investigates the methods to improve the numerical accuracy in the relevantly coarse grid to provide a guideline for the practical engineering applications where the reliability and computationally efficiency are emphasized on. The studied examines the effects of changing the differencing scheme of physical quantities and optimizing relaxation zone configuration. The results of the investigation suggest that: on the basis of code given by Appendix 2, changing the differencing scheme of the artificial interface-compression flux in the VOF formulation from “Gauss linear” to “Gauss interfaceCompression” in the“fvScheme” file improves numerical accuracy with an acceptable increase in computational cost, therefore, this change is recommend for obtaining cost-effective yet accurate wave generation numerical results on coarse grids; modifying the discretization scheme of time in file “fvScheme” from “Euler” to “CrankNicolson” in the file leads to an error called “floating point exception”, and thus this modification should be avoided; other redefinition of differencing methods in file “fvScheme” are less favorable as they either result in numerically unstable or cause unacceptable increase in resource consumption. Moreover, lengthening the relaxation zone at the outlet boundary does not exhibit potential on numerical accuracy improvement but reduces unwanted water-level elevation being attributed to the wave reflection.

6 Wave-current coupling reproduction

6.1 Feasibility study of stokesSecondwCurrent model

In this section, the feasibility of user-defined wave-current coupling solver stokesSecondwCurrent is studied by reproducing the wave-current interaction phenomena in the viscous NWT under multiple meshes and comparing the corresponding results with theoretical values. Specifically, the wave condition labeled with WC0 is respectively reproduced in the coarse 2D, Medium 2D, Fine 2D and VeryFine 2Dmeshes. Two wave gauges are also placed at the same positions as those used in the previous sections to record the wave elevation and period. The data captured by these probes from simulations is also validated against the Matlab code programmed with reference to the theory proposed by John D. Fenton. It should be noted that this theory is also capable of theoretically predicting the wave profile and wave period under wave-current coupling conditions simply by defining the Euler velocity u_E as the current velocity. Through the comparison between the theoretical and numerical results, the accuracy of stokesSecondwCurrent model is examined, and the requirements on mesh quality for wave-current coupling reproduction are also identified.

[Table 6.1] The calculation results given by stokesSecondwCurrent under 2D WC0 condition

Mesh level	Time consumption	Error on wave height (x=50)
Coarse 2D	10h 30mins	-3.7894%
Medium 2D	12h 56mins	-0.2514%
Fine 2D	19h 07mins	$+1.9550\%$
VeryFine 2D	23h 28mins	$+1.5283\%$

Simulations are conducted in the environment of waves2Foam for a physical time of 120 s, and the wave profile of these cases as well as theoretical prediction are illustrated in Figure 6.1, and the results of these cases are detailed in Table 6.1. The visualized NWT of “Medium 2D stokesSecondwCurrent WC0”case is shown by Figure 6.2. In the table, the error of free-surface elevation at the location of two probes, calculation time and the corresponding mesh level are provided.

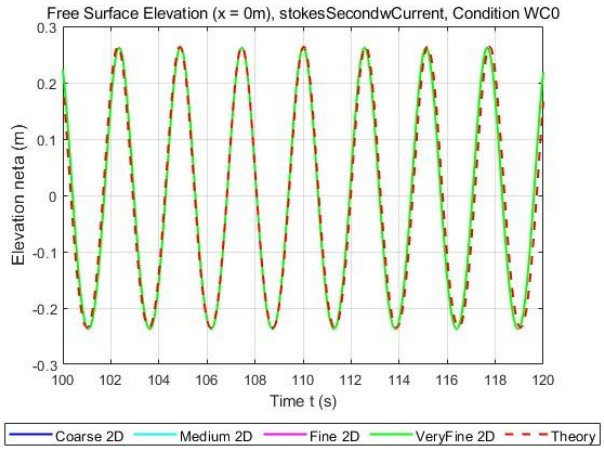

(a) The wave height at the inlet boundary

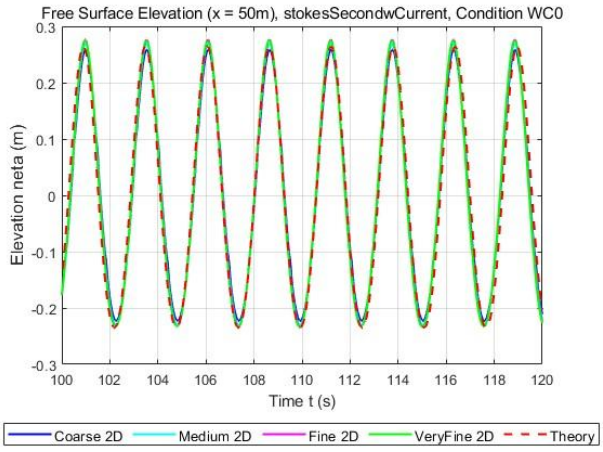

(b) The wave height at the location 50 m downstream from the inlet boundary

[Figure 6.1] The comparison on wave height between numerical results given by stokesSecondwCurrent in waves2Foam and theoretical values under WC0 condition

According to Table 6.1 and Figure 6.1, conclusion can be made that user-defined solver stokesSecondwCurrent is feasible to reproduce the wave-current coupling phenomena and exhibit satisfactory accuracy performance. As the Figure 6.1 illustrated, the numerical results obtained in this study agree well with the theoretical predictions, typically at the inlet boundary - almost perfectly consistent with theoretical predictions, whereas, numerical errors with varying degrees are observed in the calculation domain of different cases. From the comparison results, it might be concluded that with the increase of mesh density, the solver stokesSecondwCurrent exhibits a tendency of overestimating the wave height, as the wave-height error gradually rise from −3.7894% (underestimating the wave height) in Coarse 2D mesh to +1.5283% (overestimating the wave height) in VeryFine 2D mesh. This finding indicates that, when reproducing wave-current coupling phenomena using stokesSecondwCurrent solver, merely refining the mesh does not necessarily improve the numerical accuracy, instead selecting appropriate mesh density may both provide highly precise numerical predictions and reduce computational resource cost. Moreover, this discovery also demonstrates the high performance of the wave -current coupling solver. As a result, this research suggest that when using the stokesSecondwCurrent solver, in ordering to obtain numerical result with best accuracy, the number of cells in a single wave length should be more than 200 while less than 250 and the grids within a wave height should varies from 20 to 30. It should be noted that the recommended mesh density here is defined with reference to the wave parameters of the uncoupled wave component, specifically, without considering the Doppler effect introduced by the current.

(a) The free-surface deformation in the viscous-NWT

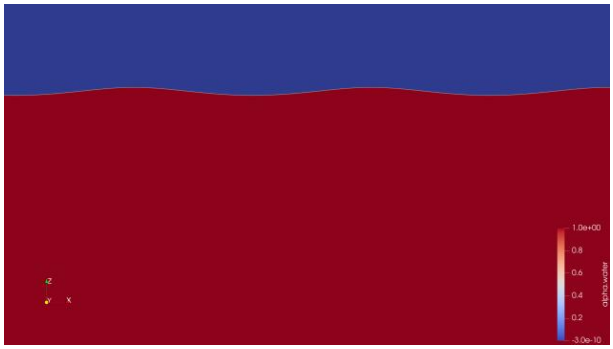

(b) The free-surface deformation in the viscous-NWT (partially enlarged view)

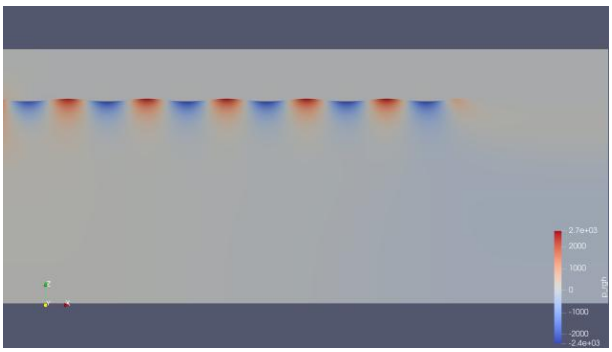

(c) The pressure distribution in the viscous-NWT

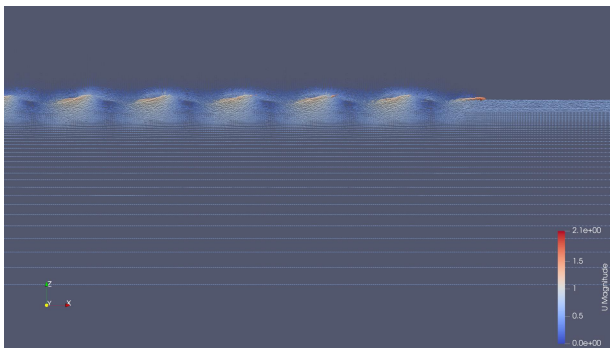

(d) The velocity vector distribution in the viscous-NWT

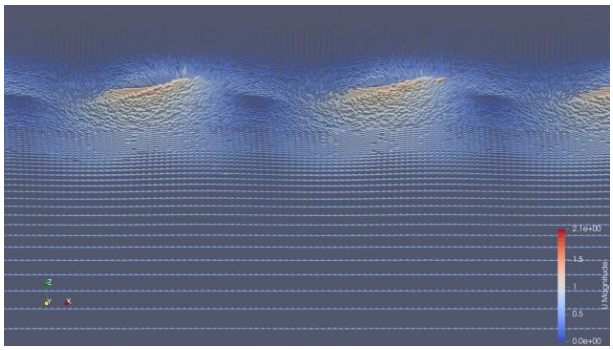

(e) The velocity vector distribution in the viscous-NWT (partially enlarged view)

[Figure 6.2] The visualized viscous-NWT of the “Medium 2D stokesSecondwCurrent WC0” case

Apart from the good agreement of free-surface elevation between computational results and theoretical values, as shown in Figure 6.2 no abnormal fluctuation over time is observed in the wave period which shows the numerical stability of the simulation. Furthermore, the free-surface elevation, distribution of pressure field and velocity vector field, shown in the figure, are also consistent with the expected physical behavior. Specifically, the vector distribution of fluid well agrees with the expected physical phenomenon, as the velocity vectors deeply beneath the water-level shows no variation on their magnitudes and their directions correspond with the define current while the magnitudes and

directions of those around the free-surface are remarkably influenced by waves.

The above mentioned conclusions confirm the feasibility of the stokesSecondwCurrent model developed within the framework of waves2Foam, and exhibit its satisfactory accuracy performance.

From the analysis of the results in Table 6.1, it might be concluded that Medium 2D mesh provides the most accurate numerical predictions of wave elevation, Thus Medium 2D mesh is chosen and is expanded into 3D meshes for further investigation of the stokesSecondwCurrent in Chapter 6.2.

6.2 Performance test of the stokesSecondwCurrent model

This part evaluates the performance and generality of the stokesSecondwCurrent, a user-defined wave-coupling model, in multiple conditions. Firstly, this solver is applied to reproduce the wave labeled with WC0 in various 3D meshes to further assess the feasibility of the application in 3D cases. This model is then employed to reproduce waves with different steepness or with various current speed. In these simulations, Medium 2D is adopted in ordering to ensure the precision of the numerical results. The computational data is also compared against the Matlab code discussed in Chapter 3.1.

6.2.1 Wave-current coupling reproduction in 3D meshes

In this subsection, stokesSecondwCurrent model in waves2Foam is used for 3D wave-current reproduction in ordering to verify the feasibility of the model in 3D cases. As mentioned above, the 3D meshes are created on the basis of Medium 2D mesh, and the detail definition is given in Chapter 4.2. The Coarse 3D , Medium 3D and Fine 3D mesh are employed in the chapter for the validation of the wave-current coupling solver in 3D viscous-NWT. Similar to the study in Section 5.2, two wave gauges are placed at the inlet boundary and 50 m down stream from inlet boundary, positioned at the mid-span of the domain in the y-direction, to capture the wave height and wave period.

[Table 6.2] The calculation results given by stokesSecondwCurrent under 3D WC0 condition

Mesh level	Time consumption	Error on wave height (x=50)
Coarse 3D	23h 05mins	+1.6952%
Medium 3D	62h 43mins	+1.3831%
Fine 3D	70h 37mins	+1.3371%

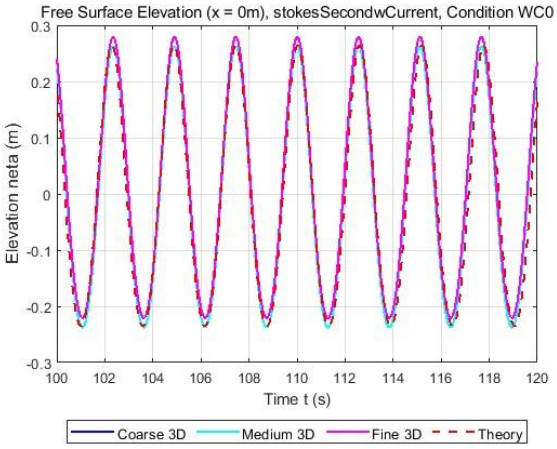

(a) The wave height at the inlet boundary

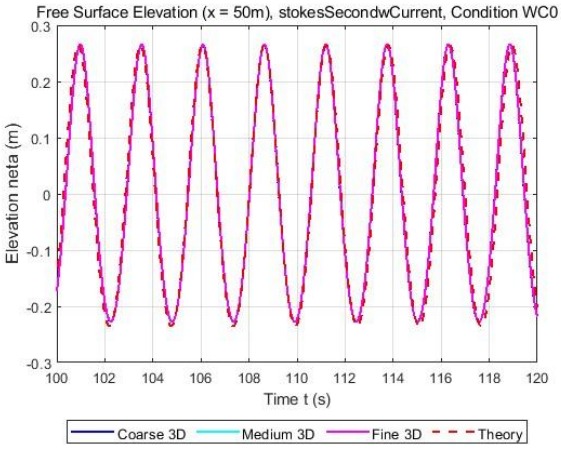

(b) The wave height at the location 50 m downstream from the inlet boundary

[Figure 6.3] The comparison on wave height between numerical results given by stokesSecondwCurrent in waves2Foam and theoretical values under WC0 condition (3D)

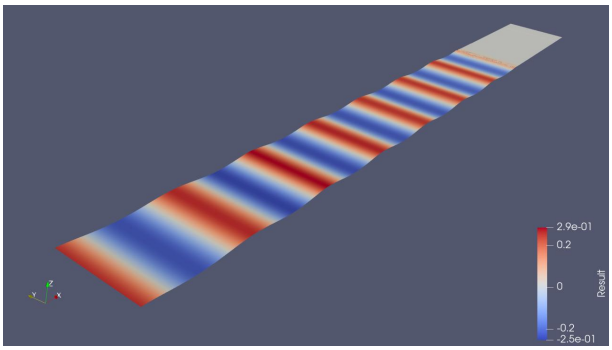

(a) The wave-induced free-surface deformation in viscous-NWT

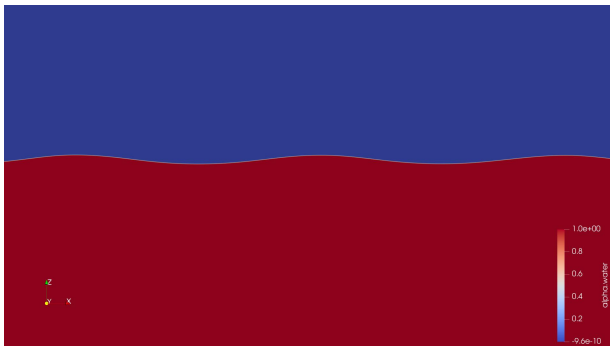

(b) The wave-induced free-surface deformation in viscous-NWT (partially enlarged view)

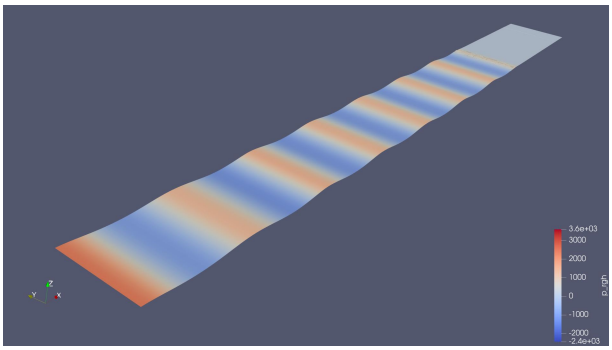

(c) The pressure distribution on the free-surface

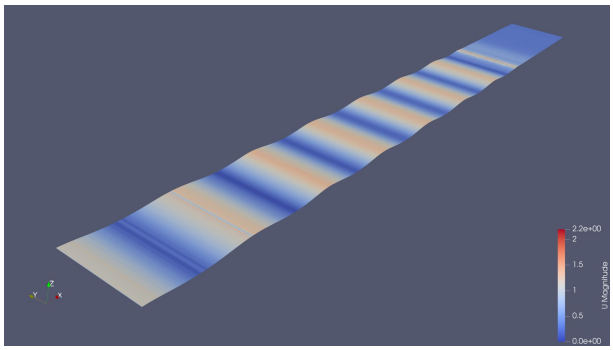

(d) The velocity contour on the free-surface

[Figure 6.4] The visualized viscous-NWT of the “Medium 3D stokesSecondwCurrent WC0” case

By using stokesSecondwCurrent, 3D CFD analysis are implemented with the computational setting of 5 nodes with 48 threads per node for a physical time of 120 s, and the wave profile of these

cases are illustrated in Figure 6.3, and visualized NWT of “Medium 3D stokesSecondwCurrent WC0” case is shown by Figure 6.4, the results are detailed in Table 6.2. In the table, the wave-height errors at the location of two probes, calculation time, mesh level and the corresponding wave models are provided.

According to the results listed above, it can be concluded that user-defined solver stokesSecondwCurrent is feasible to precisely reproduce the wave-current coupling phenomena in 3D meshes. The data given by Table 6.2 and Figure 6.3 indicates that the numerical results obtained in this part well agree with the theoretical values. From the comparison, the error in wave elevation are +1.6952%, +1.3831% and +1.3371% under the Coarse 3D, Medium 3D and Fine 3D mesh, respectively, showing the high accuracy of the solver. Noting that the wave elevations are overestimated in these 3D cases, which may result in conservative and redundant design of marine structures for practical engineering applications. Moreover, the wave period remains stable over time, confirming the numerical stability of the stokesSecondwCurrent solver under 3D conditions. The visualized results in NWT, as shown in Figure 6.4, also indicate that the wave-induced free-surface elevation, distribution of pressure field and velocity field are consistent with the expected physical behavior. In conclusion, the user-defined model - stokesSecondwCurrent - is validated as capable of accurately reproducing wave-current coupling phenomena in the 3D NWT.

6.2.2 Wave-current coupling reproduction in multiple condition

The performance and generality of user-defined wave current coupling model, stokesSecondwCurrent, is investigated in this part. The wave steepness and current velocity is successively modified for the investigation. The simulations in the assessment are conducted on the basis of Medium 2D mesh,and on the basis of that wave labeled with WC16, WC10, WC+1.1, WC+2.2 AND WC-0.6 are reproduced. The results of these cases are employed to study the accuracy of wave height by comparing the numerical result with theoretical values given by the Matlab code introduced in Section 3.1. Similar to the studies in the previous sections, two probes are positioned at inlet boundary and 50 m downstream from that boundary.

[Table 6.3] The calculation results given by stokesSecondwCurrent under various 2D wave conditions

Wave condition number	Time consumption	Error on wave height (x=50)
WC16	34h 13mins	+2.2256%
WC10	44h 59mins	+4.2346%
WC+1.1	40h 01mins	+3.3512%
WC+2.2	78h 09mins	+7.0973%
WC-0.6	44h 59mins	−14.1345%

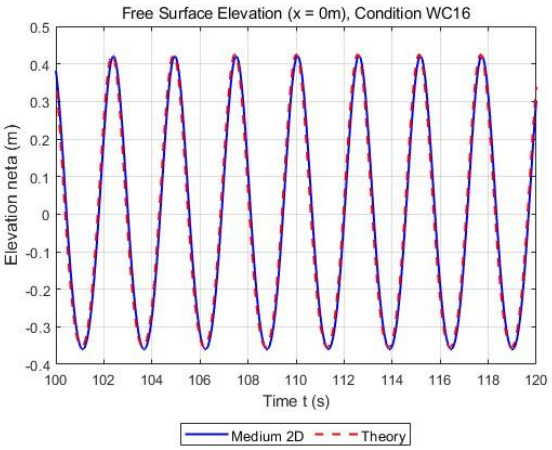

(a) The wave height at the inlet boundary

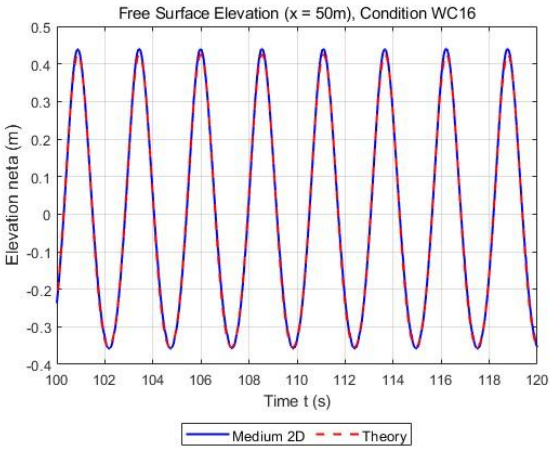

(b) The wave height at the location 50 m downstream from the inlet boundary

[Figure 6.5] The comparison on wave height between numerical results given by stokesSecondwCurrent in waves2Foam and theoretical values under WC16 condition

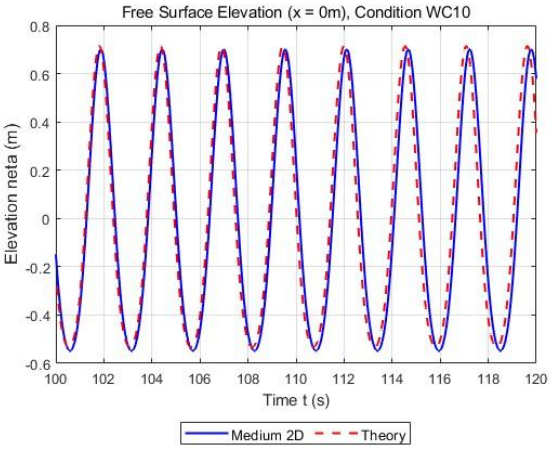

(c) The wave height at the inlet boundary

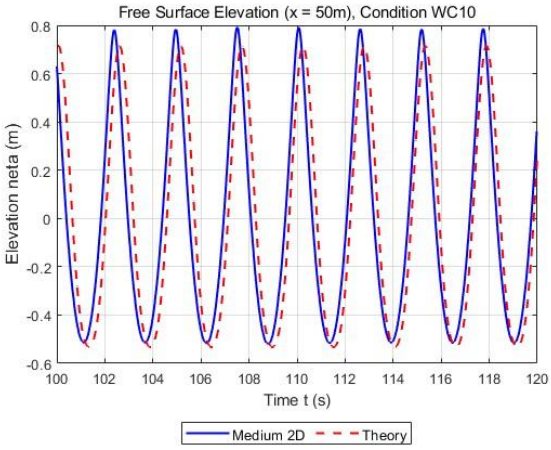

(d) The wave height at the location 50 m downstream from the inlet boundary

[Figure 6.6] The comparison on wave height between numerical results given by stokesSecondwCurrent in waves2Foam and theoretical values under WC10 condition

(a) The free-surface deformation in viscous-NWT

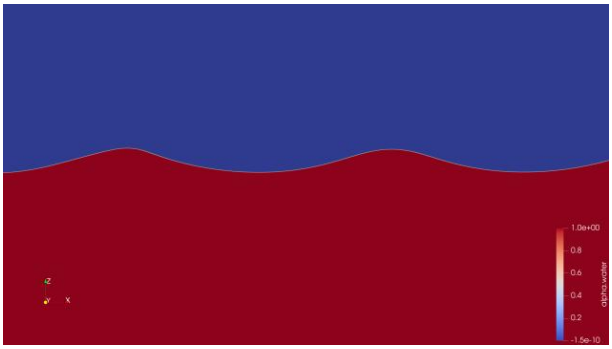

(b) The free-surface deformation in viscous-NWT (partially enlarged view)

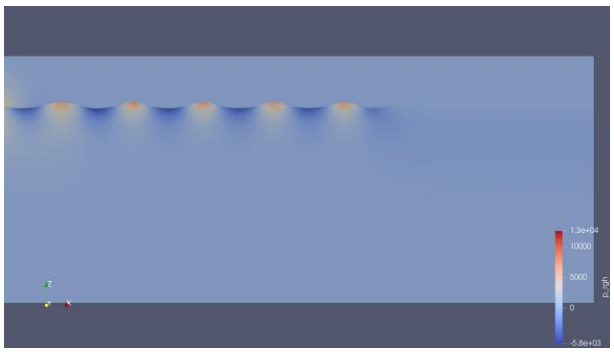

(c) The pressure distribution in viscous-NWT

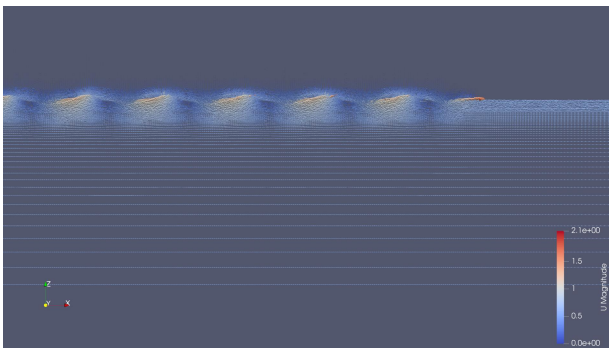

(d) The velocity vector distribution in viscous-NWT

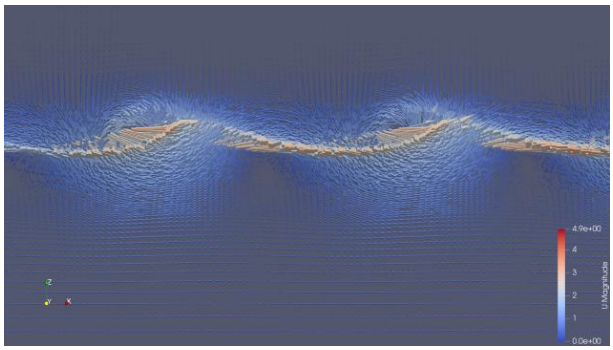

(e) The velocity vector distribution in viscous-NWT (partially enlarged view)

[Figure 6.7] The visualized viscous-NWT of the "Medium 2D stokesSecondwCurrent WC10" case

By using stokesSecondwCurrent, two simulations with the shifted wave steepness and three cases with modified current velocity are conducted for a physical time of 120 s. The wave profile of these cases are respectively illustrated in Figure 6.5, Figure 6.6, Figure 6.8, Figure 6.9 and Figure 6.10. The visualized NWT of "Medium 2D stokesSecondwCurrent WC10" case is shown by Figure 6.7, and the results of accuracy analysis are detailed in Table 6.4. In the table, the error of wave height at the location of two wave gauges, calculation time and the corresponding wave condition are provided.

As shown in Figure 6.5 and Figure 6.6, the stokesSecondwCurrent model demonstrates

outstanding performance and shows feature of high accuracy across multiple cases with different wave height. At the inlet boundary, the wave-elevation curves for both the WC16 and WC10 simulations (corresponding to wave steepness of $\frac{1}{16}$ and $\frac{1}{10}$) show excellent agreement with the theoretical predictions, and no abnormal fluctuation in wave period is observed. However, at the location 50 m from the inlet boundary, the numerical curves slightly deviate from the theoretical ones, with wave-elevation errors of +2.2256% and +4.2346% for the WC16 and WC10 cases, respectively. Moreover, unlike the "VeryFine 2D stokesFifth W10" case where significant numerical wave damping occurs within the computational domain, no obvious numerical wave attenuation is observed in the "Medium 2D stokesFifth WC10" case, confirming the high accuracy and robustness of the stokesSecondwCurrent model. It should be noted that these errors are positive, indicating that the stokesSecondwCurrent model overestimates the wave height, which may lead to a conservative design in the engineering applications. In the "Medium 2D stokesFifth WC16" case, almost no abnormal mean water-level elevation is captured, whereas in the "Medium 2D stokesFifth WC10" case, small-amplitude elevation occur, suggesting that the waves were not fully absorbed in the outlet relaxation zone due to the higher wave steepness and non-linearity. The waves are reflected at the outlet boundary leading to the unwanted mean water-level elevation in the case.

Figure 6.8, Figure 6.9 and Figure 6.10 illustrate the performance of the stokesSecondwCurrent model under various conditions with identical wave parameters but different current velocities. Similar to previous results, no significant deviation is observed between the numerical and theoretical wave-elevation curves across all cases and no abnormal elevation of the mean water level is observed, indicating the numerical stability of the model under the tested conditions. However, the wave-height error increases with the current velocity, as the errors are +3.3512% and +7.0973% in the WC+1.1 and WC+2.2 cases respectively. This trend is likely attributed to the intensified nonlinear interaction between the wave and the current at higher flow speeds. In all these cases, the wave heights are overestimated, which may lead to a conservative design in engineering applications. Conversely, when the wave and current propagate in opposite directions, the user-defined stokesSecondwCurrent model is found to be inapplicable, as the wave height is severely underestimated, with an error reaching -14.1345%.

In conclusion, the user-defined solver - stokesSecondwCurrent - performs well providing accurate

numerical prediction of wave-current coupling phenomena under multiple wave-current conditions expect for the case where wave and current propagate in the opposite directions.

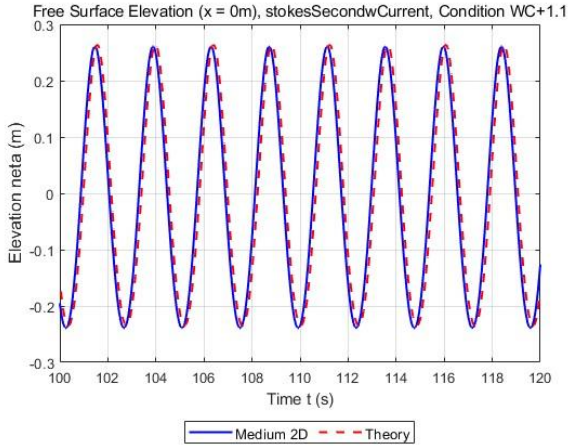

(a) The wave height at the inlet boundary

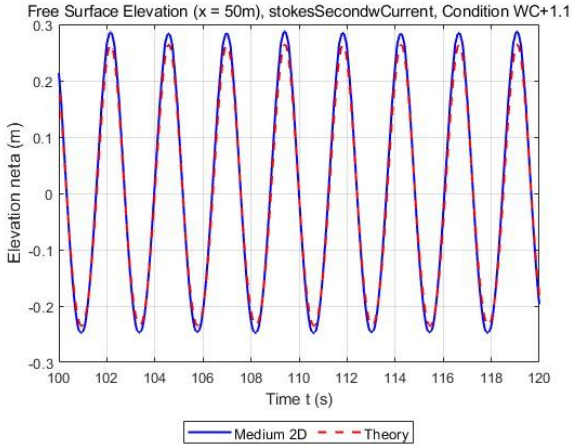

(b) The wave height at the location 50 m downstream from the inlet boundary

[Figure 6.8] The comparison on wave height between numerical results given by stokesSecondwCurrent in waves2Foam and theoretical values under WC+1.1 condition

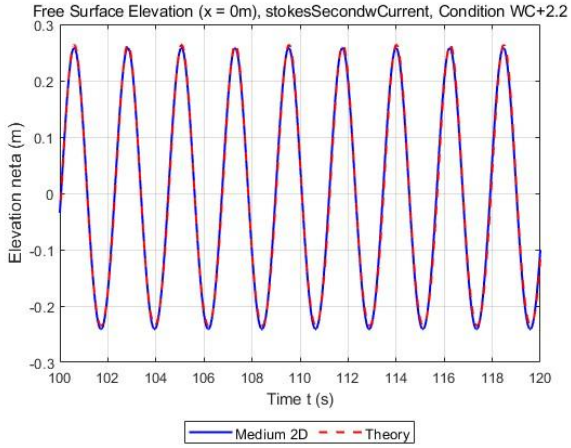

(a) The wave height at the inlet boundary

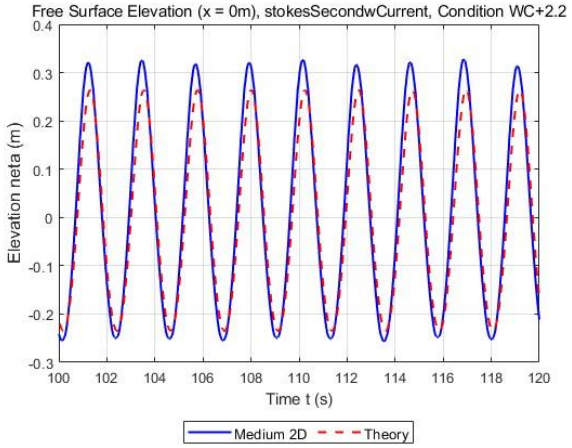

(b) The wave height at the location 50 m downstream from the inlet boundary

[Figure 6.9] The comparison on wave height between numerical results given by stokesSecondwCurrent in waves2Foam and theoretical values under WC+2.2 condition

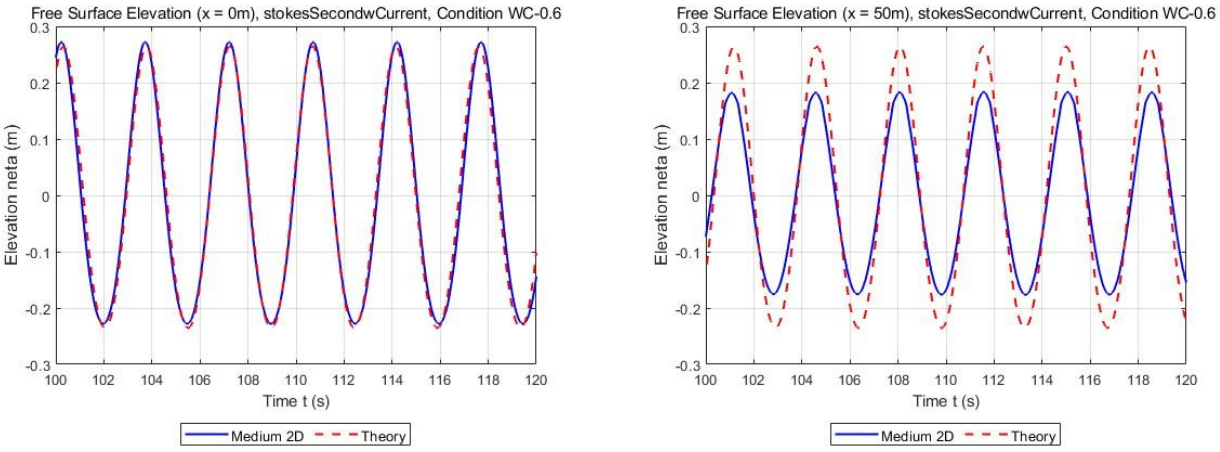

(a) The wave height at the inlet boundary

(b) The wave height at the location 50 m downstream from the inlet boundary

[Figure 6.10] The comparison on wave height between numerical results given by stokesSecondwCurrent in waves2Foam and theoretical values under WC-0.6 condition

6.3 Fluid dynamic force on a fixed floating-body

[Table 6.4] The parameters of waves in the simulation in Section 6.3

Wave parameters	Values
Water depth d (m)	1.6000
Wave period T (s)	0.7000
Wave height H (m)	0.0300
Wave amplitude a (m)	0.0150
Wave length λ (m)	0.9200
Wave steepness ε	1/30
Current velocity U_C(m/s)	0.2000

This subsection verifies whether wave-current coupling model, stokesSecondwCurrent, reproduces fluid dynamic loads on a marine structure accurately. To reach this goal, a benchmark (Gong, W.et.al) is adopted as reference.[36] Following their research, a viscous NWT, as illustrated in Figure 6.11, is established, and a fixed 2D cylinder-shaped floating body is created in the calculation domain. In this section, both wave and current loads on the structure are considered, and their detailed parameters are listed in Table 6.4. The grid, visualized in Figure 6.12, is generated with reference to the parameters of wave as well as current, and cells around the cylinder is refined in ordering to study the FSI phenomenon. The wave-induced forces in both directions and hydrodynamic moment acting on the body in the 2D plane are obtained by respectively applying a force sensor and a moment sensor

on the floating body. The data provided by these sensors are compared with the corresponding graphs in the benchmark. Noting that no turbulence model exists in the simulation of this section.

Similar to Sections 5.3, simulations are conducted in Genkai with the physical time of 20 s. Figure 6.13 shows the comparison between numerical results this study obtained and the experimental as well as computational values proposed by benchmark. The visualized free-surface deformation, pressure distribution, velocity layout and velocity vector field around the cube are shown in Figure 6.14.

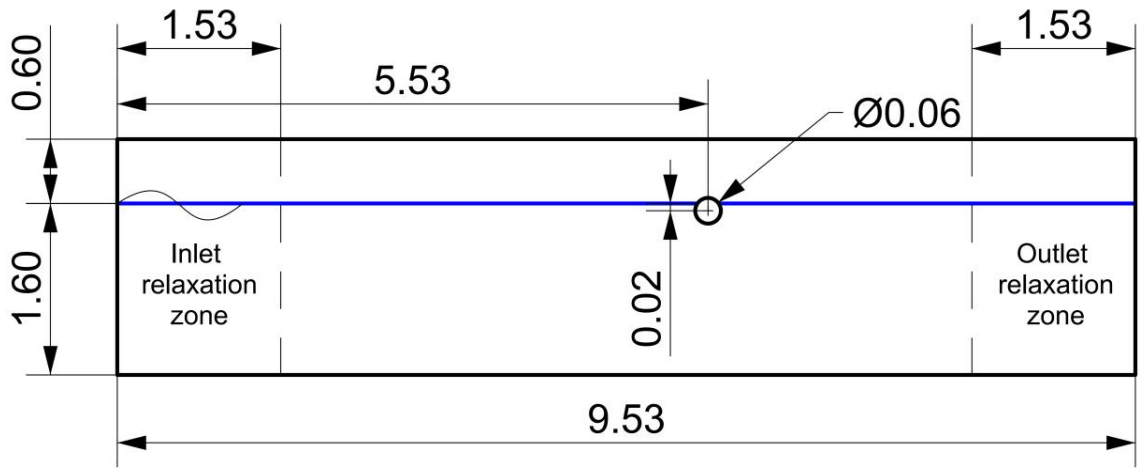

[Figure 6.11] The definition of 2D viscous-NWT for verification of wave loads predicted by stokesSecondwCurrent

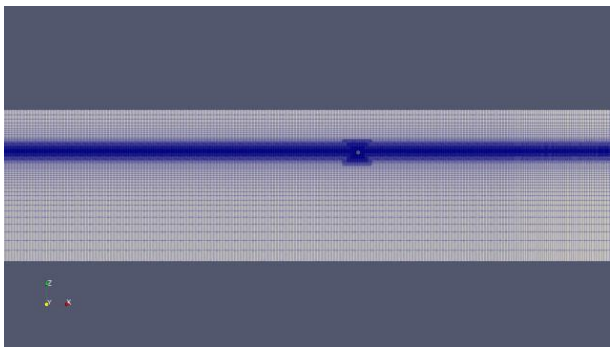

(a) The mesh configuration (overall view)

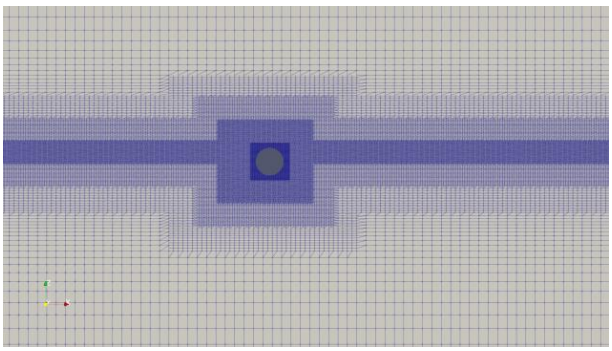

(b) The mesh configuration around target floating body

[Figure 6.12] The mesh configuration of 2D viscous-NWT for the verification of wave loads predicted by stokesSecondwCurrent

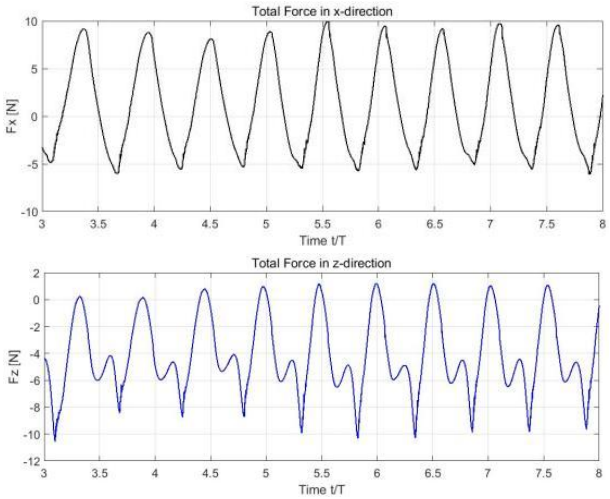

(a) The numerical results this research obtained

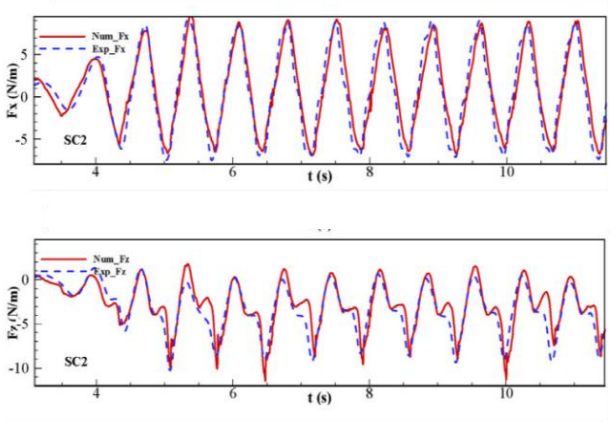

(b) The experimental and numerical results given by benchmark

[Figure 6.13] The comparison on wave loads between numerical results given by stokesSecondwCurrent in waves2Foam and values given by benchmark

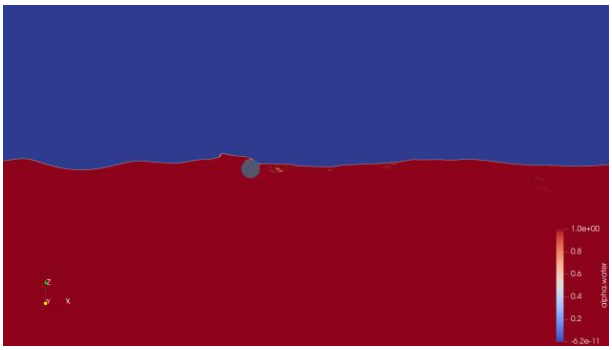

(a) The free-surface deformation around the floating body under investigation

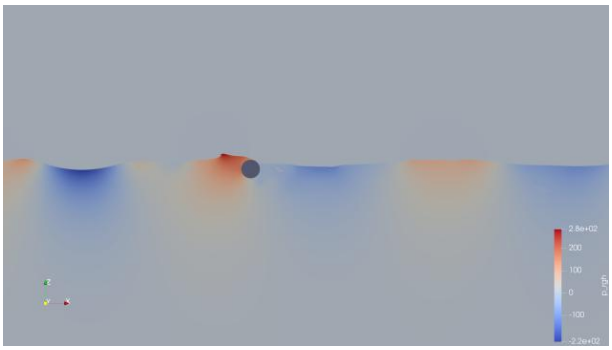

(b) The pressure distribution around the floating body under investigation

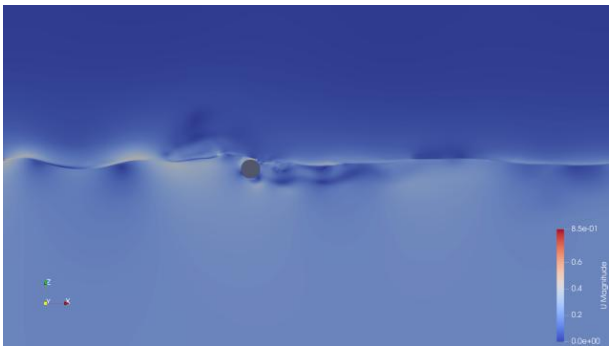

(c) The velocity contour around the floating body under investigation

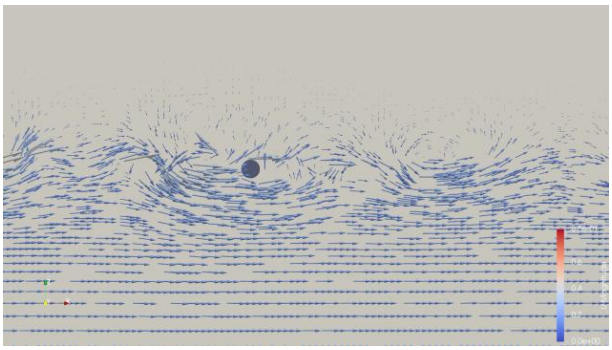

(d) The velocity vector distribution around the floating body under investigation

[Figure 6.14] The visualized viscous-NWT of the simulation for the verification of hydrodynamic loads predicted by stokesSecondwCurrent

It can be concluded from Figure 6.13 that user-define wave-current coupling model -

stokesSecondwCurrent, provides an accurate prediction showing high agreement with the experiments as well as computational results proposed in the benchmark. The overall trend and shape of the curves in Figure 6.13 about forces in each direction are consistent with those of the reference results in the benchmark, the peak and trough values also show good correspondence.

As shown in Figure 6.14, the visualized fluid field also well agrees with expatiation, exhibiting no abnormal physical behaviour. The numerical simulation reproduces the free-surface deformation around the floating body well, showing no sign of abnormal free-surface breaking. Furthermore, the distribution of pressure field, velocity field and velocity vector field around the cylinder are also consistent with the expected physical behavior. The fluid velocity vectors beneath the free-surface well consistent with the designated current direction showing no variation on their magnitudes, yet those around the water-level fluctuate induced by waves, demonstrating the correctness of the wave-current model.

In conclusion, the results obtain from this subsection demonstrates that stokesSecondwCurrent is capable of forecasting the loads on a marine structure, providing both precise and stable numerical predictions about hydrodynamic forces.

6.4 Investigation into accuracy improvement

This part explores the possibility of improving the accuracy of wave-current coupling reproduction in relevantly coarser meshes to meet the requirement of engineering applications, which require to obtain relevantly precise results with controllable resource consumption. To achieve this objective, methods such as optimizing the discretization schemes for each physical quantity and enlarging the length of relaxation zone are tested. Due to the fact that Medium 2D mesh is capable of providing numerical predictions with sufficient accuracy, the effects of these two methods are initially examined in Coarse 2D meshes and their influences on the accuracy are further verified in Medium 2D meshes to ensure the the generality of the conclusion. In this subsection, all simulations reproduce one identical condition, wave-current case labeled with WC0. Similarly, to capture the free-surface elevation, two probes are placed in the NWT and the positions of which are consistent with the setting in the previous subsections of this chapter. The results of wave height captured by these calculations are compared with the theoretical values given Matlab code mentioned above in Section 3.1.

Similarly to Section 5.4, on the basis of “Coarse 2D stokesSecondwCurrent WC0” case and

"Medium 2D stokesSecondwCurrent WC0" case, several modified simulation cases were constructed with reference to the redefinition given by Table 5.9. Noting that the original content of "fvScheme" file in "Coarse 2D stokesSecondwCurrent WC0" case for wave-current coupling reproduction is given by Appendix 3. The redefined simulation cases are implemented for 120s, and the numerical results of those be modified on the basis of Medium 2D mesh are given by Table 6.5 and Figure 6.15.

[Table 6.5] The numerical errors of the cases modified from the "Coarse 2D stokesSecondwCurrent W0" case

Case label	Time consumption	Error on wave height (x=50)
Coarse 2D stokesSecondwCurrent WC0	10h 30mins	-3.7894%
Coarse 2D stokesSecondwCurrent WC0 - TimeSecondOrder	Error	Error
Coarse 2D stokesSecondwCurrent WC0 - GradLimited	13h 12mins	-4.5168%
Coarse 2D stokesSecondwCurrent WC0 - DivUSecondOrder	33h 45mins	-4.2092%
Coarse 2D stokesSecondwCurrent WC0 - DivAlphaCompressed	15h 32mins	-2.9524%
Coarse 2D stokesSecondwCurrent WC0 - 35outlet	12h 33mins	-3.9368%
Coarse 2D stokesSecondwCurrent WC0 - 4outlet	12h 40mins	-4.0611%

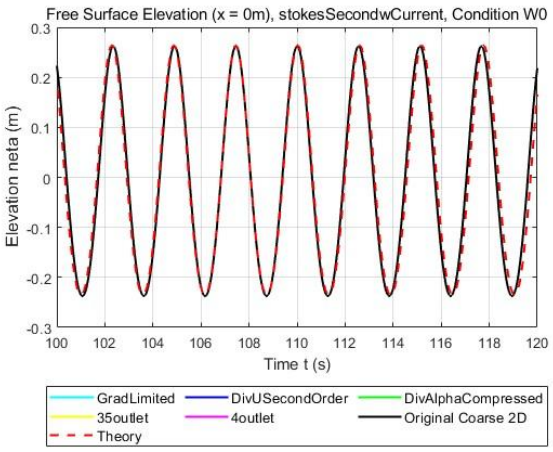

(a) The wave height at the inlet boundary

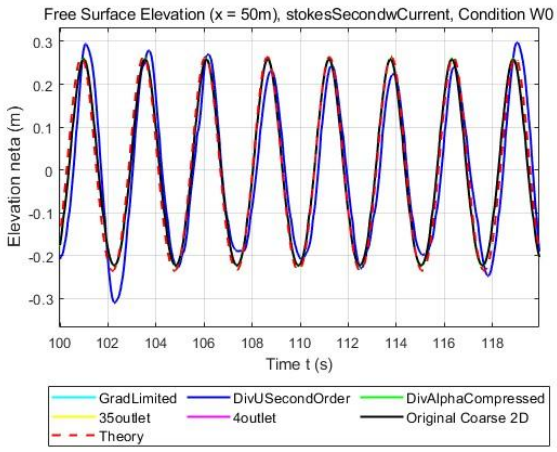

(b) The wave height at the location 50 m downstream from the inlet boundary

[Figure 6.15] The wave profile of the cases modified from the "Coarse 2D stokesSecondwCurrent W0" case

According to Table 6.5 and Figure 6.15, it can be concluded that modifying the differencing scheme of the relevant physical terms has a significant influence on the numerical results. By changing the differencing method of time in file "fvScheme" from "Euler" to "CrankNicolson" in the "Coarse 2D stokesSecondwCurrent WC0 - TimeSecondOrder" case, a floating point exception error occurs, similar to the consequence when applying the same modification to the wave generation simulations.

This error appears only a few s after the calculation is launched, and the visualized results at the moment the issue occurs are shown in Figure 6.16. Although no abnormal physical behaviour is observed in the flow field, pressure distribution field and velocity vector distribution, the time step is reduced to be infinitely small in order to satisfy the Courant number limitation. This finding indicates that the floating point exception, in another word numerical divergence, may be caused by abnormally large velocity vectors generated within the computational domain. Thus, it can be concluded that switching the time differencing scheme to the second-order method reduces the numerical stability of the simulation and should be avoided when reproducing wave-current coupling phenomena using the stokesSecondwCurrent solver. Modifying the discretization method of the spatial gradient operator ∇ for physical variables except for fluid's volume fraction from "Gauss linear" to "cellLimited Gauss linear" in "fvScheme" file, similar to the result when the same change is implemented to the wave generation case in Section 5.4, negatively influenced the accuracy and simulation efficiency, as the wave-height error drops to -4.5168% and calculation time consumption increases for 30%. Due to these unfavorable influence on numerical accuracy, this modification should be avoided when using stokesSecondwCurrent model. Shifting the differencing method of the discretization scheme for the momentum convection term in Navier-Stokes equation from "Gauss upwind" to " Gauss linearUpwind grad(U)" in the file "fvScheme" lead to significant computational consumption rise, as the calculation time is tripled under the same computational settings with the original case, while the numerical accuracy also drops. Additionally, as shown in Figure 6.15, the curve in deep blue which represents the result of the corresponding case remarkably fluctuates over the time. The peak and trough values of the curve vary from one period to another, indicating that the numerical stability of the case is adversely affected by this redefinition of the differencing method for the the momentum convection term. Thus, this modification should also be avoid when reproducing the wave-current coupling phenomena. However, changing the discretization scheme of the artificial interface-compression flux in the VOF formulation from "Gauss linear" to "Gauss interfaceCompression" in the "fvScheme" file is proved to have the potential to improve numerical accuracy. This modification results in an overestimation of the wave height by the solver stokesSecondwCurrent, leading to the improvement on accuracy as the wave height is originally under estimated on the Coarse 2D mesh. The wave-height error of this modified case is -2.9524%, which is significantly lower than that of the original unchanged case, yet still larger

than the error obtained in the original unmodified simulation on the Medium 2D grid. Meanwhile, the time consumption of the case increases to 15.5 hours which is even longer than that of the “Medium 2D stokesSecondwCurrent WC0” case - roughly 13 hours. As a result, although this redefinition shows potential for improving numerical accuracy, it becomes pointless when considering the increased computational cost, since simply refining the grid yields a better outcome.

(a) The free-surface deformation in the viscous-NWT

(b) The pressure distribution in the viscous-NWT (partially enlarged view)

(c) The velocity contour of the case

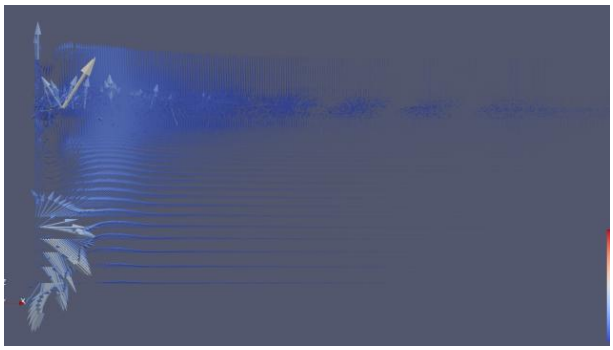

(d) The velocity vector distribution in the NWT

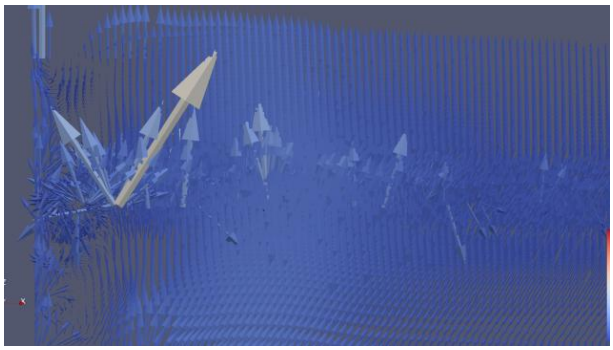

(e) The velocity vector distribution in the viscous-NWT (partially enlarged view)

[Figure 6.16] The visualized viscous-NWT of the“Medium 2D stokesSecondwCurrent WC0 - TimeSecondOrder” case at the moment when error occurs

As shown in Table 6.5 and Figure 6.15, lengthening the relaxation zone at the outlet boundary does not positively affect the numerical accuracy and computational efficiency. The time consumption of the corresponding modified cases is significantly longer than 10.5 hours - the computational time of the unmodified case. Moreover, the accuracy performance of these two cases is also worse than that of the "Medium 2D stokesSecondwCurrent WC0" case which is -3.7894%, as the errors on wave height of "Coarse 2D stokesSecondwCurrent WC0 - 35outlet" case and "Coarse 2D stokesSecondwCurrent WC0 - 4outlet" case are -3.9368% and -4.0611% respectively. Whereas, similar to the finding in Section 5.4, increase the length of the relaxation zone also reduces the unwanted water-level elevation induced by the wave reflection at the outlet boundary.

Similar to the process in the Section 5.4, to verify the correctness and generality of the conclusion obtained above, the same process of accuracy improvement study is implemented on the Medium 2D mesh. The same modifications detailed in the Table 5.9 are conducted on the basis of the "Medium 2D stokesSecondwCurrent W0" case, and the corresponding cases are created. Table 6.6 and Figure 6.17 indicates the results of these simulations, and from the results, same conclusion can be made that none of the redefinition given by Table 5.9 positively affect the numerical accuracy and thus the original settings of differencing schemes as well as relaxation zone layout are optimal.

In conclusion, none of the aforementioned modifications to the fvSchemes file improves numerical accuracy while maintaining a controllable increase in computational cost. This suggests that the original differencing scheme settings in the file—shown in Appendix 3—together with the unchanged relaxation-zone layout, are likely the optimal configuration.

[Table 6.6] The numerical errors of the cases modified from the "Medium 2D stokesSecondwCurrent W0" case

Case label	Time consumption	Error on wave height (x=50)
Medium 2D stokesSecondwCurrent WC0	12h 56mins	-0.2514%
Medium 2D stokesSecondwCurrent WC0 - TimeSecondOrder	Error	Error
Medium 2D stokesSecondwCurrent WC0 - GradLimited	14h 14mins	-0.8584%
Medium 2D stokesSecondwCurrent WC0 - DivUSecondOrder	25h 27mins	$+0.6949\%$
Medium 2D stokesSecondwCurrent WC0 - DivAlphaCompressed	19h 22mins	$+0.2152\%$
Medium 2D stokesSecondwCurrent WC0 - 35outlet	13h 43mins	-1.2019%
Medium 2D stokesSecondwCurrent WC0 - 4outlet	13h 54mins	-0.7829%

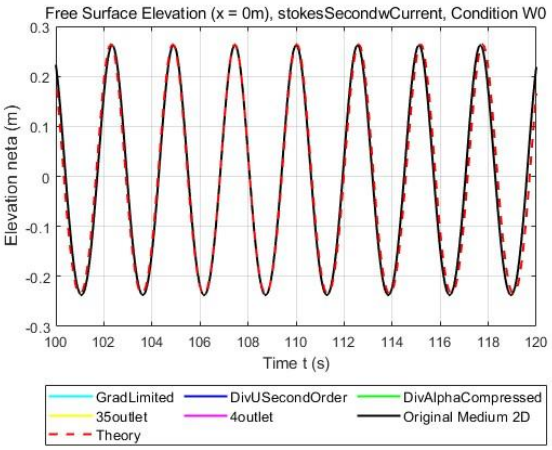

(a) The wave height at the inlet boundary

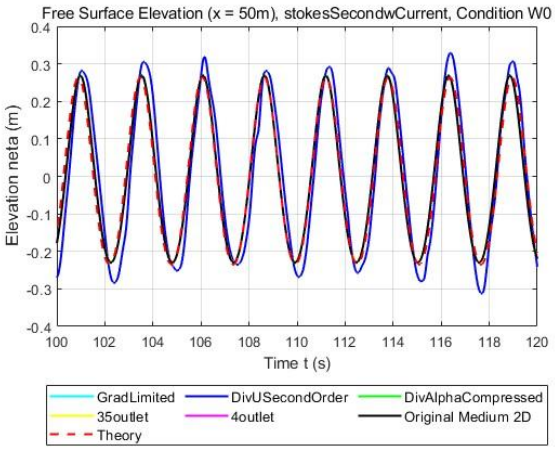

(b) The wave height at the location 50 m downstream from the inlet boundary

[Figure 6.17] The wave profile of the cases modified from the "Medium 2D stokesSecondwCurrent W0" case

6.5 Conclusion and discussion

In Chapter 6, the feasibility of the user-defined wave-current coupling solver - stokesSecondwCurrent is validated, and then the generality as well as accuracy performance of which is systematically studied. Finally, investigation is conducted to identify methods to reduce numerical error on relevantly coarse mesh when using stokesSecondwCurrent solver to reproduce wave-current coupling phenomena. Section 6.1 is the verification and validation study of the wave-current solver, in which the convergence study is also implemented to obtain a guideline for determining the mesh requirements needed to achieve high-accuracy numerical predictions (wave-height error below $\pm 2\%$). In Section 6.2, the performance of the solver - stokesSecondwCurrent is tested on 3D mesh and under multiple wave-current conditions, and the generality of the model is also examined. Section 6.3 investigates whether the user-defined model is capable of precisely forecasting loads on a marine structure by conducting a simulation with a 2D fixed cylinder-shape floating body in the fluid field. A systematic study is subsequently conducted in Section 6.4 to identify the effects of approaches, such as modifying the differencing schemes of physical terms or optimizing the relaxation-zone layout, on improving the numerical accuracy of simulations on coarse meshes.

From the analysis in Section 6.1, conclusion can be made that user-defined solver in waves2Foam - stokesSecondwCurrent is capable of precisely reproducing wave-current coupling phenomena. The errors between numerical predictions given by the solver and theoretical values varies from 3.7894% to 0.2514% in different meshes and the grid that provide results with lowest error on wave-height is

Medium 2D. Differ from the conclusion made in Section 5.1 where the accuracy of wave model increase with mesh density, stokesSecondwCurrent model shows a tendency of overestimating wave-induce free-surface elevation when grids are refined. Thus, merely increasing the mesh density does not necessarily lead to improved results when using the stokesSecondwCurrent model, and the recommended grid resolution is 200 to 250 cells per wavelength and 20 to 30 cells per wave height.

In Section 6.2, the performance of the user-defined solver stokesSecondwCurrent is examined under various conditions, including 3D meshes and wave-current loads with different wave steepness values and current velocities. Investigation in this subsection suggests that the wave model performs well on 3D grids, providing highly accurate numerical predictions, with wave-height errors on all meshes remaining below 2%. This finding demonstrates the feasibility of the stokesSecondwCurrent solver for 3D simulations. Study about the performance and generality of the wave-current coupling solver in the section, also suggests that stokesSecondwCurrent solver is capable of reproducing wave-current coupling phenomena and providing precise numerical forecasts on wave-height and period in almost all cases including some extreme ones. With the rise of wave component's steepness, the error on wave height rise and the error reaches to $+4.2346\%$ under WC10 condition. Notably, when the steepness of wave component exceeds $\frac{1}{25}$, the solver exhibits a tendency to overestimate the wave-height which may lead to conservative marine structure design. Thus, although the accuracy of the wave model decrease under such conditions, it remains acceptable for engineering application. Similarly, when the velocity of current component elevates, the error of the model also rises, for example in the "Medium 2D stokesSecondwCurrent WC+2.2" case wave-height error reaches $+7.0973\%$. However, due to the same reason, the wave-current coupling model is still feasible for practical engineering application. The stokesSecondwCurrent solver is found to be inappropriate for cases where the wave and current propagate in opposite directions, as the model significantly underestimates the wave height - the error of which is -14.1345% - and thus severely affect the safety design of marine structures. Overall, the user-defined solver for wave-current coupling performs well providing numerical predictions with satisfactory precision in multiple cases.

Sections 6.3 verified the feasibility of forecasting hydrodynamic loads on a marine structure under wave-current coupling conditions with stokesSecondwCurrent model. A fixed 2D cylinder-shaped floating body is created in the calculation domain, and forces in both directions together with moment

acting on the structure are measured by the installed probes and compared against a benchmark for validation. The numerical results highly agree with the values given by benchmark, as the temporal characteristics and overall trend of the load-time curves agree well with the benchmark data, demonstrating the feasibility of the wave-current solver on forecast hydrodynamic loads.

The last section - Section 6.4 - of the chapter explores the approaches to improve the numerical accuracy of wave-current coupling reproduction on Coarse 2D mesh. In the section, the effect of both discretization scheme modification method and relaxation zone layout optimization method are initially examined on Coarse 2D mesh and subsequently tested in Medium 2D mesh to ensure the generality of the conclusions. The result of which indicates that none of the approaches listed in Table 5.9 are favorable on improving the numerical accuracy. Changing the differencing scheme of physical parameters in “fvScheme” file either reduces numerical accuracy or increases computational consumption, so does lengthening the outlet relaxation zone. However, expanding the relaxation zone at the outlet boundary, effectively suppresses the unwanted water-level elevation induced by wave reflection,which becomes crucial when the wave steepness or current velocity is high. In conclusion, when using stokesSecondwCurrent model to reproduce wave-current coupling phenomena, the settings in “fvScheme” file is recommended to consistent with code shown in Appendix 3 and the configuration of relaxation is suggested to follow the layout illustrated in Figure 4.1.

7 Overset-mesh-based 6DOF motion solver

7.1 Feasibility study of the overWaveDyMFoam solver

In this chapter, the feasibility of the user-defined solver for overset mesh simulation - overWaveDyMFoam - in waves2Foam is verified by comparing the numerical prediction of the dynamic response of a 2D free floating cubic-shaped body under wave loads against the values given by a benchmark[35]. The benchmark adopted here is consistent with that in Section 5.3, and the viscous-NWT is created with reference to the paper.

[Table 7.1] The parameters of waves in the simulation in Chapter 7

Wave parameters	Values
Water depth d (m)	0.4000
Wave period T (s)	1.2000
Wave height H (m)	0.0400
Wave amplitude a (m)	0.0200
Wave length λ (m)	0.8100
Wave steepness ε	4/81

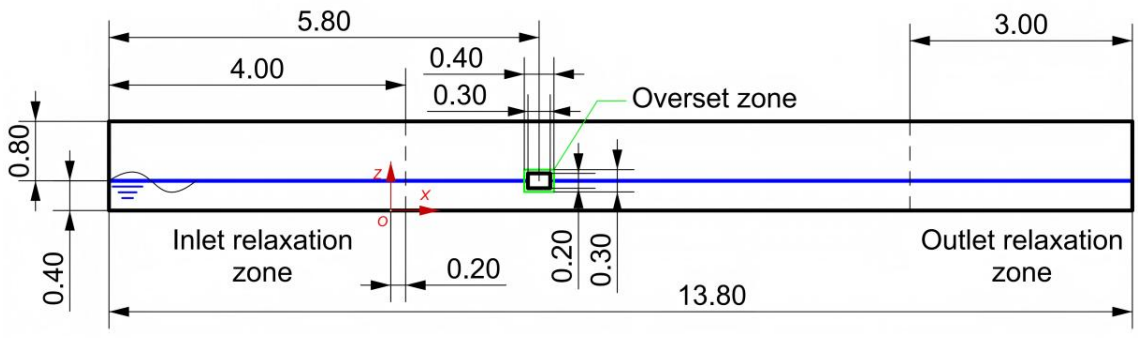

[Figure 7.1] The definition of 2D viscous-NWT for the verification case of solver overWaveDyMFoam

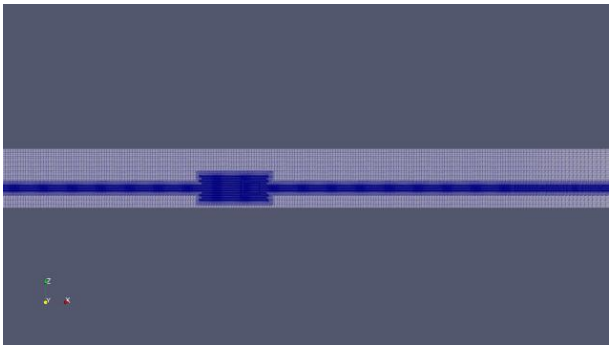

(a) The background mesh

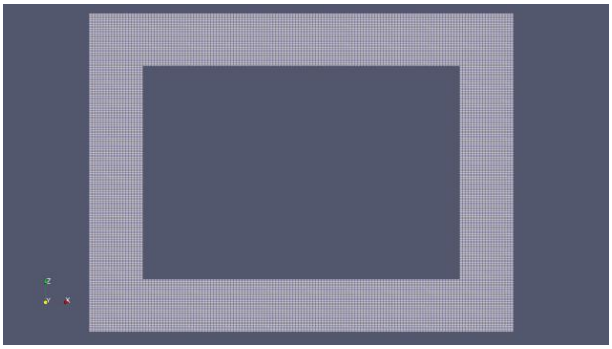

(b) The overset-zone mesh around the floating body

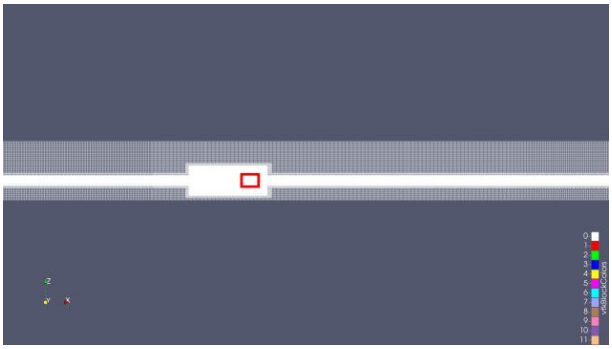

(c) The configuration of the merged mesh
(overall view)
(white area: background, red area: overset-zone)

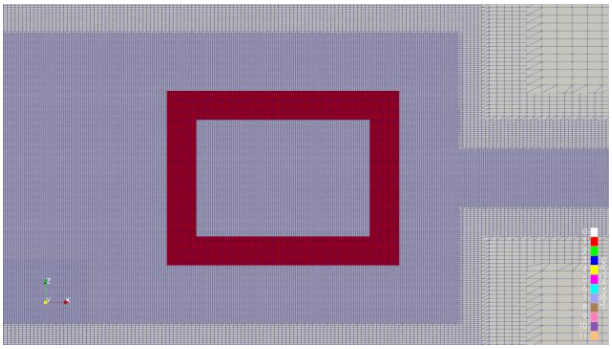

(d) The configuration of the merged mesh
(partially enlarged view)
(white area: background, red area: overset-zone)

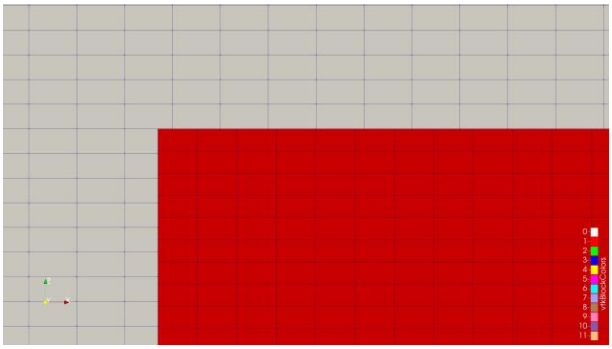

(e) The difference on cell size of background mesh and overset-zone mesh
(white area: background, red area: overset-zone)

[Figure 7.2] The mesh configuration of 2D viscous-NWT for the verification case of solver overWaveDyMFoam

The detailed definition of the calculation domain is shown in Figure 7.1. In this chapter the NWT configuration is similar to that of in Section 5.3, while the water depth is modified from 1.2 m to 0.4 m. A 2D floating body is also added to this case, yet the position and scale of it are also changed. In this chapter, the floating body has a length of 0.3 m, a width of 0.2 m, a draft of 0.1 m and a mass of 29.946 kg, with its center of mass located at the water-air interface. Noting that here the floating body is a free floating 2D structure and motions in only three degrees (surge, heave and pitch) are allowed.

Overset mesh is adopted to describe the dynamic response of the 2D floating body. As shown in Figure 7.2, the background mesh is generated and locally refined around the free-surface to capture its deformation. Additionally, the background mesh is also refined around the area where the overset mesh is merged into. A grid is also generated around the floating body as an overset-zone mesh, and the cell sizes of which are slightly smaller than the background mesh in the vicinity of the free surface to ensure interpolation accuracy. Subsequently, these two meshes are merged as the grid of the simulation in this chapter.

In this chapter, to enhance the credibility of the verification study about solver overWaveDyMFoam, 3 simulations with different settings are implemented. A simulation with fixed floating body is initially conducted to ensure the solver - overWaveDyMFoam - predict hydrodynamic loads on the floating body in waves precisely. In this case, floating body and overset mesh are introduced, where as the degrees of freedom of the floating body are constrained. The forces and moments acting on the floating body obtained from this simulation are summarized in Figure 7.3. In the second simulation, three degrees of freedom of the floating body are released to analyze its free-decay behavior in calm water and to simultaneously verify the correctness of the 6DOF solver module of overWaveDyMFoam. The motions of the 2D box in this case are recorded and are shown in Figure 7.4. Finally, on the basis of the second simulation, a wave with parameters detailed in Table 7.1 is introduced to the calculation domain to analyze the dynamic response of the floating body under wave loads. Additionally, in this case the $k-\omega$ SST turbulence model is employed to account for the effects of turbulence and fluid viscosity on the dynamic response of the floating body under wave loads. The results of the this simulation are illustrated in Figure 7.5. Noting all the cases are conducted with solver overWaveDyMFoam in the framework of waves2Foam, and the results of these cases about the motion values of floating body are all visualized in non-dimensional form.

All the above mentioned simulations are implemented in the super computer of Kyushu University - Genkai, and the calculation occupies 2 nodes with 48 threads per node. All these cases are simulated for a total duration of 12 s (10 wave periods), and the data from the steady-state stage are extracted and subsequently visualized.

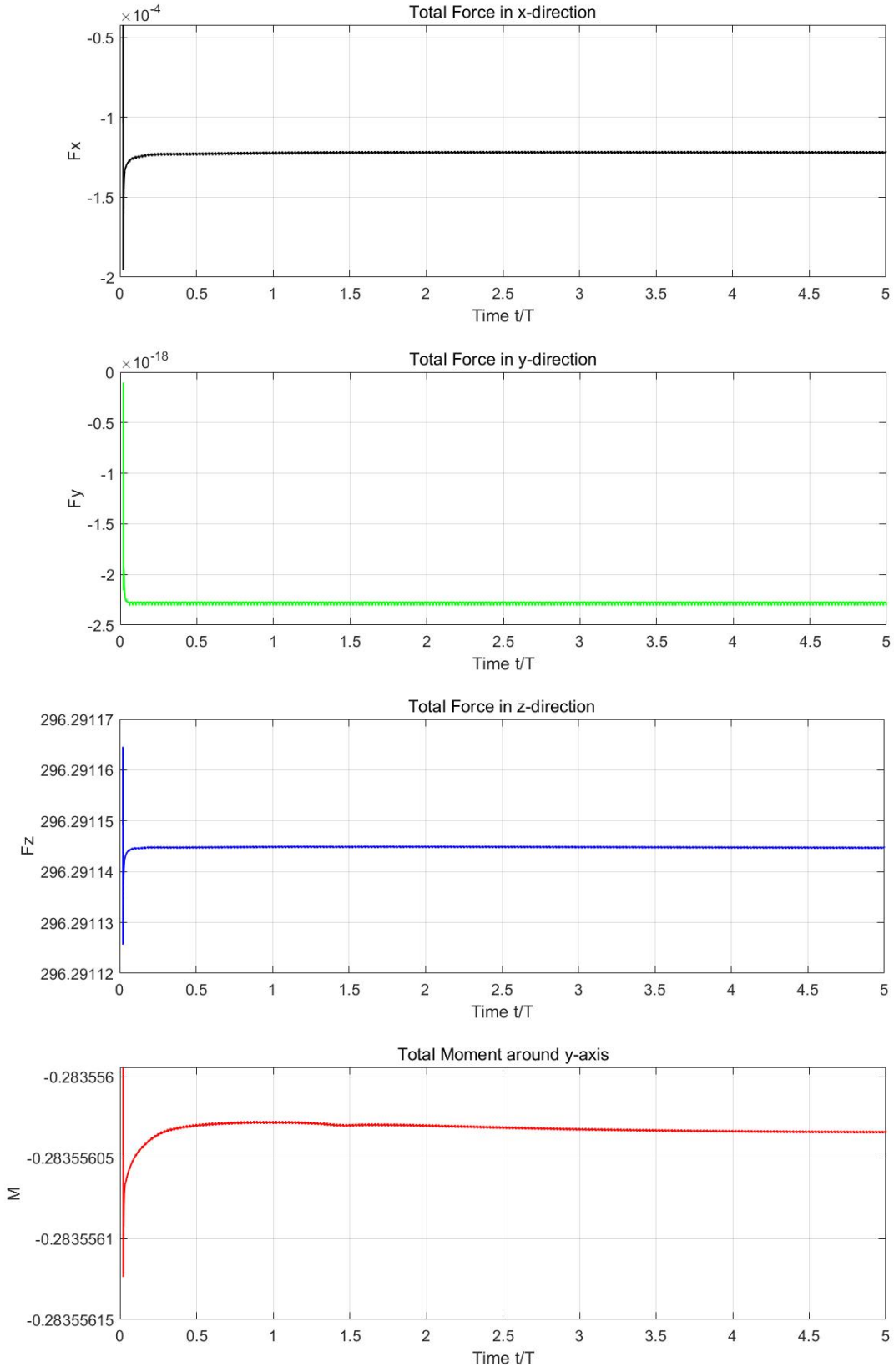

[Figure 7.3] The hydrodynamic loads on the fixed 2D cubic-shaped floating body

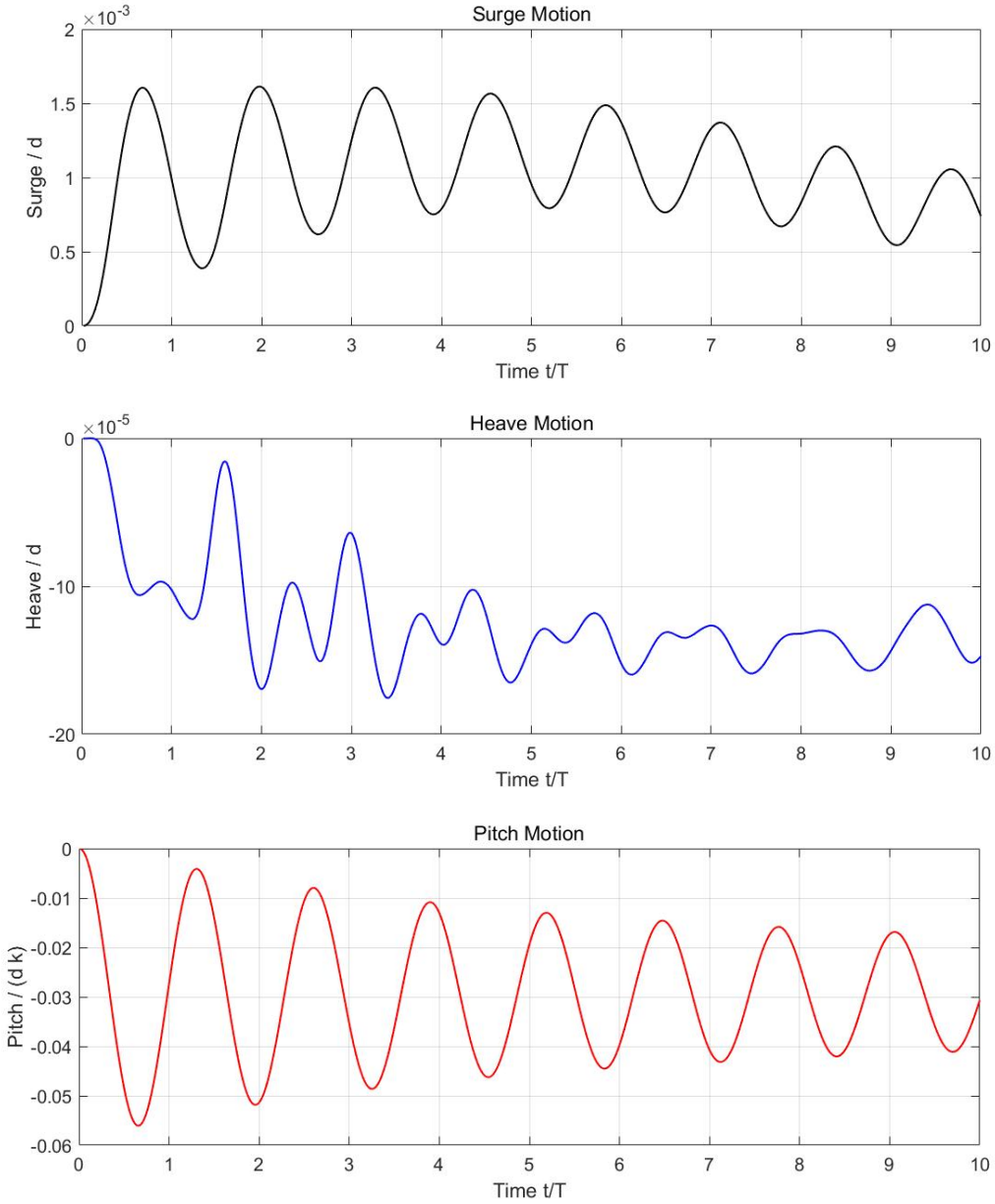

[Figure 7.4] The free-decay motions of the 2D cubic-shaped floating body in clam water

As shown in Figure 7.3, hydrodynamic loads on the 2D box predicted by the solver overWaveDyMFoam highly agrees with the physical expectation. The horizontal force F_x, F_y on the floating body fluctuates around zero over the time with a micro amplitude on the order of 10^{-4} or 10^{-18}. Similar oscillation is also observed in the graph of vertical force and the amplitude of fluctuation is also in the order of 10^{-5}. This micro amplitude fluctuation is commonly reported in simulation of multiple phase flow problems and is mainly attributed to unavoidable numerical noise arising from the discretization of the VOF interface, pressure-velocity coupling, and time-stepping schemes. Thus, conclusion can be made that the horizontal loads acting on the floating body are zero,

and the vertical force on the structure, in another word buoyancy, is 296.29 N. Moreover, apart from the initial torque peak observed at the start of the simulation, the pitch moment remains stable over time, showing fluctuation with only negligible amplitude. These results are consistent with physical expectation, as no horizontal load should exist on a fixed 2D structure in clam water, and the buoyancy balances its gravity, indicating that overWaveDyMFoam is capable of predicting hydrodynamic loads on a floating body.

The free-decay motions of the floating body in clam water is shown in Figure 7.4, and the results in the graphs validate the correctness of 6DOF solver module of overWaveDyMFoam. As the graphs showing, the amplitudes of the surge, heave, and pitch motions of the floating structure are minor, and decrease over the time, shows no tendency of increasing with time, indicating the convergence and stability of the simulation. It can be observed from the figure that in addition to the oscillatory motion a minor mean surge drift is present for the floating body. This might be attribute to the minor asymmetries in the pressure distribution around the floating body induced by numerical noise. However, the magnitude of the mean surge drift is small, on the order of 10^{-4}, and thus this drift is negligible. Additionally, apart from the fluctuation a mean heave offset with negligible amplitude is also observed for the floating body. This might be caused by the minor unbalance between the buoyancy and gravity of structure, and thus the floating box is adjusting its draft to reach a new equilibrium floating attitude. Overall, the free-decay motions of the floating body highly agrees with physical expectation, demonstrating the feasibility of the overWaveDyMFoam solver on 6DOF dynamic analysis.

As shown in Figure 7.5, the overWaveDyMFoam solver accurately predicts the dynamic response of the floating body in waves, as the numerical values proposed by the solver well agree with experimental and computational date given by the benchmark. This result demonstrates the feasibility of the overWaveDyMFoam solver on analyzing the 6DOF motion of a floating body. As shown in the graphs, the surge motion of the floating box consists of a mean surge drift and a periodic oscillation, as the surge displacement exhibits a stepwise increase over time. Both the peak and trough values of the surge response show good agreement with the benchmark date, demonstrating the high accuracy of the solver. In addition, the spacing between successive peaks is approximately equal to one wave period, which also consistent with physical expectations, indicating the correctness of the overWaveDyMFoam solver. The heave motion of the floating box does not exhibits the present of

mean heave offset, while the peak and trough values of the motion highly agrees with the benchmark data. Although the peak and trough values of heave motion slightly fluctuate over time, the oscillation amplitude is negligible, and thus the stability of the solver is satisfactory. Moreover, the stability of the solver is also evidenced by the period of the heave displacement remains stable over the time and equals to the wave period. As shown in Figure 7.5, the pitch motion of the floating body exhibit a satisfactory agreement with the benchmark values, evidenced by the peak and trough values of the pitch displacement are consistent with that of the benchmark. Moreover, the period of the pitch motion also remains stable over the time and equals to the wave period, which is also in agreement with physical expectations. The excellent agreement between numerical prediction given by overWaveDyMFoam and experimental data of benchmark well demonstrates the high accuracy and stability of the user-defined solver - overWaveDyMFoam, validating its feasibility of forecasting the dynamic response of floating body under wave loads.

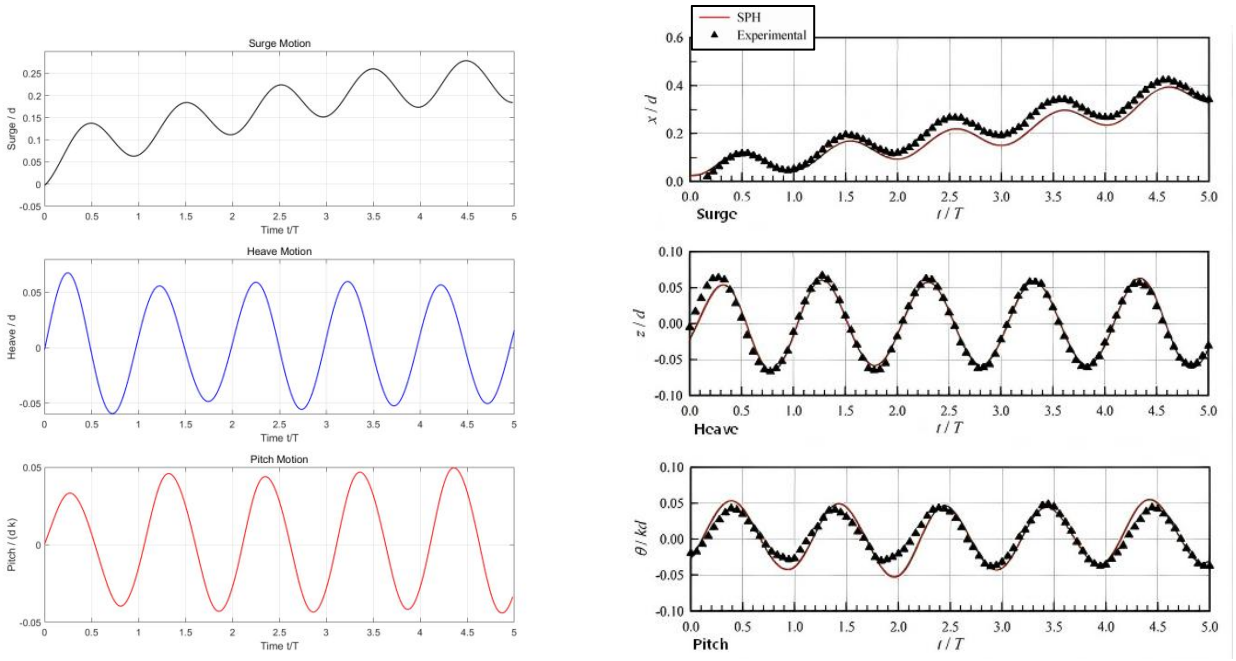

(a) The dynamic response of the floating body this research obtained

(b) The dynamic response of the floating body given by the benchmark

[Figure 7.5] The dynamic response of the 2D cubic-shaped floating body in waves

7.2 Conclusion and discussion

In this chapter, the feasibility of user-defined solver for overset-mesh-based 6DOF motion analysis - overWaveDyMFoam is examined and verified. Three simulations, hydrodynamic load

analysis, free-decay motion analysis of a floating body in clam water and dynamic response of a floating body in waves, are conducted to comprehensively validate the feasibility of the solver. The results of these cases demonstrate the correctness, accuracy, numerical stability, and good convergence properties of the solver, indicating that the overWaveDyMFoam solver is capable of accurately predicting dynamic response of floating body in wave. These findings also confirms that the overWaveDyMFoam solver developed in this study successfully introduces the overset mesh methodology into waves2Foam, enabling users to perform overset-mesh-based 6DOF simulations within the framework of the program.

8 Conclusion and discussion

In this study, the function of OpenFOAM as well as its plug-in code waves2Foam for wave generation and wave-current coupling reproduction are systematically studied. A wave-current coupling solver and an overset-mesh-based 6DOF motion solver are developed, verified, and subsequently evaluated within the waves2Foam framework. The feasibility and performance of the developed solvers are assessed, and for wave generation and wave-current coupling reproduction in practical engineering applications is also devised. Eventually, this research obtained the following conclusions.

1. The feasibility of generating nonlinear waves with OpenFOAM is validated, yet the accuracy performance of both stokesII and stokesV model are unsatisfactory. This is attributed to the strong non-linearity of the waves, which triggers significant numerical damping in the computational domain and leads to a remarkable underestimation of the wave height, with the error reaching -24.4289% even on the VeryFine2D mesh.

2. In order to accurately generate large nonlinear waves, the introduction of waves2Foam, a plug-in code of OpenFOAM, is essential. Because, the accuracy of both second-order and fifth-order Stokes wave models of waves2Foam is higher than those of OpenFOAM under the same mesh configuration and wave condition.

3. Among all the build-in wave models of the waves2Foam, stokesFifth - the one developed on the basis of fifth-order Stokes wave theory - is the optimal model for nonlinear wave generation. The feasibility of which is validated in both 2D and 3D meshes, and this wave model also performs well under multiple wave condition including extremely steep waves, demonstrating its high accuracy and generality. Moreover, this wave model is also proved to be capable of forecasting hydrodynamic loads on floating structures.

4. When generating nonlinear waves using stokesFifth model of waves2Foam, in order to obtain highly accurate results (error on wave height is lower than $\pm 2\%$), the following requirements for mesh configuration should be satisfied. In 2D simulations, when the wave steepness is smaller than $\frac{1}{25}$, there should be 300 cells in one wavelength and 30 cells in one wave height; when the wave steepness ranging from $\frac{1}{25}$ to $\frac{1}{16}$, there should be no fewer than 350 cells per wavelength and 35 cells per wave

height; when the wave steepness exceeds of $\frac{1}{16}$, the numerical damping in the fluid field become significant and mesh density with 450 cells per wavelength and 45 cells per wave height is necessary; however if the wave height increases further and the wave steepness is greater than $\frac{1}{10}$, the numerical damping in the fluid field become significant and numerical damping on wave height occurs no matter how fine the mesh is. In 3D cases, the recommended minimal mesh density in the third direction is 80 cells per wave length. Moreover, lengthening the relaxation zone at the outlet boundary does not measurably improves the numerical accuracy, yet reduce the unwanted mean water-level elevation, induced by wave reflection at the boundary. Therefor, in order to limits the unwanted mean water-level elevation, it is recommended that the length of outlet relaxation zone should be no shorter than three times of wave length, and more than four times of wave length under extreme conditions. The recommended length of inlet relaxation zone is two wave length.

5. The user-defined solver - stokesSecondwCurrent is validated to be capable of accurately reproducing wave-current coupling phenomena and exhibiting high performance under multiple conditions. The feasibility of the solver is verified under both 2D and 3D grids, and the generality of the model is validated by simulation cases with various wave steepness and current velocity. This model performs well under most wave-current conditions, providing highly precise numerical predictions except from the case where the wave and current propagates in opposite directions. In this case, the model significantly underestimates the wave height - the error on wave height reaching -14.1345%, which poses a risk to the safety design of marine structures. In contrast, under other conditions, the model tends to overestimate the wave height, leading to overly conservative designs in practical engineering applications. Furthermore, the solver stokesSecondwCurrent is also proved to be capable of forecasting hydrodynamic loads on marine structure with appropriate accuracy.

6. When reproducing wave-current coupling phenomena with stokesSecondwCurrent, achieving high accuracy (error on wave height is lower than $\pm 2\%$), the following requirements for mesh configurations should be satisfied. Due to the fact that the stokesSecondwCurrent solver exhibit a tendency of overestimating wave height with the increase of mesh density, merely refining the grid does not necessarily improve the numerical accuracy. Thus, the recommended mesh setting for 2D simulations is 200 to 250 cells per wavelength and 20 to 30 cells per wave height, while for 3D simulations, there should be more than 80 cells per wave length in the third direction. Additionally,

lengthening the outlet relaxation zone only reduces the wave reflection induced unwanted mean water-level elevation, yet does not improve the wave accuracy. As a result, it is recommended that the length of outlet relaxation zone should be no shorter than three times of wave length, and the suggested inlet relaxation zone length is two times of wave length.

7. This research investigates the methods to improve the numerical accuracy of wave generation and wave-current coupling reproduction on the basis of relevantly coarse mesh, obtaining the following results. On the basis of Appendix 2, shifting the discretization method of the artificial interface-compression flux in the VOF formulation from “Gauss linear” to “Gauss interfaceCompression” in “fvScheme” file improves the numerical accuracy of wave generation, allowing users to reduce the mesh density and the computational cost while maintaining high accuracy. For wave-current coupling reproduction, the optimal settings of “fvScheme” file is given by Appendix 3, and any change on the differencing scheme of physical parameters in the file leads to accuracy drops. The accuracy is not influenced by the relaxation zone layout, and thus the configuration of which is suggested to consistent with the above mentioned settings.

8. The feasibility of user-defined overset-mesh-based 6DOF motion solver -overWaveDyMFoam - is verified, and thus it can be concluded that the solver is capable of precisely predict the dynamic response of floating body under wave loads. The study also confirms that the overWaveDyMFoam solver developed in this study successfully introduces the overset mesh into the waves2Foam.

References

[1] International Energy Agency (IEA), “Key world energy statistics 2023”, International Energy Agency, Paris (2023).

[2] BP, “BP statistical review of world energy 2021”, BP p.l.c., London (2021).

[3] U.S. Energy Information Administration (EIA), “Country analysis brief: Japan”, U.S. Energy Information Administration, Washington, D.C. (2022).

[4] National Bureau of Statistics of China, “China energy statistical yearbook 2011”, China Statistics Press, Beijing (2011).

[5] Paulling J.R., “Tension leg platforms for deep water”, Journal of Petroleum Technology, Vol. 33, No. 12, pp. 2447–2458 (1981).

[6] Karsan D.I., “Design and installation of the Green Canyon tension leg platform”, Offshore Technology Conference, OTC 6055, Houston, USA (1989).

[7] Ma K.T., Patel M.H., “Dynamic response of tension leg platforms in deep water”, Marine Structures, Vol. 10, No. 3, pp. 199–224 (1997).

[8] Chakrabarti S.K., Handbook of Offshore Engineering, Vol. 2, Elsevier, Oxford (2005).

[9] Randolph M.F., Gourvenec S., Offshore Geotechnical Engineering, CRC Press, Boca Raton (2011).

[10] Jonkman J.M., “Dynamics modeling and loads analysis of an offshore floating wind turbine”, NREL/TP-500-41958, National Renewable Energy Laboratory, Golden, CO (2007).

[11] Butterfield S., Musial W., Jonkman J., Sclavounos P., “Engineering challenges for floating offshore wind turbines”, NREL/CP-500-38776, National Renewable Energy Laboratory, Golden, CO (2005).

[12] Ishida S., Utsunomiya T., Sato I., “Model tests of a tension-leg platform type floating offshore wind turbine”, Journal of Offshore Mechanics and Arctic Engineering, Vol. 135, 041903 (2013).

[13] Fernandez J., Sanchez A., “Experimental deployment of a tension-leg platform floating offshore wind turbine at PLOCAN”, Renewable Energy, Vol. 195, pp. 1125–1138 (2022).

[14] Myhr A., Bjerkseter C., Ågotnes A., Nygaard T.A., “Levelised cost of energy for offshore floating wind turbines”, Renewable Energy, Vol. 66, pp. 714–728 (2014).

[15] Weller H.G., Tabor G., Jasak H., Fureby C., “A tensorial approach to computational continuum mechanics using object-oriented techniques”, Computers in Physics, Vol. 12, No. 6, pp. 620–631 (1998).

[16] Jasak H., “OpenFOAM: Open source CFD in research and industry”, International Journal of Naval Architecture and Ocean Engineering, Vol. 1, No. 2, pp. 89–94 (2009).

[17] Greenshields C.J., OpenFOAM User Guide, OpenFOAM Foundation Ltd., London (2021).

[18] Hirt C.W., Nichols B.D., “Volume of fluid (VOF) method for the dynamics of free boundaries”, Journal of Computational Physics, Vol. 39, No. 1, pp. 201–225 (1981).

[19] Ubbink O., Issa R.I., “A method for capturing sharp fluid interfaces on arbitrary meshes”, Journal of Computational Physics, Vol. 153, No. 1, pp. 26–50 (1999).

[20] Rusche H., “Computational fluid dynamics of dispersed two-phase flows at high phase fractions”, PhD Thesis, Imperial College London, London (2002).

[21] Jacobsen N.G., Fuhrman D.R., Fredsøe J., “A wave generation toolbox for the open-source CFD library OpenFOAM®”, International Journal for Numerical Methods in Fluids, Vol. 70, No. 9, pp. 1073–1088 (2012).

[22] Lin P., Liu P.L.-F., “Internal wave-maker for Navier–Stokes equations”, Journal of Waterway, Port, Coastal, and Ocean Engineering, Vol. 125, No. 4, pp. 207–215 (1999).

[23] Larsen B.E., Dancy H., “Open boundaries in short wave simulations – a new approach”, Coastal Engineering, Vol. 7, No. 3, pp. 285–297 (1983).

[24] Higuera P., Lara J.L., Losada I.J., “Realistic wave generation and active wave absorption for Navier–Stokes models: Application to OpenFOAM”, Coastal Engineering, Vol. 71, pp. 102–118 (2013).
[25] Higuera P., Lara J.L., Losada I.J., “Simulating coastal engineering processes with OpenFOAM”, Coastal Engineering, Vol. 71, pp. 119–134 (2013).
[26] Higuera P., Lara J.L., Losada I.J., “Three-dimensional numerical wave generation with moving boundaries”, Coastal Engineering, Vol. 101, pp. 35–47 (2015).
[27] Hu S., “Development of a numerical wave tank for complex sea state simulation based on OpenFOAM”, Master Thesis, Shanghai Jiao Tong University, Shanghai (2024).
[28] Higuera P., Lara J.L., Losada I.J., “OLAFOAM: A numerical model for wave generation and absorption”, Coastal Engineering, Vol. 73, pp. 65–77 (2013).
[29] Higuera P., Lara J.L., Losada I.J., “IHFOAM: A numerical model for wave–structure interaction using OpenFOAM”, Coastal Engineering, Vol. 83, pp. 182–201 (2014).
[30] Chenari B., Saadatian S.S., Ferreira A.D., “Numerical modelling of regular wave propagation and breaking using waves2Foam”, Journal of Clean Energy Technologies, Vol. 3, No. 4, pp. 276–281 (2015).
[31] Fenton J.D., “Nonlinear wave theories”, in: Le Méhauté B., Hanes D.M. (Eds.), Ocean Engineering Science, Vol. 9, Part A, Wiley, New York, pp. 3–25 (1990).
[32] Bruinsma N., Paulsen B.T., Jacobsen N.G., “Validation and application of a fully nonlinear numerical wave tank for simulating floating offshore wind turbines”, Ocean Engineering, Vol. 147, pp. 647–658 (2018).
[33] Perić M., “Best practices for wave flow simulations”, The Naval Architect, Royal Institution of Naval Architects, pp. 22–27 (2018).
[34] Amini-Afshar M., “Numerical wave generation in OpenFOAM®”, Master Thesis, Chalmers University of Technology, Göteborg (2010).
[35] Ren B., He M., Dong P., Wen H., “Nonlinear simulations of wave-induced motions of a freely floating body using WCSPH method”, Applied Ocean Research, Vol. 50, pp. 1–12 (2015).
[36] Bai J., Ma N., Gu X., “Study of interaction between wave–current and a horizontal cylinder located near the free surface”, Applied Ocean Research, Vol. 67, pp. 44–58 (2017).

Appendix

Appendix 1 - Mathematical expressions of the constant coefficients in Stokes wave theory

$$A_{11} = \frac{1}{\sinh(kd)}$$

$$A_{22} = \frac{3S^2}{2(1-S)^2}$$

$$A_{31} = \frac{-4 - 20S + S^2 - 13S^3}{8\sinh[kd(1-S)^3]}$$

$$A_{33} = \frac{-2S^2 + 11S^3}{8\sinh[kd(1-S)^3]}$$

$$A_{42} = \frac{12S - 14S^2 - 264S^3 - 45S^4 - 13S^5}{24(1-S)^5}$$

$$A_{44} = \frac{10S^3 - 174S^4 + 291S^5 + 278S^6}{48(3+2S)(1-S)^5}$$

$$A_{51} = \frac{-1184 + 32S + 13232S^2 + 21712S^3 + 20940S^4 + 12554S^5 - 500S^6 - 3341S^7 - 670S^8}{64\sinh[kd(3+2S)(4+S)(1-S)^6]}$$

$$A_{53} = \frac{4S + 105S^2 + 198S^3 - 1376S^4 - 1302S^5 - 117S^6 + 58S^7}{32\sinh[kd(3+2S)(1-S)^6]}$$

$$A_{55} = \frac{-6S^3 + 272S^4 - 1552S^5 + 852S^6 + 2029S^7 + 430S^8}{64\sinh[kd(3+2S)(4+S)(1-S)^6]}$$

$$B_{11} = 1$$

$$B_{22} = \coth\left[\frac{kd(1+2S)}{2(1-S)}\right]$$

$$B_{31} = \frac{-3(1 + 3S + 3S^2 + 2S^3)}{8(1-S)^3}$$

$$B_{33} = -B_{31}$$

$$B_{42} = \coth\left[\frac{kd\left(6 - 26S - 182S^2 - 204S^3 - 25S^4 + 26S^5\right)}{6(3+2S)(1-S)^4}\right]$$

$$B_{44} = \coth\left[\frac{kd\left(24 + 92S + 1222S^2 + 66S^3 + 67S^4 + 34S^5\right)}{24(3+2S)(1-S)^4}\right]$$

$$B_{51} = -(B_{53} + B_{55})$$

$$B_{53} = \frac{9\left(132 + 17S - 2216S^2 - 5897S^3 - 6292S^4 - 2687S^5 + 194S^6 + 467S^7 + 82S^8\right)}{128(3+2S)(4+S)(1-S)^6}$$

$$B_{55} = \frac{5\left(300 + 1579S + 3176S^2 + 2949S^3 + 1188S^4 + 675S^5 + 1326S^6 + 827S^7 + 130S^8\right)}{384(3+2S)(4+S)(1-S)^6}$$

Appendix 2 - Content of “fvScheme” file for wave generation

```
/*--------------------------------*- C++ -*----------------------------------*\
| =========                 |                                                 |
| \\      /  F ield         | OpenFOAM: The Open Source CFD Toolbox           |
|  \\    /   O peration     | Version:  v2106                                 |
|   \\  /    A nd           | Website:  www.openfoam.com                      |
|    \\/     M anipulation  |                                                 |
\*---------------------------------------------------------------------------*/
FoamFile
{
    version     2.0;
    format      ascii;
    class       dictionary;
    object      fvSchemes;
}
// * * * * * * * * * * * * * * * * * * * * * * * * * * * * * * * * * * * * * * * * * * * * * * * * * * * * * * * * //
ddtSchemes
{
    default         Euler;
}

gradSchemes
{
    default         Gauss linear;
    grad(U)         Gauss linear;
    grad(alpha1)    Gauss linear;
}

divSchemes
{
    div(rhoPhi,U)   Gauss upwind;
    div(U)          Gauss linear;
    div(phi,alpha)  Gauss vanLeer;
    div(phirb,alpha) Gauss linear;
    div(((rho*nuEff)*dev2(T(grad(U))))) Gauss linear;
//Activate when turbulence model exist
/*
```

```
    div(phi,k)          Gauss upwind;
    div(phi,epsilon) Gauss upwind;
div(phi,omega) Gauss upwind;
*/
}

laplacianSchemes
{
    default             Gauss linear corrected;
}

interpolationSchemes
{
    default             linear;
}

snGradSchemes
{
    default             corrected;
}

oversetInterpolation
{
    method              cellVolumeWeight;
}

oversetInterpolationSuppressed
{
    grad(p_rgh);
    surfaceIntegrate(phiHbyA);
}

fluxRequired
{
    default             no;
    p_rgh;
    pcorr;
    alpha.water;
}

wallDist
```

```
        90
{
    method                  meshWave;
}
// ************************************************************************* //
```

Appendix 3 - Content of “fvScheme” file for wave-current coupling reproduction

```
/*--------------------------------*- C++ -*----------------------------------*\
| =========                      |                                            |
| \\      /  F ield              | OpenFOAM: The Open Source CFD Toolbox      |
|  \\    /   O peration          | Version:  v2106                            |
|   \\  /    A nd                | Website:  www.openfoam.com                 |
|    \\/     M anipulation       |                                            |
\*---------------------------------------------------------------------------*/
FoamFile
{
    version     2.0;
    format      ascii;
    class       dictionary;
    object      fvSchemes;
}
// * * * * * * * * * * * * * * * * * * * * * * * * * * * * * * * * * * * * * * * * * * * * * * * * * * * * * * * * //
ddtSchemes
{
    default         Euler;
}

gradSchemes
{
    default         Gauss linear;
    grad(U)         Gauss linear;
    grad(alpha1)    Gauss linear;
}

divSchemes
{
    div(rhoPhi,U)   Gauss upwind;
    div(U)          Gauss linear;
    div(phi,alpha)  Gauss vanLeer;
    div(phirb,alpha) Gauss linear;
    div(((rho*nuEff)*dev2(T(grad(U))))) Gauss linear;
//Activate when turbulence model exist
/*
    div(phi,k)      Gauss upwind;
```

```
    div(phi,epsilon) Gauss upwind;
div(phi,omega) Gauss upwind;
*/
}

laplacianSchemes
{
    default         Gauss linear corrected;
}

interpolationSchemes
{
    default         linear;
}

snGradSchemes
{
    default         corrected;
}

oversetInterpolation
{
    method          cellVolumeWeight;
}

oversetInterpolationSuppressed
{
    grad(p_rgh);
    surfaceIntegrate(phiHbyA);
}

fluxRequired
{
    default         no;
    p_rgh;
    pcorr;
    alpha.water;
}

wallDist
{
```

```
    method          meshWave;
}
// ************************************************************************* //
```

Acknowledgement

At the end of this paper for master degree of Pusan National University, I would like to express my deepest gratitude to those who assisted me in the past few years.

Firstly, I would like to deeply appreciate the professors. Thanks for the kindly assistance and instruction of Prof. Park from Pusan National University. During my stay in Korea, Prof. Park patiently listened to my problems on research and gave precious advice which significantly helped me to overcome academic challenges. Also, Prof. Park gave me a precious chance of studying in Korea for half years which remarkably influenced my life, enabling my study of master degree to be memorable. I would also like to appreciate the supervisor of mine in Kyushu University - Prof. Hu, who gave me an opportunity of studying and living in Japan. The stay in Japan is an unforgettable period of time in my life, promoting my personal and academic growth. Also, the academic advice and highly valuable computational resources given by Prof. Hu were also significant toward my research and this paper. Additionally, I would like to express my gratitude to Prof. Wang, the founder of Campus Asia project. It was him who allows me to further study in Korea and have a chance of obtaining double master degrees in both Pusan National University and Kyushu University. I sincerely appreciate these professors at the end of my master degree course, it will not be possible for me to accomplish this paper without their kind help.

Secondly, I would like to celebrate the completion of the paper and leave a message of “Otsukare” for myself. The path toward the completion of this work was not without challenges, being filled by accidents and challenges. Countless difficulties occurs in the research, yet were all overcome under the highly valuable instruction and the spirit of perseverance.

Thirdly, I am also thankful to colleagues and members of the laboratory in both Pusan Nation University and Kyushu University for their valuable discussions and assistance. Without the assistance of such a group of warm-hearted colleagues, this study can finally be completed.

Finally, I would like to thank my family and friends for their unwavering support, encouragement, and understanding during the completion of this thesis.